

Electronic Thesis and Dissertation Repository

4-20-2012 12:00 AM

Photocatalytic Reactors for Air Treatment: Energy Efficiencies and Kinetic Modeling

Juan M. Garcia Hernandez
The University of Western Ontario

Supervisor
Hugo de Lasa
The University of Western Ontario

Graduate Program in Chemical and Biochemical Engineering
A thesis submitted in partial fulfillment of the requirements for the degree in Doctor of Philosophy
© Juan M. Garcia Hernandez 2012

Follow this and additional works at: <https://ir.lib.uwo.ca/etd>

 Part of the [Catalysis and Reaction Engineering Commons](#)

Recommended Citation

Garcia Hernandez, Juan M., "Photocatalytic Reactors for Air Treatment: Energy Efficiencies and Kinetic Modeling" (2012). *Electronic Thesis and Dissertation Repository*. 459.
<https://ir.lib.uwo.ca/etd/459>

This Dissertation/Thesis is brought to you for free and open access by Scholarship@Western. It has been accepted for inclusion in Electronic Thesis and Dissertation Repository by an authorized administrator of Scholarship@Western. For more information, please contact wlsadmin@uwo.ca.

PHOTOCATALYTIC REACTORS FOR AIR TREATMENT: ENERGY EFFICIENCIES AND KINETIC MODELING

(Spine title: **Photocatalytic Reactors for Air Treatment**)

(Thesis format: Monograph)

by

Juan Manuel Garcia Hernandez

Graduate Program in Chemical and Biochemical Engineering

A thesis submitted in partial fulfillment
of the requirements for the degree of
Doctor of Philosophy

The School of Graduate and Postdoctoral Studies
The University of Western Ontario
London, Ontario, Canada

©Juan Manuel Garcia Hernandez, 2012

CERTIFICATE OF EXAMINATION

Supervisor

Examiners

Dr. Hugo de Lasa

Dr. Ajay K. Ray

Supervisory Committee

Dr. Charles Xu

Dr. Benito Serrano

Dr. Fariborz Taghipour

Dr. Ron R. Martin

The thesis by

Juan Manuel Garcia Hernandez

entitled:

**Photocatalytic Reactors for Air Treatment: Energy Efficiencies
and Kinetic Modeling**

is accepted in partial fulfillment of the
requirements for the degree of
Doctor of Philosophy

Date

Chair of the Thesis Examination Board

Abstract

Indoor air pollution is an increasing environmental concern. Heterogeneous photocatalysis is a promising strategy for the elimination of air pollutants in enclosed environments. However, studies involving gas-phase heterogeneous photocatalysis are relatively few compared with the substantial literature on photocatalytic water treatment.

It is necessary to pay special attention to the photocatalytic reactor design allowing for optimal use of irradiation. Therefore, in addition to the rate of photoconversion, an energy yield describing the light utilization efficiency and how this energy efficiency varies at different operating conditions should be defined. A parameter for this analysis is the quantum efficiency. This parameter can also help in reaction pathway discrimination.

Definitions of quantum yields should be based on ratios involving photoconverted molecules over the rate of light intensity absorbed at a given wavelength. Although determining the rate of light intensity absorbed at a given wavelength is a relative easy task in homogeneous systems, it is a rather difficult assignment for heterogeneous reactions. In this case, light is not only absorbed but also scattered and reflected by the suspended semiconductor particles.

In this PhD dissertation, the energy efficiency of the photocatalytic conversion of gas-phase organic pollutants was studied using a redesigned and scaled up Photo-CREC-Air Reactor (the letters CREC stand for Chemical Reactor Engineering Centre). This photocatalytic unit has the unique feature of allowing an accurate analysis of the irradiation field by establishing macroscopic balances and in-situ measurements. The reactor operates in a batch mode with the photocatalyst supported by a stainless steel mesh being irradiated by 8 UV lamps. Kinetic modelling, Quantum Yields (*QY*) and Photochemical Thermodynamic Efficiency Factors (*PTEF*) were calculated using data from acetone, acetaldehyde and isopropanol photocatalytic degradation in ambient air utilizing the commercial Degussa P25 photocatalyst. It is shown that the Photo-CREC-Air Reactor is suitable for the determination of kinetic and adsorption parameters, given its design which allows excellent irradiation usage and fluid-catalyst contact. In this

respect, quantum yields for acetone, acetaldehyde and isopropanol supersede the value of 1 (equivalent to 100%) with *PTEFs* remaining in all cases below the level of 1 as required by thermodynamics.

Keywords

Air, acetone, acetaldehyde, isopropanol, heterogeneous photocatalysis, Photo-CREC-Air Reactor, photocatalytic reactor, kinetic modeling, energy efficiency.

Acknowledgments

I would like to thank my supervisor Dr. Hugo de Lasa for his invaluable guidance, support, encouragement, criticism and patience during the development of this project.

I would also like to thank Professor Benito Serrano for all his suggestions, comments and useful advice.

I am grateful to the CREC staff, members and colleagues. It has been a pleasure to share with you and learn from all of you.

My sincere appreciation goes to the administrative staff in the Department of Chemical and Biochemical Engineering, the University Machine Services, people at The University of Western Ontario that helped me in the completion of my PhD program and those I forgot between the pages.

I offer my gratitude to The National Council of Science and Technology in Mexico (CONACyT-México) for the scholarship provided.

I am indebted to my close friends, old and new. They are by my side when going through happy and difficult moments equally, regardless distance and time.

Finally I must say that everything I do, big or small, fast or slow, good or even bad is always dedicated to my family.

Table of Contents

CERTIFICATE OF EXAMINATION	ii
Abstract	iii
Acknowledgments	v
Table of Contents	vi
List of Tables	x
List of Figures	xi
List of Appendices	xv
Nomenclature	xvi
Chapter 1	1
1 Introduction	1
Chapter 2	4
2 Literature Review	4
2.1 Introduction	4
2.2 Heterogeneous Photocatalysis	4
2.3 Photocatalysts	5
2.3.1 TiO ₂ Photocatalysts	6
2.4 Photocatalytic Reactors and Light Sources	7
2.4.1 Honeycomb Monolith Reactors	7
2.4.2 Fluidized Bed Reactors	8
2.4.3 Annular Reactors	10
2.4.4 Packed bed Reactors	11
2.4.5 Fibre Optic Based Reactors	12
2.4.6 Light sources	13
2.5 Photo-CREC-Air Reactors	15
2.5.1 Characteristics of the Photo-CREC-Air Reactor	16

2.5.2 Antecedents in the use of Previous Photo-CREC-Air Reactor Versions	18
2.6 Energy Efficiencies in Photocatalytic Reactors	20
2.6.1 Quantum Yields	21
2.6.2 Photochemical Thermodynamic Efficiency Factor (<i>PTEF</i>)	23
2.7 Photocatalytic Kinetics Models	24
2.8 Conclusions	26
Chapter 3	27
3 Scope of the Research	27
3.1 General Objectives of the Research	27
3.2 Specific Objectives of the Research	28
3.2.1 Photocatalyst Preparation and Kinetic Studies	28
3.2.2 Irradiation and Flow Field Studies	28
3.2.3 Energy Efficiency Evaluation	29
Chapter 4	30
4 Experimental Setup	30
4.1 Introduction	30
4.2 Photo-CREC-Air Reactor	30
4.3 UV Sources	34
4.4 Photocatalyst Support	35
4.5 Photocatalyst Impregnation	38
4.6 Irradiation Field Analysis	38
4.7 Flow Field Analysis	41
4.8 Conclusions	43
Chapter 5	44
5 Experimental Methods	44
5.1 Sample Analysis	44
5.2 Experimental Procedure	45

5.3	Blank Experiments	45
5.4	Mass Balances	47
Chapter 6		49
6	Results and Discussion I: Kinetic Modeling	49
6.1	Introduction»	49
6.2	Photocatalysis Kinetics Modeling	49
6.3	Acetone Photocatalytic Degradation Modeling	52
6.4	Acetaldehyde Photocatalytic Degradation Modeling	55
6.5	Isopropanol Photocatalytic Degradation Modeling	58
6.6	Conclusions	64
Chapter 7		65
7	Results and Discussion II: Energy Efficiencies in Previous Versions of the Photo-CREC-Air Reactor	65
7.1	Introduction	65
7.2	Quantum Efficiency in Previous Photo-CREC-Air Reactor Versions	65
7.3	Photochemical-Thermodynamic Efficiency Factor (<i>PTEF</i>) in Previous Photo-CREC-Air Reactor Versions	69
7.4	Conclusions	72
Chapter 8		73
8	Results and Discussion III: Energy Efficiency in the 55.1 L Version of the Photo-CREC-Air Reactor	73
8.1	Introduction	73
8.2	Energy Efficiency Factors	74
8.3	Stoichiometric Equations and Photoreaction Rates	77
8.3.1	Acetone Photocatalytic Degradation Stoichiometry	78
8.3.2	Acetaldehyde Photocatalytic Degradation Stoichiometry	78
8.3.3	Isopropanol Photocatalytic Degradation Stoichiometry	79
8.4	Photocatalytic Modeling	79
8.4.1	Acetone Photocatalytic Degradation Modeling	80

8.4.2 Acetaldehyde Photocatalytic Degradation Modeling	83
8.4.3 Isopropanol Photocatalytic Degradation Modeling	86
8.5 Energy Efficiency Calculations	90
8.6 Conclusions	97
Chapter 9	98
9 Conclusions and Recommendations	98
9.1 Main Conclusions	99
9.2 Recommendations for Future Work	99
References	101
Appendices	112
Curriculum Vitae	125

List of Tables

Table 1: Bandgap energy of various photocatalysts.....	6
Table 2: Properties and features of the artificial UV light sources	15
Table 3: Quantum Parameter Definitions.....	22
Table 4: Kinetic and Data Modeling Parameters for acetone photocatalytic degradation with Degussa P25 photocatalyst.....	81
Table 5: Kinetic and Data Modeling Parameters for acetaldehyde photocatalytic degradation with Degussa P25 photocatalyst	85
Table 6: Kinetic and Data Modeling Parameters for isopropanol photocatalytic degradation with Degussa P25 photocatalyst	90
Table 7: Comparison of Efficiency Parameters (Quantum Efficiency and <i>PTEF</i>)	94

List of Figures

Figure 1: Schematic of the Processes that take place when a semiconductor particle receives band-gap illuminated	5
Figure 2: Schematic diagram of the monolith reactor	8
Figure 3: Schematic diagram of the fluidized-bed reactor	9
Figure 4: Schematic diagram of the annular reactor	10
Figure 5: Photocatalytic reactors used by Esterkin et al., (2002)	12
Figure 6: Schematic diagram of the optical fiber photocatalytic	13
Figure 7: Schematic diagram of the Former Photo-CREC-Air reactor	17
Figure 8: Former Version of the Photo-CREC–air Venturi section	18
Figure 9: Picture of Photo-CREC-Air Reactor showing its main components. The protecting enclosure holding the 8 near UV lamps is open for a better description of Photo-CREC-Air components	31
Figure 10: Detailed drawing of the Photo-CREC-Air Reactor dimensions	32
Figure 11a: Diagram of the Photo-CREC-Air Reactor, isometric view	33
Figure 11b: Description of the Venturi divergent section in the Photo-CREC-Air Reactor	33
Figure 12: Detail of the reaction section in the Photo-CREC-Air Reactor showing the near-UV lamps distributed circumferentially around the reaction section	35
Figure 13: Cylindrical mesh used as catalyst support	36
Figure 14: Stainless steel mesh cylinder coated with Degussa P25	37
Figure 15: Picture showing the Degussa P25 photocatalyst covering the metallic mesh	37

Figure 16: Top and Side View of the Perforated Reaction Section Top Plate	39
Figure 17: Schematics of the specially designed Periscopic Irradiation Receiver showing the angle of acceptance	40
Figure 18a: Schematic Diagrams of the Periscope Irradiation Receiver showing the irradiation acceptance angle placed at three positions: Periscope placed between the glass tube and the near UV lamps measuring “ P_e ”	41
Figure 18b: Schematic Diagrams of the Periscope Irradiation Receiver showing the irradiation acceptance angle placed at three positions: Periscope placed between the impregnated mesh and the glass tube measuring “ P_{el} ”	41
Figure 19: Schematic Diagram and Description of air circulation in Photo-CREC-Air Reactor	42
Figure 20: Cross Flow sensor probe and support (TSI Inc.) used to measure the velocity inside the reaction section	43
Figure 21: GC temperature program used for the experiments	44
Figure 22: QY_{app} for acetone using experimental data reported by Ibrahim and de Lasa (2004) with the catalyst Hombikat UV-100. Three initial concentrations in $\mu\text{mol/L}$: 40, 50 and 60	66
Figure 23: QY_{app} for acetone using experimental data reported by Ibrahim and de Lasa (2004) with the catalyst Degussa P25. Three initial concentrations in $\mu\text{mol/L}$: 40, 50 and 60	67
Figure 24: QY_{app} for acetaldehyde using experimental data reported by Ibrahim and de Lasa (2004) with the catalyst Hombikat UV-100. Three initial concentrations in $\mu\text{mol/L}$: 30, 40 and 50	67
Figure 25: QY_{app} for acetaldehyde using experimental data reported by Ibrahim and de Lasa (2004) with the catalyst Degussa P25. Three initial concentrations in $\mu\text{mol/L}$: 30, 40 and 50	68

Figure 26: $PTEF_{app}$ for acetone using experimental data reported by Ibrahim and de Lasa (2004) with the catalyst Hombikat UV-100. Three initial concentrations in $\mu\text{mol/L}$: 40, 50 and 60	70
Figure 27: $PTEF_{app}$ for acetone using experimental data reported by Ibrahim and de Lasa (2004) with the catalyst Degussa P25. Three initial concentrations in $\mu\text{mol/L}$: 40, 50 and 60	70
Figure 28: $PTEF_{app}$ for acetaldehyde using experimental data reported by Ibrahim and de Lasa (2004) with the catalyst Hombikat UV-100. Three initial concentrations in $\mu\text{mol/L}$: 30, 40 and 50	71
Figure 29: $PTEF_{app}$ for acetaldehyde using experimental data reported by Ibrahim and de Lasa (2004) with the catalyst Degussa P25. Three initial concentrations in $\mu\text{mol/L}$: 30, 40 and 50	71
Figure 30: Changes of acetone concentrations with reaction time using the Degussa P25 as catalyst. Three initial concentrations in $\mu\text{mol/L}$ were considered: 49(\diamond), 37(Δ) and 24.5(o). (Continuous line represents model predictions using Equation 19)	82
Figure 31: Changes of CO_2 concentrations with reaction time during the photocatalytic degradation of acetone using the Degussa P25 as catalyst. Three initial concentrations of acetone in $\mu\text{mol/L}$ were considered: 49(\diamond), 37(Δ) and 24.5(o). (Continuous line represents model predictions)	83
Figure 32: Changes of acetaldehyde concentrations with reaction time using Degussa P25 as catalyst. Three initial concentrations in $\mu\text{mol/L}$ were considered: 320(\diamond), 240(Δ) and 160(o). (Continuous line represents model predictions using Equation 22)	85
Figure 33: Changes of CO_2 during the photocatalytic degradation of acetaldehyde using Degussa P25 as catalyst. Three initial concentrations of acetaldehyde in $\mu\text{mol/L}$ were considered: 320(\diamond), 240(Δ) and 160(o). (Continuous line represents model predictions)	86
Figure 34: Changes in the concentration of all species present during the photocatalytic degradation of isopropanol using Degussa P25 as catalyst. Three initial concentrations of isopropanol in $\mu\text{mol/L}$ were considered: 100(\diamond), 150(Δ) and 200(o). (Continuous and dashed lines represent model predictions using Equations 30, 31 and 32)	89

Figure 35: <i>QY</i> for acetone with Degussa P25 as photocatalyst. Three initial concentrations were considered in $\mu\text{mol/L}$: 49, 37 and 24.5	91
Figure 36: <i>PTEF</i> for acetone using Degussa P25 as photocatalyst. Three initial concentrations were considered in $\mu\text{mol/L}$: 49, 37 and 24.5	92
Figure 37: <i>QY</i> for acetaldehyde using Degussa P25 as photocatalyst. Three initial concentrations in $\mu\text{mol/L}$: 320, 240 and 160	93
Figure 38: <i>PTEF</i> for acetaldehyde using Degussa P25 as photocatalyst. Three initial concentrations in $\mu\text{mol/L}$: 320, 240 and 160	93
Figure 39: <i>QY</i> for isopropanol using Degussa P25 as photocatalyst. Three initial concentrations in $\mu\text{mol/L}$: 200, 150 and 100	95
Figure 40: <i>PTEF</i> for isopropanol using Degussa P25 as photocatalyst. Three initial concentrations in $\mu\text{mol/L}$: 200, 150 and 100	95
Figure C1: Spectral intensity of a new Pen-Ray lamp as measured by the Sola Scope 2000 Spectroradiometer (Ibrahim, 2001)	117
Figure D1: Spectral intensity inside the reaction section of the Photo-CREC-Air reactor reporting the fraction of the total energy involved in the average photon energy calculation	120
Figure E1: Spectral intensity for a new 15 W black-light-bulb near-UV lamp as measured with the spectrophotometer Stellarnet EPP2000	122
Figure E2: Typical lamp axial radiation flux as measured at the surface of the photocatalyst support	123
Figure E3: Spectral intensity profiles for three locations in the axial direction of the reaction section: Near the bottom, the middle and near the top	124

List of Appendices

Appendix A: Mechanism of Formation of OH^\bullet Radicals in Photocatalytic Processes for Air Treatment	112
Appendix B: Reaction Enthalpy for the Formation of OH^\bullet Radicals in Photocatalytic Reactors for Air Treatment.....	114
Appendix C: Calculation of the Average Photon Energy and the Fraction of Q_{irr} with a Wavelength Smaller than 388 nm (14.7 L Photo-CREC-Air Unit)	116
Appendix D: Calculation of the Average Photon Energy and the Fraction of Q_{ads} with a Wavelength Smaller than 388 nm (55.1 L Photo-CREC-Air Unit)	119
Appendix E: Lamp Characterization	122

Nomenclature

A	illuminated area of catalyst, m^2
A_{irr}	irradiated mesh area holding the catalyst, m^2
c	speed of light in vacuum, m s^{-1}
C	concentration, $\mu\text{mol m}^{-3}$
C_i	concentration of i species, $\mu\text{mol m}^{-3}$
C_j	concentration of j species, $\mu\text{mol m}^{-3}$
$C_{ACETALDEHYDE,T}$	total concentration of acetaldehyde, $\mu\text{mol/L}$
$C_{ACETONE,T}$	total concentration of acetone, μmol
$C_{ISOPROPANOL,T}$	total concentration of isopropanol, μmol
C_S^0	dimensionless Langmuir parameter
E_{av}	average energy of a photon, J
$E(\lambda)$	energy of a photon at a given wavelength, J
h	Planck's constant J s photon^{-1}
$I(\lambda)$	intensity of light, W cm^{-2}
$k_{ACETALDEHYDE}$	reaction rate constant for acetaldehyde, $\mu\text{mol m}^{-3} \text{min}^{-1}$
$k_{ACETONE}$	reaction rate constant for acetone, $\mu\text{mole m}^{-3} \text{min}^{-1}$
$k_{ISOPROPANOL}$	reaction rate constant for iopropanol, $\mu\text{mole m}^{-3} \text{min}^{-1}$
k_i	intrinsic kinetic constant for i species, $\mu\text{mol m}^{-3} \text{min}^{-1}$
k_I	reaction rate constant of the first reaction involved in the isopropanol photodegradation, $\mu\text{mol m}^{-3} \text{min}^{-1}$

k_2	reaction rate constant of the second reaction involved in the isopropanol photodegradation, $\mu\text{mol m}^{-3} \text{min}^{-1}$
k_{leak}	parameter accounting pollutant leak, $\text{m}^{-3} \text{min}^{-1}$
K	adsorption constant
K_i^A	adsorption constant for i species, $\text{m}^3 \mu\text{mol}^{-1}$
K_j^A	adsorption constant for j species, $\text{m}^3 \mu\text{mol}^{-1}$
$K^A_{ACETALDEHYDE}$	acetaldehyde adsorption constant, $\text{m}^3 \mu\text{mol}^{-1}$
$K^A_{ACETONE}$	acetone adsorption constant, $\text{m}^3 \mu\text{mol}^{-1}$
$K^A_{ISOPROPANOL}$	isopropanol adsorption constant, $\text{m}^3 \mu\text{mol}^{-1}$
$K'_{ACETALDEHYDE}$	dimensionless acetaldehyde adsorption constant
$K'_{ACETONE}$	dimensionless acetone adsorption constant
$K'_{ISOPROPANOL}$	dimensionless isopropanol adsorption constant
$C_{ACETALDEHYDE,g}$	concentration of acetaldehyde in the gas phase, $\mu\text{mol m}^{-3}$
$C_{ACETONE,g}$	concentration of acetone in the gas phase, $\mu\text{mol m}^{-3}$
$C_{ISOPROPANOL,g}$	concentration of isopropanol in the gas phase, $\mu\text{mol m}^{-3}$
$N_{ACETALDEHYDE,T}$	total number of moles of acetaldehyde
$N_{ACETONE,T}$	total number of moles of acetone
$N_{ISOPROPANOL,T}$	total number of moles of isopropanol
$N_{ACETALDEHYDE,g}$	number of moles of acetaldehyde in the gas phase
$N_{ACETONE,g}$	number of moles of acetone in the gas phase

$N_{ISOPROPANOL,g}$	number of moles of isopropanol in the gas phase
$N_{ACETALDEHYDE,s}$	number of moles of acetaldehyde adsorbed on the solid
$N_{ACETONE,s}$	number of moles of acetone adsorbed on the solid
$N_{ISOPROPANOL,s}$	number of moles of isopropanol adsorbed on the solid
P_e	rate of photons emitted by the lamps
P_{el}	rate of photons reaching the photocatalyst surface
P_t	rate of photons not absorbed by the photocatalyst
$q_{ACETALDEHYDE}$	amount of acetaldehyde adsorbed, $\mu\text{mol g}^{-1}$
$q_{ACETONE}$	amount of acetone adsorbed, $\mu\text{mol g}^{-1}$
$q_{ISOPROPANOL}$	amount of isopropanol adsorbed, $\mu\text{mol g}^{-1}$
$q_{ACETALDEHYDE,max}$	maximum amount of acetaldehyde adsorbed on solid, $\mu\text{mol g}^{-1}$
$q_{ACETONE,max}$	maximum amount of acetone adsorbed on the solid, $\mu\text{mol g}^{-1}$
$q_{ISOPROPANOL,max}$	maximum amount of isopropanol adsorbed on the solid, $\mu\text{mol g}^{-1}$
Q_{used}	rate of irradiated energy used to form OH^\bullet radicals, W
Q_a	rate of irradiated energy absorbed in photocatalytic reactor, W
Q_r	rate of irradiated energy reaching the catalyst, W
QY	quantum yield based on OH^\bullet radical consumption and rate of photons absorbed by photocatalyst
QY_{app}	apparent quantum yield based on OH^\bullet radical consumption and rate of photons reaching photocatalyst surface

r	reaction rate
$r_{ACETALDEHYDE}$	reaction rate of acetaldehyde, $\mu\text{mol m}^{-2} \text{min}^{-1}$
$r_{ACETONE}$	reaction rate of acetone, $\mu\text{mol m}^{-2} \text{min}^{-1}$
$r_{ISOPROPANOL}$	reaction rate of isopropanol, $\mu\text{mol m}^{-2} \text{min}^{-1}$
$r_{ACETALDEHYDE,g}$	rate of acetaldehyde photocatalytic degradation as observed by concentration changes in the gas phase, $\mu\text{mol m}^{-2} \text{min}^{-1}$
$r_{ACETONE,g}$	rate of acetone photocatalytic degradation as observed by concentration changes in the gas phase, $\mu\text{mol m}^{-2} \text{min}^{-1}$
$r_{ISOPROPANOL,g}$	rate of isopropanol photocatalytic degradation as observed by concentration changes in the gas phase, $\mu\text{mol m}^{-2} \text{min}^{-1}$
$r_{OH^\bullet,T}$	total reaction rate of formation of OH^\bullet radical groups per unit weight of irradiated catalyst, $\mu\text{mol gcat}_{\text{irr}}^{-1} \text{s}^{-1}$
$r_{OH^\bullet,j}$	reaction rate of OH^\bullet radicals in reaction step j , $\mu\text{mol gcat}_{\text{irr}}^{-1} \text{s}^{-1}$
$r_{i,j}$	reaction rate of component i in reaction step j , $\mu\text{mol gcat}_{\text{irr}}^{-1} \text{s}^{-1}$
V	total system volume, m^3
W	weight of adsorbent material, g
W_{irr}	total amount of irradiated catalyst, g

Acronyms

<i>CREC</i>	Chemical Reactor Engineering Centre
<i>PTEF</i>	Photochemical Thermodynamic Efficiency Factor
<i>QY</i>	Quantum Yield

Subscripts

<i>ads</i>	adsorbed
<i>app</i>	apparent
<i>av</i>	average
<i>irr</i>	irradiated
<i>max</i>	maximum
<i>min</i>	minimum

Greek letters

γ	fraction of the adsorbed energy contributed by photons with $\lambda < 388$ nm
ν	stoichiometric coefficient for the consumption of OH^\bullet group
ν_i	stoichiometric coefficient for the consumption of model pollutant
$\nu_{ACETALDEHYDE}$	stoichiometric coefficient of acetaldehyde
$\nu_{ACETONE}$	stoichiometric coefficient of acetone
$\nu_{ISOPROPANOL}$	stoichiometric coefficient of isopropanol
$\nu_{OH^\bullet, j}$	stoichiometric coefficient of OH^\bullet radical in reaction step j
$\nu_{H_2O, j}$	stoichiometric coefficient of H_2O in reaction step j
$\nu_{h, j}$	stoichiometric coefficient of component h in reaction step j
$\nu_{i, j}$	stoichiometric coefficient of component i in reaction step j
θ_{A_1}	$1/(k_{ACETONE}K^A_{ACETONE})$, min

θ_{A2}	$1/k_{ACETONE}, m^3 \cdot min \cdot \mu mol^{-1}$
θ_{AA1}	$1/(k_{ACETALDEHYDE}K^A_{ACETALDEHYDE}), min$
θ_{AA2}	$1/k_{ACETALDEHYDE}, m^3 \cdot min \cdot \mu mol^{-1}$
θ_1	$1/(kK^A_{ISOPROPANOL}), min$
θ_2	$1/k_1, m^3 \cdot min \cdot \mu mol^{-1}$
θ_3	$K^A/(k_1K^A_{ISOPROPANOL}), m^3 \cdot min \cdot \mu mol^{-1}$
θ_4	$1/(k_2K^A_{ACETONE}), min$
θ_5	$K^A_{ISOPROPANOL}/(k_2K^A_{ACETONE}), m^3 \cdot min \cdot \mu mol^{-1}$
θ_6	$1/k_2, m^3 \cdot min \cdot \mu mol^{-1}$
η_{OH^\bullet}	fraction of photon energy to form OH^\bullet radicals
λ	radiation wavelength, nm
λ_{max}	upper bound of wavelength in the range of interest, nm
λ_{min}	lower bound of wavelength in the range of interest, nm
$\zeta_{ACETALDEHYDE}$	dimensionless solid phase acetaldehyde concentration
$\zeta_{ACETONE}$	dimensionless solid phase acetone concentration
$\zeta_{ISOPROPANOL}$	dimensionless solid phase isopropanol concentration
ΔH_{OH^\bullet}	enthalpy of formation of an OH^\bullet group adsorbed on the photocatalyst, $J \cdot mol^{-1}$
$\Delta H^\circ_{f,OH^\bullet(g)}$	standard enthalpy of formation of OH^\bullet radical, $J \cdot mol^{-1}$
$\Delta H^\circ_{f,H_2O(g)}$	standard enthalpy of formation of water vapor, $J \cdot mol^{-1}$
$\Delta H^\circ_{f,O_2(g)}$	standard enthalpy of formation of O_2 , $J \cdot mol^{-1}$

Chapter 1

Introduction

Air pollution is an increasing environmental concern. Particularly, indoor air pollution is an issue that in recent years has attracted significant attention due to the health hazards that it poses to people. We spend between 70 to 90 % of our lifetime indoors. (Finlayson-Pitts and Pitts, 2000; Aguado et al., 2004) Furthermore, indoor air is often more contaminated than outdoor air (Spengler and Chen, 2000).

The decontamination of indoor air has been addressed through different strategies: increased ventilation, pollution control at the emission source and air cleaning (Ao et al., 2005). However, some of these strategies show critical drawbacks. The implementation of increased ventilation may transport more pollutants from the outdoors. Pollution control at the emission source is many times impractical in large urban environments, where numerous sources of air pollutants are present. Therefore, air cleaning is thought to be the most practical alternative to remedy indoor air pollution. In this respect, advanced oxidation technologies and more specifically heterogeneous catalysis represents one of the best options for efficient removal of a wide range of pollutants.

Heterogeneous photocatalysis has received considerable attention given its potential applications to remove organic air contaminants contained in aircrafts and spacecrafts, office buildings and factories. Despite the fact that studies involving gas-phase heterogeneous photocatalysis are relatively few compared with the substantial literature on photocatalytic water treatment (Kaneko and Okura, 2002; de Lasa et al., 2005; Paz, 2009), the number of contribution in this area is considerably growing nowadays.

A photocatalytic reaction can be defined as a chemical reaction influenced or initiated by light. Irradiation promotes charge separation on the photocatalyst and provides radical species, as a result. The main participants in the photocatalytic process are a light source, a catalyst, and various chemical species. Heterogeneous photocatalysis requires an interface between a solid photocatalyst and a liquid or a gas phase containing the chemical species (organic pollutants). The photocatalytic reaction proceeds via a series of events with the electron-hole pair formation being the

initiation step. This step is followed by the electron-hole h^+ utilization for oxidation and eventually the e^- electron use for species reduction. All this leads to the potential formation of hydroxyl radicals, super oxides anions and hydrogen peroxide, all three produced from atmospheric oxygen (Cerdá et al., 1977). There is however, the possibility of electron-hole recombination. This is actually, one of the main factors potentially limiting energy efficiency in photocatalytic processes.

Regarding the application of photocatalysis in air treatment, most research has been done to envisage the production of active catalysts, catalyst improvement and optimal operating conditions. However, it is of special importance to study the design of photocatalytic reactors from the point of view of optimal use of irradiation. The light utilization efficiency and the manner in which this irradiation utilization is influenced by the reactor operation conditions must be described. A key tool for this analysis is the quantum efficiency. This parameter is a reactor-dependent parameter. The quantum yield can also help in reaction pathway discrimination. Different definitions of quantum efficiency have been proposed leading to different approaches in assessing the photocatalytic reactor energy performance (Serpone and Emeline, 2002; Ibrahim and de Lasa, 2003). Ibrahim (2001) and de Lasa et al. (2005) have provided detailed summaries of the possible quantum yield definitions.

Many of the definitions for quantum yields reported in the technical literature are based on the rate of radiation intensity reaching the catalyst (incident photon flux) and are of uncertain value (Ibrahim, 2001; Hoffmann et al., 1995; Tahiri et al., 1996; Kish, 2010). The quantum yield should be based on ratios involving photoconverted molecules over the rate of radiation intensity absorbed at a given wavelength (photon flux). While determining the rate of radiation intensity absorbed at a given wavelength is a relatively easy task in homogeneous systems, it is a rather difficult assignment for heterogeneous reactions. In this case, radiation is not only absorbed but also scattered and reflected by the suspended semiconductor particles.

The Photocatalytic Thermodynamic Efficiency Factor (*PTEF*) is a parameter based on thermodynamic considerations. This parameter was first proposed by Serrano and de Lasa (1997) for water purification to overcome the uncertainty of lack of bounds for quantum efficiency. This thesis shows the first application of the *PTEF* in air treatment.

The Photo-CREC-Air Reactor used in this PhD dissertation has been designed with TiO_2 supported by a mesh. This configuration represents a step forward in photocatalysis studies by the CREC-UWO team (Chemical Reactor Engineering Center at Western University). This special design offers optimal mesh irradiation and most favorable fluid-mesh contact. Furthermore, this unit highlights certain features for measurement of the irradiation at different points inside the reaction section. This allows accounting for the various irradiation components such as scattered, absorbed and reflected irradiation involved in a photocatalytic process.

The main section of the Photo-CREC-Air Unit is the reaction section. This includes a stainless steel mesh cylinder supporting a commercial TiO_2 based photocatalyst. This mesh cylinder is enclosed by a UV transparent quartz cylinder surrounded by 8 UV radiation lamps. The fluid is directed through the metallic mesh supporting the catalyst. There is a bullet nose at the bottom of the reaction section. This promotes a cross flow with a uniform distribution over the substrate that increases the contact between the fluid and the photocatalyst. The unit operates in a batch mode with a set amount of model pollutant injected into a set amount of volume air. Once the model pollutant is injected, concentration changes of model pollutant over time are carefully monitored.

This PhD dissertation reports the photocatalytic degradation of acetone, acetaldehyde and isopropanol in the most recent version of a 55.1 liter scaled up Photo-CREC-Air Reactor. This new Photo-CREC-Air Unit provides: i) high photocatalyst mesh loading, ii) enhanced photocatalyst irradiation, iii) special devices for performing macroscopic irradiation balances. These results are compared to those obtained in a former 14.7 liter Photo-CREC-Air Reactor. This comparison is made on the basis of apparent quantum efficiencies which are defined as ratios of OH^\bullet consumption rates over the number of photons reaching the surface of the photocatalyst. It is the aim of this study to take advantage of the new Photo-CREC-Air Unit for both kinetic modeling as well as for quantum yield and *PTEF* calculations.

Chapter 2

Literature Review

2.1 Introduction

Photocatalysis is the segment of catalysis, which covers the range of the reactions proceeding under the action of light. Among them, we can distinguish phenomena such as catalysis of photochemical reactions, photo-activation of catalysts, and photochemical activation of catalytic processes. This term is defined by the IUPAC as follows “Photocatalysis is the catalytic reaction involving light absorption by a catalyst or substrate.” A more detailed definition may be the following “Photocatalysis is a change in the rate of chemical reactions or their generating under the action of light in the presence of the substances (photocatalysts) that absorb light quanta and are involved in the chemical transformations of the reaction participants, repeatedly coming with them into intermediate interactions and regenerating their chemical composition after each cycle of such interactions” (Parmon, 1997).

2.2 Heterogeneous Photocatalysis

During the last decades much attention has been paid to the reactions that take place on the irradiated surface of semiconductor metal oxides and sulfides. These compounds are semiconductors, i.e. they have a moderate energy band-gap (1-3 eV) between their valence and conduction bands. Under irradiation by photons of greater than band-gap energies, the valence band electrons can be excited to the conduction band, creating highly reactive electron-hole pairs. After migration to the solid surface, these may undergo electron-transfer processes with adsorbates of suitable redox potentials (Figure 1). In this way, these semiconductor compounds act as photosensitizers, promoting synthetic photoassisted reactions (if the reaction exhibits a positive free energy gain), or catalytic photoassisted reactions (negative gain).

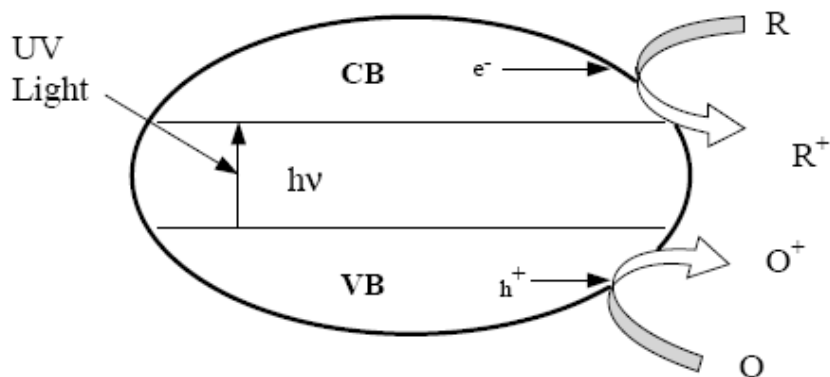


Figure 1: Schematic of the Processes that take place when a semiconductor particle receives band-gap illuminated

Studies involving gas-phase heterogeneous photocatalysis are relatively few in number compared with the substantial literature on photocatalytic water treatment (Ollis et al., 1991; Serpone and Pelizzetti, 1989). There is however nowadays a growing interest in photocatalysis for air treatment given the potential application for contaminant control and removal from air atmospheres as found in aircraft and spacecraft, office buildings and factories. At moderate conditions (room temperature, one atmosphere pressure and with molecular oxygen as the only oxidant), the mentioned semiconductors have proven to be effective photocatalysts for the thermodynamically favoured transformations of many organics to CO_2 and H_2O

2.3 Photocatalysts

Solids that can promote reactions in the presence of light and are not consumed in the overall reaction are referred to as “photocatalysts”. These are invariably semiconductors. A good photocatalyst should be (i) photoreactive, (ii) able to utilize visible and/ or near UV radiation, (iii) biologically and chemically inert, (iv) photostable (i.e. not prone to photocorrosion), (v) inexpensive and (vi) non-toxic. In order for a semiconductor to be photochemically active as a sensitizer for the above reaction the redox potential of the photogenerated valence band hole must be sufficiently positive to generate OH^\bullet radicals, which can subsequently oxidize the organic pollutant. The redox potential of the photogenerated conductance band electron must be sufficiently negative to be able to reduce adsorbed O_2 to superoxides (Mills et al., 1993).

The photoexcitation of semiconductor particles generates electron-hole pairs due to the adsorption of 390 nm or UV radiation of low wavelength (for TiO₂). If the exciting energy employed comes from solar radiation, the process is called solar photocatalysis. Si, TiO₂, ZnO, WO₃, CdS, ZnS, SrTiO₃, SnO₂, WSe₂, Fe₂O₃, etc. can be used as photocatalysts. Table 1 (Thiruvengkatachari et al., 2008) gives band energies and band gap positions of these catalysts.

Table 1: Bandgap energy of various photocatalysts (Thiruvengkatachari et al., 2008)

Photocatalyst	Bandgap energy (eV)	Photocatalyst	Bandgap energy (eV)
Si	1.17	ZnO	3.436
TiO ₂ (rutile)	3.1	TiO ₂ (anatase)	3.2
WO ₃	2.7	CdS	2.4
ZnS	3.7	SrTiO ₃	3.4
SnO ₂	3.5	WSe ₂	1.2
Fe ₂ O ₃	2.2	α -Fe ₂ O ₃	3.1
PbS	0.286	PbSe	0.165
Cu ₂ O	2.172	ZrO ₂	3.87

2.3.1 TiO₂ photocatalysts

Among many semiconductor photocatalysts, there is a general consensus among researchers that TiO₂ is more superior because of its high activity, large stability to light illumination, low price, and nontoxicity (Trillas et al., 1992). It has been shown that under similar study conditions, TiO₂ had greater photocatalytic efficiency than α -Fe₂O₃, ZrO₂, CdS, WO₃ and SnO₂. Although ZnO had a higher activity (although the surface area is less) than TiO₂, the later was photochemically more stable in aqueous media. Wu (2004) also observed higher photocatalytic activity for TiO₂ compared to ZnO and SnO₂. The two principal polymorphs of TiO₂ are anatase and rutile which are associated with bandgap energies of 3.2 and 3.1 eV, respectively.

It has been pointed out that the photocatalytic degradation reaction rate is much more rapid over anatase than in the rutile (Alfano et al., 1997), and it is mainly affected by the crystalline state and textural properties, particularly, surface area and particle size of the TiO₂ powder. The phase structure of TiO₂ greatly affects the photoreactivity.

The photocatalytic performance of TiO_2 depends not only on its bulk energy band structure, but also, to a large extent, on surface properties. The larger the surface area, the higher the photocatalytic activity.

2.4 Photocatalytic Reactors and Light Sources

The volatile organic compounds (VOC) removal by photocatalytic processes is a surface reaction process consisting of two important steps: i) the VOCs have to transfer to the reaction surface first; ii) following this, the VOCs are decomposed by the photocatalyst. Thus, the most important performance parameters of a photocatalytic oxidation (PCO) reactor are the VOC convective mass transfer rate, the reaction rate and the reaction surface area (Henderson, 2011).

Ideally, the structure of a PCO reactor should have; a) a high specific surface area per unit volume, b) a support with small-through channels allowing high air velocity and high mass transfer and c) a the Ultra Violet (UV) radiation source irradiating directly on the reaction surface. Unless using sunlight, due to electricity charges and bulb replacement, the light source will tend to be the most costly component of any photocatalytic reactor. Thus; it is essential to utilize the produced photons very effectively, ensuring that emitted photons contact the photocatalyst and initiate oxidation. In addition, a reactor surfaces have to receive irradiation from the light source, so that no flow paths through the reactor exist where the catalyst remains without irradiation.

Moreover, various photocatalytic reactors have been categorized according to the location of the UV lamps with respect to the photoreaction area. These different configurations lead to different irradiated areas, pollutant mass transfer and photocatalytic reaction efficiency (Zhao and Yang, 2003; Mo et al., 2009).

2.4.1 Honeycomb Monolith Reactors

Honeycomb monolith reactors provide nearly negligible pressure drop and are widely used in automobile exhaust emission control and for NO_x reduction in power-plant flue gases.

A honeycomb monolith reactor contains certain number of channels; each single channel typically has an internal dimension of the order of 1 mm; the cross-sectional shapes of channels are square or circular and the catalyst is coated onto the walls of channels in a very thin wash coat (Hayes et al., 1992). The advantages of monolith configuration are its low pressure drop and its high surface-area-to-volume ratio. Studies on the mathematical modeling of air flow, photon flux field and mass transfer in photocatalytic monolith reactors had been carried out to attain energy-efficient photocatalytic reactor designs (Hossain et al., 1999; Hossain and Raupp, 1999; Raupp et al., 2001; Votruba et al., 1975).

Suzuki et al. (1991) reported the use of the photocatalytic monolith for the oxidative destruction of odours. Sauer and Ollis (1994) worked on the photocatalytic oxidation of acetone in the air by using near-UV illuminated TiO_2 coated on the surface of a ceramic honeycomb monolith. An example of the monolith reactor is the one used by Raupp et al. (2001), showed in Figure 2.

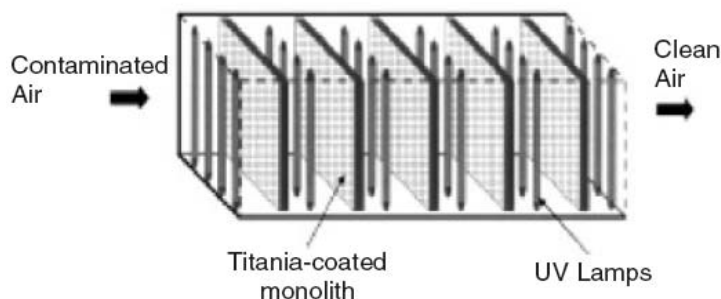


Figure 2: Schematic diagram of the monolith reactor used by Raupp et al., 2001

2.4.2 Fluidized Bed Reactors

The design of fluidized bed reactors (FBPR) makes them able of treating fairly high gas feed rates, in which the gas flows directly through the catalyst bed. Among the advantages offered by FBPRs are the efficient contact between the catalyst and the pollutants, the low mass transfer resistances, the low pressure drop, and the high TiO_2 surface exposure to UV-radiation. It is believed that fluidized bed photocatalytic reactors are more advantageous than fixed bed photocatalytic reactors because of the good contact of catalyst-light and catalyst-reactants (Lim et al., 2000).

The fluidized bed photocatalytic reactor was explored for studies of ammonia oxidation by Cant and Cole (1992). Another example fluidized-bed reactor used by Dibble and Raupp (1992) is reported in Figure 3: TiO_2 was supported on silica gel; the cross-sectional area at the top of reactor was larger than that of lower portion, this feature and a glass frit in the overhead effluent tube helped to reduce the momentum of catalyst particle and prevent the catalyst particles from flowing with the gas. More recently, some new features have been added to the design of fluidized-bed reactors.

Lim et al. (2000) combined the features of an annular and a fluidized-bed reactor to design a modified fluidized-bed reactor, where the catalyst formed an annular bed with UV radiation in the center; a quartz filter was used as a distributor to provide a uniform fluidization of the catalyst, at the same time a square mirror box surrounded the reactor to minimize the loss of light irradiation and improve the utilization of reflected and deflected light.

Nam et al. (2002) used fluidized-bed reactors with light source at the center of catalyst bed which was applied to the entire volume of the reactor and some nozzles as air distributors were installed at the bottom of the reactor to get the uniform air distribution in the catalyst bed.

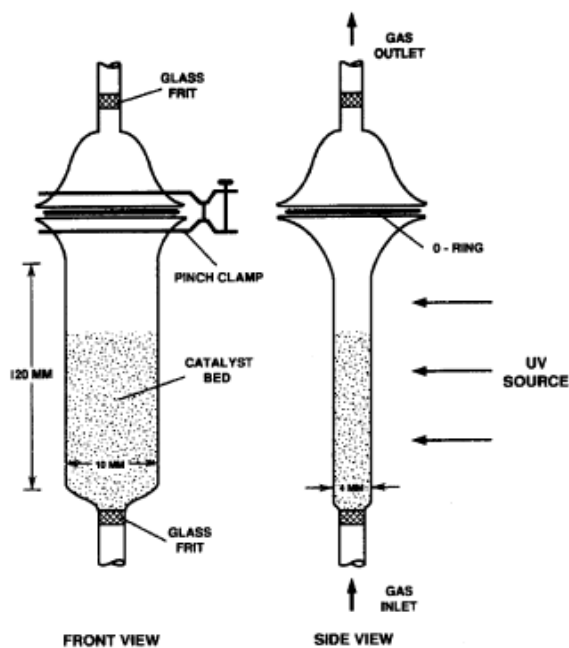


Figure 3: Schematic diagram of the fluidized-bed reactor used by Dibble and Raupp, 1992

2.4.3 Annular Reactors

The annular reactors are generally composed of two concentric cylinders that form an annular region with a certain gap. The catalyst is coated on the interior wall of the outer cylinder. The light source is located at the center and the thickness of the catalyst film coated on the surface of reactor is thin enough to let all the catalyst be irradiated by the UV-source.

However when light source is located outside the reactor the catalyst is coated on the surface of two concentric cylinders. In general, the cross section of annular reactor is small so that high gas flow velocity can be obtained ensuring that products desorbing from surface can be removed quickly (Larson et al., 1995).

Figure 4 shows one type of the annular reactor. Annular reactors with different structures have been used by several research groups: Larson et al. (1995) used a thin-film TiO_2 annular reactor to study PCO of 2-propanol at ambient temperature. Lichtin et al. (1996) used the concentric annular tubes flow reactor with a thin film of P25 TiO_2 catalyst on the inner surface to measure the degradation rate of the components of 14 binary mixtures. Lim et al. (2000) studied the photocatalytic decomposition of NO by TiO_2 particles in a reactor formed by two quartz glass tubes. Mohseni and Taghipour (2004) presented an analysis, based on computational fluid dynamics, of the flow characteristics and its impact on the overall destruction of gas phase contaminants in a photocatalytic annular reactor. The influence of fins on formaldehyde removal in annular photocatalytic reactors was studied theoretically, numerically and experimentally by Mo et al. (2008).

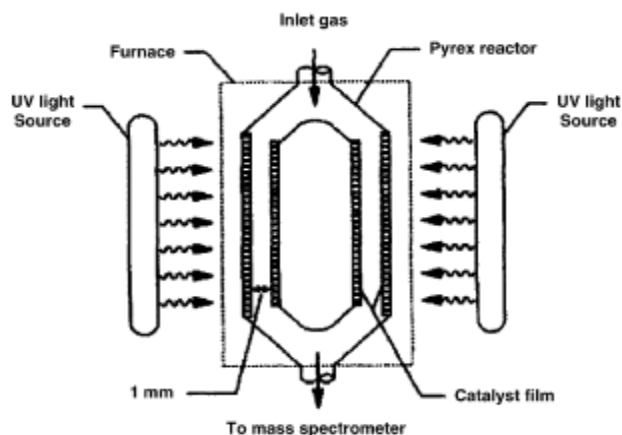


Figure 4: Schematic diagram of the annular reactor used by Larson et al., 1995

2.4.4 Packed bed Reactors

In this type of reactors the fluid stream to be treated flows through the packed bed, comes into contact with the irradiated particles holding the TiO_2 . Some of the drawbacks that this configuration may suffer are a low surface area to reactor volume ratio and low use of irradiation and this considering both light absorption and scattering (Al-Ekabi et al., 1989; Raupp et al., 1997).

Different types of fixed bed reactors have been proposed: flat or curved walls, corrugated walls, monoliths, packed beds and reticulated configurations. Important contributions aimed at modeling this type of reactors have been made by Raupp and coworkers. These authors reported a two-flux radiation model for an annular packed bed photocatalytic reactor (Raupp et al., 1997) which is an extension of the two-flux model for parallel-plate reactors proposed by Maruyama and Nishimoto (1992).

Hossain and Raupp (1998, 1999) described the radiation field in a monolith photocatalytic reactor using a theory based on radiation exchange between surfaces in channels. Changrani and Raupp (1999) proposed a reticulated foam photocatalytic reactor and solved the model with Monte Carlo simulation; these authors also used a deterministic two-dimensional (2-D) heterogeneous model to simulate this reactor (Changrani and Raupp, 2000).

At the same time, a model for absorption by TiO_2 films in a corrugated-plate photocatalytic reactor was described by Zhang et al. (2000). Later on, the radiation field in a fixed bed reactor having the titanium dioxide catalyst immobilized on an inert support (Figure 5) and made by a set of parallel, flat glass fiber meshes was discussed by Esterkin et al. (2002). In this reactor, UV radiation enters the reactor through transparent, acrylic windows; irradiation can be produced from one or both sides of the reactor.

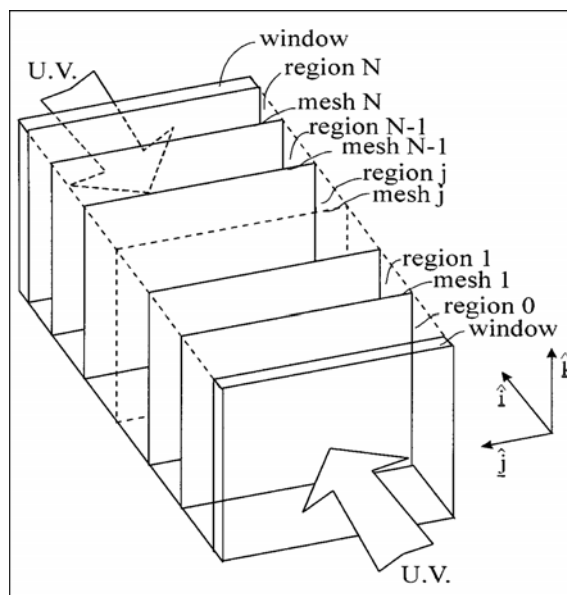


Figure 5: Photocatalytic reactors used by Esterkin et al., 2002

2.4.5 Fibre Optic Based Reactors

In a fiber optic photocatalytic reactor, instead of using a single UV radiation lamp, a bundle of optical fibers are utilized as the media for delivering UV within the photocatalytic reactor.

Marinangeli and Ollis (1977, 1980, and 1982) were the first in proposing and theoretically evaluating the use of optical fibers as both a light distributing guide and an immobilizing support for photocatalysts. These authors concluded that optical fiber photocatalytic reactor might not be practicable owing to the heat build-up on the optical fiber and its extremely thin diameter. However, these problems have been overcome by the developments of IR filter, cooling system and large-sized optical fiber.

The employment of optical fibers for the photocatalytic decomposition of organic pollutants was studied by several research groups. Optical fiber photocatalytic reactors can be suitably applied to deliver higher quantum yields owing to its relatively uniform distribution of light radiation within the photocatalytic reactors. Hofstadler et al., (1994) obtained quantum yields for the decomposition of 4-chlorophenol in a TiO_2 -coated optical fiber photocatalytic reactor similar to those obtained in a suspended TiO_2 slurry reactor (Peill and Hoffmann, 1995), and was much higher than that obtained in an annular fixed-bed photocatalytic reactor.

In addition, Peill and Hoffmann (1995), and Kribus et al. (2000) mentioned the application of optical fiber for remote UV radiation delivery without significant light depreciation, which makes it possible to treat pollutants present in places difficult to access. The operation of UV radiation source is usually considered to be the most expensive component for a photocatalytic oxidation system.

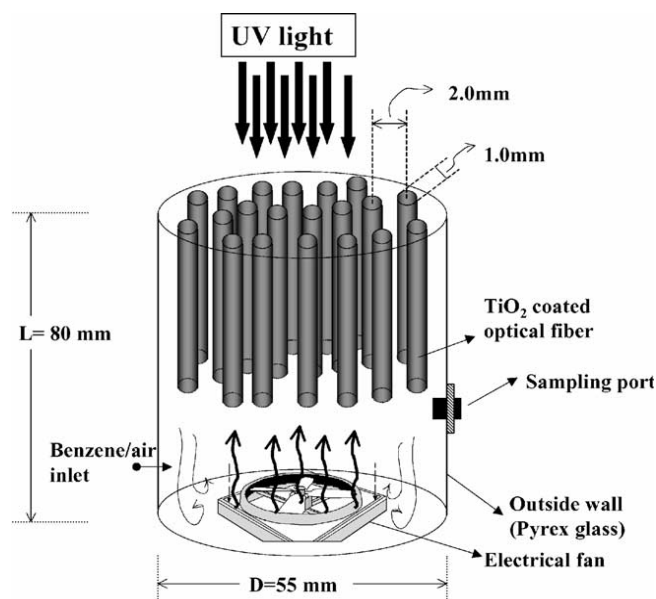


Figure 6: Schematic diagram of the optical fiber photocatalytic reactor used by Wang et al., 2003

2.4.6 Light sources

The radiation source, ultraviolet radiation and specifically near-ultraviolet radiation, is a very important component of the photocatalytic process. The light source plays a critical role (as the energy provider) on the photocatalytic degradation of the pollutants: the photocatalyst activity depends strongly on the light-irradiation (energy per unit area) or the photon flux on the surface of the catalyst.

Ultraviolet radiation refers to electromagnetic radiation in the 10-400 nm wavelength range. Radiation in the 10 to 200 nm is considered as Vacuum UV since it is absorbed by air, UVA covers from 315 to 400 nm, UVB from 280 to 315 nm and UVC from 200 to 280 nm.

The band gap of TiO₂ anatase is 3.2 eV and the irradiation portion that can participate in the photocatalytic reaction is the one below 388 nm; commonly near-UV radiation

with the wavelength of near 300-370 nm. This type of lamp is used to provide the energy to induce the process of the photo-sensation. While on the other hand the bio-hazardous UV-254 nm is avoided to be employed.

Artificial UV lamps can power photocatalytic processes and are made of different metals including mercury, sodium, zinc/cadmium and rare gases (neon, argon). The mercury emission lines are usually in the desired range of energy for driving the photochemical reactions. Artificial UV lamps (Table 2) can be grouped in three categories (Bolton et al., 1995): low pressure mercury lamp, medium pressure mercury lamp and high pressure mercury lamp categories.

The heterogeneous photocatalysis can also be driven by solar light since the TiO_2 activation spectrum overlaps with the solar spectrum (Nimlos et al., 1993).

Approximately 4%-5% of the sunlight reaching the surface of the Earth is in the 300-400 nm near-ultraviolet range and this portion of the solar spectrum can be used to drive photocatalytic reactions (Bolton et al., 1995; Matthews, 1993; Wilkins and Blake, 1994).

Some disadvantages of solar energy, however, are its intermittency and variability with both factors being geographically dependant (Wilkins and Blake, 1994). Bolton et al., (1995) have mentioned that solar energy cannot be used effectively for homogeneous photochemical processes since typical reagents such as H_2O_2 and O_3 do not significantly absorb radiation above 300 nm and none of the radiation received at the surface of the earth is below 300 nm.

Therefore, the application of solar light is clearly favored in photocatalytic heterogeneous processes versus its application in homogenous photocatalytic reactors.

Table 2: Properties and features of the artificial UV radiation sources reported by Bolton et al., (1995)

	Low Pressure Mercury Lamp	Medium Pressure Mercury lamp	Advanced Medium Pressure Mercury Lamp
Life Time (h)	>5000	>2000	>3000
Output Range	80% in a narrow range around 254nm	Broad but not much below 250 nm	Strong below 250 nm
Energy Density	Low (~1 W/cm)	Moderate (~125 W/cm)	High (~250 W/cm)
Electrical to Photon Energy	High (~30%)	Moderate (~15% for 200-300 nm)	High (~30% for 200- 300 nm)

The types of light sources used in the research include Xe arc lamp (Nimlos et al., 1996) with 300-800 nm radiation, Hg-arc lamp (Sauer and Ollis, 1994; Hennezel et al., 1998; Chen and Ray, 1999) and Black-light lamp (Nimlos et al., 1996; Dibble and Raupp, 1992; Cao, 1999; Lim et al., 2000; Peral et al., 1997).

The impact of UV-radiation wavelength on the photocatalytic oxidation stoichiometry has been studied under different experimental conditions (Jacoby, 1993). Benoit-Marquie et al., (2000) found that Xe-excimer lamp (emitting at 308 nm), whose incident photonic emission was higher than a medium pressure Hg-arc light (22.1-32.6 mw/cm²), increased the conversion rate significantly. Yamazaki (1999) examined the effect of light intensity under the reactant gas stream of 250 ppmv ethylene, 2.1×10^5 ppmv O₂, and 2.2×10^3 ppmv H₂O at the inlet molar flow rate of 6.6×10^6 g.s/mol; the results showed that the reaction rate was first-order with light intensity. The research of Obee (1996) indicated that the internal shading in the porous structure affected the adsorption rate of the photons so as to influence the conversion rate.

2.5 Photo-CREC-Air Reactors

A first version of the Photo-CREC-air unit was designed for air cleaning applications. This first version of the Photo-CREC-air unit considered important facts such as

minimum pressure drop, firm attachment of the catalyst to the support, good transmission and distribution of the UV radiation and good contact between the mesh and the fluid (Ibrahim and de Lasa, 2002). Some of the particular issues of this Photo-CREC-air reactor unit were the limited power provided by the external, near UV lamps placed in parabolic reflectors. A glass mesh region basket supported the TiO_2 . This basket was irradiated with near UV and contacted with an air stream.

2.5.1 Characteristics of the Photo-CREC-Air Reactor

The main body of this first version of the Photo-CREC-Air reactor consisted of a closed-loop system with 14.7 litres of capacity and was made of zinc-plated pipes connected with aluminized-steel 90 elbows and a stainless steel Venturi section. There were eight Pen-Ray 1-watt lamps symmetrically placed around the reaction section; the radiation penetrated through windows cut out of acrylic sheets in a divergent section of the Venturi. The Photo-CREC-air batch reactor unit with auxiliary components is described in Figure 7 (Ibrahim, 2001).

This reactor was operated in a batch mode with a given amount of model pollutant injected in a set volume of air. The fluid flow pattern in the unit and the assessment of the UV radiation reaching the impregnated mesh was also characterized. Assuming a plane of symmetry in both the x and y directions made possible the use of smaller cell sizes and improved the convergence.

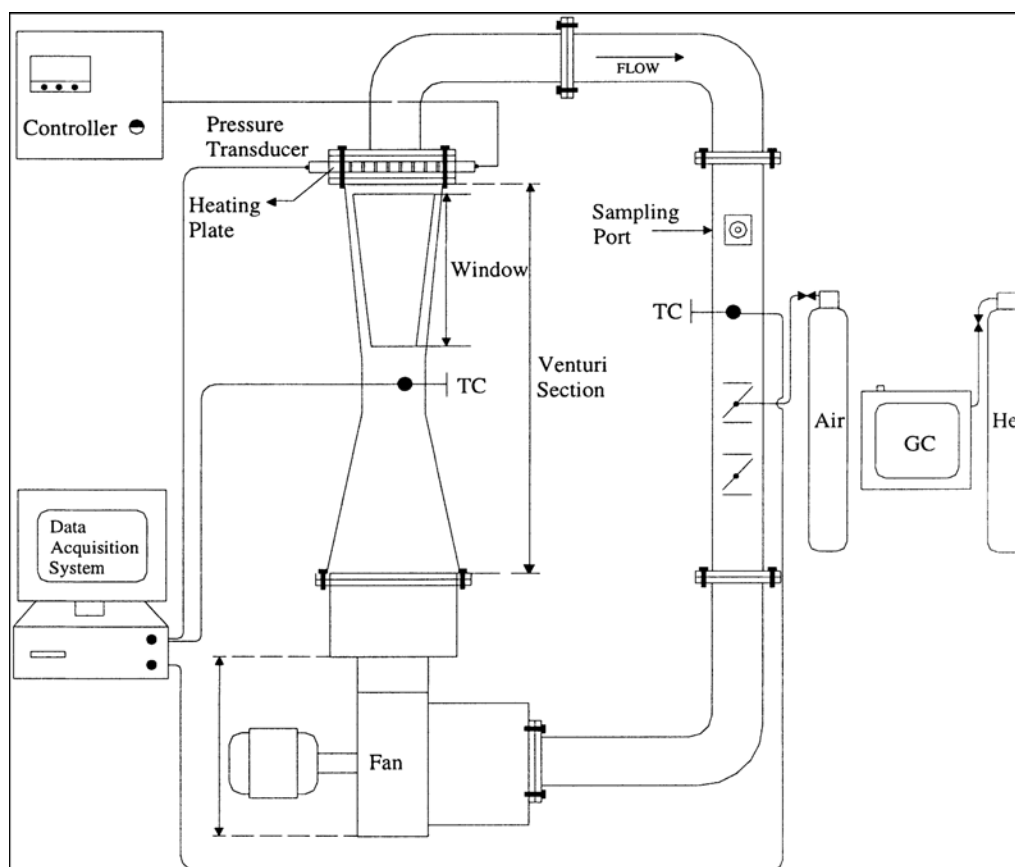


Figure 7: Schematic diagram of the Former Photo-CREC-Air reactor (Ibrahim and de Lasa, 2004)

Air exiting the blower entered the Venturi divergent section, flowed through the Venturi throat and contacted the TiO_2 -impregnated mesh (Figure 8(b)). Eight Pen-Ray Mercury UV-lamps, with a power output of $1213 \mu \text{W cm}^{-2}$ at 20mA (AC) and a principal radiation wavelength of 365 nm, mounted outside of the Venturi divergent section (Figure 8(a)) and housed inside parabolic reflectors irradiated the TiO_2 -impregnated mesh. The parabolic reflectors were designed so that the irradiation focal point was placed at a semi-infinite distance from the source, thereby improving the incidence efficiency Ibrahim (2001).

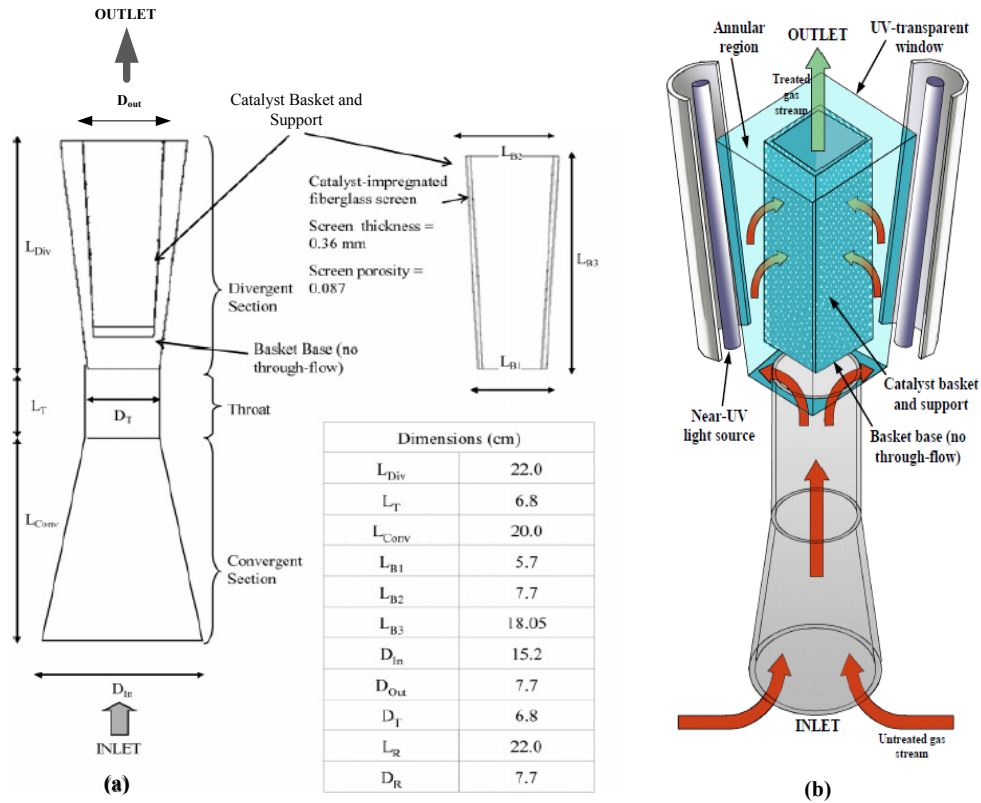


Figure 8: Former Version of the Photo-CREC-air Venturi section: (a) Venturi and basket dimensions. (b) Mesh irradiation by externally mounted near-UV lamps and Venturi divergent section isometric view

2.5.2 Antecedents in the use of Previous Photo-CREC-Air Reactor Versions

A first and previous version of the Photo-CREC-Air was designed and assembled as a prototype device for air cleaning applications by CREC researchers in 1996. Since then and given the important studies that follow up, this led to further modifications to improve Photo-CREC-Air performance and applicability. The work done by Ibrahim (1998) pointed out the need of changing design details related to UV energy transmission and utilization.

These needed modifications were later assessed and analyzed (Ibrahim, 2001; Ibrahim and de Lasa, 2002) until reaching a better design that showed a superior potential for the reduction of VOCs compounds.

It is important to mention the high performance of this former version of the Photo-CREC-Air unit was confirmed on the basis of the rates of model pollutants obtained (Ibrahim and de Lasa, 2002). The associated high energy efficiencies were reported as apparent quantum efficiencies larger than 100% (Ibrahim and de Lasa, 2003; Garcia-Hernandez et al., 2010). These high efficiencies provided a view of the high potential of the photocatalytic process for air purification.

However, the Photo-CREC-Air reactor design still required new modifications and investigation in order to exploit the aforementioned advantages, mainly in terms of reactor fluid flow and catalyst preparation. Ibrahim (2001) reported a series of recommendations that can be summarized as follows:

- On-line auto sampling is highly recommended to reduce inaccuracies in sample collection and data measurements.
- Improvement of the windows by replacing the sealant material in order to resist higher temperatures.
- Developing experiments with mixture of model pollutants and concentrations at the sub-ppm level that better resemble the actual conditions in industrial and commercial environments.
- Analyzing the supporting mesh from the point of view of pre-treatment effects and their influence over the photocatalytic activity.
- Evaluating the influence of operational aspects to enhance the photocatalytic activity and take advantage of the reported high quantum efficiencies.

More recently, Romero-Vargas Castrillon (2005) developed an important study about the Photo-CREC-Air reactor flow field and its implications over the performance through the use of Computational Fluid Dynamics. The aerodynamic simulations (Romero-Vargas Castrillon et al., 2006) showed the need of certain modifications in the design to allow the scale up the unit keeping its high energy efficiency. These same authors reported a set of possible modifications of the original Photo-CREC-Air reactor design. The main features of the modified design were as follows: i) a straight cylindrical section that replaced the divergent section and allowed the placement of a single wraparound window instead of four trapezoidal windows, ii) a wiremesh basket

sidewalls was replaced by a perforated plate. So that, the mass flow and time distributions were uniformized.

Romero-Vargas Castrillon (2005) proposed the following recommendations based on the results of the CFD simulations:

- Performing similar analysis for radiation models in the modified reactor configuration.
- Extending the application of the modified design to water treatment by using the same type of simulations.
- Studying the performance of the Photo-CREC-Air reactor under continuous operation conditions, although this requires further modifications in the design.

It is worth mentioning that all the valuable information and knowledge obtained with the design of the previous versions of the Photo-CREC-Air reactor as well as the experimental and theoretical results reported were the foundations for the unit design of this PhD dissertation.

The new Photo-CREC-Air reactor, as in the present study, has shown outstanding performance through the implementation of the most advanced radiation measurement techniques and photocatalysis applications. The details of the current Photo-CREC-Air reactor are described in further sections of this thesis.

2.6 Energy Efficiencies in Photocatalytic Reactors

One of the most significant obstacles in the application of photocatalytic processes is the energy consumption. Operating costs associated with the production of photons frequently limit the possible application of photoreacting processes. Therefore it is important to know how efficiently the radiative energy is used in the reactor, or how this energy varies while operating under different conditions.

Consequently, in photocatalytic processes, in addition to the effort directed at obtaining high active catalysts and at identifying best operating conditions to carry out the chemical reactions involved, it is also necessary to pay special attention to those factors of the reactor design restricting the optimal use of the radiation energy.

A key indicator for this analysis is the reactor quantum efficiency. Different definitions have been proposed for the radiative energy efficiency of photocatalytic reactors. This led to different ways of assessing their energy performance (Cerdá et al., 1977; Serpone and Emeline, 2002; Ibrahim and de Lasa, 2003).

2.6.1 Quantum Yields

The experimental determination of the activity as a part of the characterization of photocatalysts in heterogeneous systems is certainly a challenge (Emeline et al., 2006).

A few parameters have been suggested for the characterization of photocatalytic activities in heterogeneous systems; one is the “quantum yield”, which has been defined in different manners by several authors. Ibrahim (2001) and de Lasa et al., (2005) presented detailed summaries of the diverse definitions of quantum efficiency parameters as well as their concise description. Those definitions are reported in Table 3 along with a couple of new definitions.

One should note that many of the quantum yield definitions are based on a ratio that involves the number of photoconverted molecules over the number of photons entering the photocatalytic reactor.

This definition involves a first possible flaw in the energy efficiency analysis in a photocatalytic reactor. The radiation considered in determining the energy efficiency of a photocatalytic reactor must be that one corresponding to the photons absorbed by the photocatalyst (Serrano and de Lasa, 1997), and more specifically the absorbed photons with a wavelength small enough to supersede the catalyst energy bandgap (Garcia-Hernandez et al, 2010).

Table 3: Quantum Parameter Definitions

Parameters	Definition and References
Primary Quantum Yield (<i>Primary QY</i>)	$\frac{\text{number of pollutant molecules degraded from a primary process}}{\text{number of photons absorbed}}$ Cassano et al., (1995); Davydov et al., (1999)
Overall Quantum Yield (<i>Overall QY</i>)	$\frac{\text{number of pollutant molecules degraded from a primary and secondary process}}{\text{number of photons absorbed}}$ Cassano et al., (1995)
Quantum Yield (<i>Apparent QY</i>)	$\frac{\text{number of pollutant molecules degraded}}{\text{number of photons absorbed}}$ Peil and Hoffmann (1995); Valladares and Bolton (1993); Yamazaki-Nishida et al., (1994)
Apparent Quantum Yield or Global Quantum Yield (<i>QE</i>)	$\frac{\text{number of pollutant molecules degraded from a primary process}}{\text{number of photons entering the reactor}}$ Fox and Dulay (1993); Nimlos et al., (1993); Sczechowski et al., (1995); Zhang et al., (1994)
Minimum Apparent Quantum Yield ($QY_{app,min}$)	$\frac{\text{number of pollutant molecules degraded}}{\text{number of photons reaching the photocatalyst with } \lambda \leq 388 \text{ nm}}$
Minimum Apparent Quantum Yield ($QY_{app,min}^*$)	$\frac{\text{number of OH}^* \text{ consumed}}{\text{number of photons reaching the photocatalyst with } \lambda \leq 388 \text{ nm}}$

On the other hand quantum efficiencies should also consider changes of a more phenomenologically relevant parameter such as the number of OH^* groups consumed

during the photocatalytic process instead of the number of pollutant molecules photodegraded.

While in principle assessing the rate of OH^\bullet groups consumed and the rate of absorbed photons is the proper basis for an adequate quantum efficiency definition, this is a simple calculation. This requires accounting for; i) light scattering and photon absorption rates via macroscopic irradiation balances, i) net rate consumption of OH^\bullet groups.

2.6.2 Photochemical Thermodynamic Efficiency Factor (*PTEF*)

The efficiency of the photocatalytic reactor can also be defined using thermodynamic principles as the ratio of irradiation energy absorbed and irradiation energy used for the formation of OH^\bullet radicals which then interact with adsorbed species. More specifically the Photochemical Thermodynamic Efficiency Factor (*PTEF*) proposed originally by Serrano and de Lasa (1997) for photoconversion of pollutants in water can be used as a parameter to establish energy efficiency utilization,

$$PTEF = \eta = \frac{Q_{used}}{Q_a} \quad (1)$$

The irradiation energy used for desired formation of OH^\bullet can also be represented by the term $r_{OH^\bullet} \cdot \Delta H_{OH^\bullet} \cdot W_{irr}$, then the *PTEF* becomes

$$PTEF = \eta = \frac{-\nu / \nu_1 r_{OH^\bullet} \Delta H_{OH^\bullet} W_{irr}}{Q_a} \quad (2)$$

with r_{OH^\bullet} being the rate of formation of OH^\bullet radical groups per unit weight of irradiated catalyst, ν and ν_1 are the stoichiometric coefficients for the consumption of OH^\bullet group and for the model pollutant respectively, ΔH_{OH^\bullet} the enthalpy of formation of an OH^\bullet group and W_{irr} the total amount of irradiated catalyst. The *PTEF* can also be defined as a function of A_{irr} (the area of irradiated catalyst) if the rate of formation of OH^\bullet radical groups is expressed on a per unit irradiated catalyst area:

$$PTEF = \eta = \frac{-\nu/V_1 r_{OH^\bullet} \Delta H_{OH^\bullet} A_{irr}}{Q_a} \quad (3)$$

It can also be noticed that a quantum yield based on the fraction of photons absorbed by the photocatalyst leading to the formation of OH^\bullet radicals, can be defined as a function of $PTEF$ as follows,

$$QY = \frac{PTEF}{\eta_{OH^\bullet}} \quad (4)$$

where η_{OH^\bullet} is the fraction of photon energy used in forming an OH^\bullet radical, given by

$$\eta_{OH^\bullet} = \frac{\Delta H_{OH^\bullet}}{E_{av}} \quad (5)$$

And ΔH_{OH^\bullet} is the enthalpy of formation of an OH^\bullet group ($J \text{ mol}^{-1}$) and E_{av} is the average energy of a photon (J).

2.7 Photocatalytic Kinetics Models

The mechanism of TiO_2 photocatalytic processes in air treatment has not been sufficiently studied at the laboratory scale. It is important to state that the dissociation of pollutants approaching the surface of photocatalyst by the simple adsorption is unlikely. The most popular kinetic models proposed in photocatalysis are one site or competitive adsorption Langmuir-Hinshelwood type, with model pollutants and intermediates eventually competing for a single site.

The existence of layers of water formed from air humidity covering the TiO_2 surface has been pointed out by some authors (Pichat, 2010; Garcia-Hernandez et al., 2010). The presence of these molecules of water adsorbed on the photocatalyst surface has several effects. It has been highlighted the fact that water molecules do participate in the photocatalytic process both as hydroxyl radical (OH^\bullet) sources, competitive adsorbents and reaction products. Hence, it is obvious that the presence of water (humidity) in air may have a significant effect on the photocatalytic efficiency and on the chemical mechanism of degradation (Thevenet et al., 2008; Paz, 2010).

Usually the concentration of water vapor is below 20,000 ppmv indoors and the concentrations of pollutants in air are even smaller (Peral et al., 1997; Daisey et al., 2003; Garcia-Hernandez et al., 2010). The competition among the air pollutants seems to be negligible due to these low concentrations. However, it is quite possible that the surface of the photocatalyst, such as TiO_2 , exposed to air is covered by water molecules. Therefore, interactions between TiO_2 covered by water and the pollutants must be considered when laboratory studies are performed.

The mechanistic aspects of photocatalytic reactions on TiO_2 are complex. However, one of the most common radical species observed in hydrocarbon combustion and photocatalytic reactions is the hydroxyl radical (OH^\bullet). The OH^\bullet radicals are strong oxidizing agents and known to be important chain carriers, so they are expected to act as main promoters in some reactions such as photocatalytic degradation.

The formation of OH^\bullet has been supposed to occur by different pathways; however these possibilities are still on discussion (Salvador, 2007).

- Direct electron transfer from photo-excited TiO_2 to adsorbed OH^\bullet ions and water molecules.
- Location of a hole at a surface oxygen anion and protonation of the resulting radical-anion.
- Reduction reactions of O_2 as it have been assumed in liquid water with no presence of TiO_2 .
- Reactions taking place on TiO_2 exposed to humid air once some water molecules are adsorbed on the surface of the catalyst.

The mechanism of formation of radicals in photocatalytic processes for air treatment with TiO_2 as catalyst could be the same as those proposed for TiO_2 in liquid water (Pichat, 2010; Garcia-Hernandez et al., 2010). The formation of OH^\bullet radicals at the surface of UV-irradiated TiO_2 in liquid water has been under study for a long time (Bickley and Stone, 1973; Serpone and Khairutdinov, 1996; Serrano et al, 2009). This mechanism implies that OH^\bullet radicals can be formed by reaction of holes with $\text{H}_2\text{O}/\text{OH}^-$ and surface O_2^- , and three-electron reduction of O_2 via the intermediate formation of H_2O_2 .

The participation of some detected radicals and chemical species different from OH^\bullet in photocatalytic degradation of hydrocarbons has been suggested and inferred from reported results (Ibrahim and de Lasa, 2004; Kim and Choi, 2007; Sopyan, 2007; Garcia-Hernandez et al., 2010). The nature of H_2O_2 as an oxidizing and reducing agent makes think it is involved in the photocatalytic mechanism. However, the participation of H_2O_2 in any case leads to the formation of OH^\bullet radicals. Formation of molecular oxygen and its posterior reduction in TiO_2 photocatalysis remains debated. Some experiments have shown that O_2 atoms can play a role in photocatalytic oxidations; however, this role seems minor. In contrast, an OH^\bullet radical formed on TiO_2 can easily replace a H_2O molecule in the adsorbed layer and react with the pollutants. Therefore the leading role of OH^\bullet radicals in photocatalytic processes either in air or water treatment is well supported.

The calculations and analysis performed throughout this thesis dissertation are based on the assumption of the OH^\bullet radicals as the main participant species in the photocatalytic processes analyzed. The approach implemented to define the formation of these radicals as well as the calculation of the energy required for this formation reactions play a fundamental role in further section of this work. A detailed explanation of the mechanism of formation of these OH^\bullet radicals is showed in Appendix A. Appendix B describes the calculation of the reaction enthalpy for the formation of the OH^\bullet radicals.

2.8 Conclusions

The use of photocatalytic processes in the decontamination of both aqueous and gaseous systems is a technology of great prospects given it can lead to complete mineralization of many types of organic pollutants.

This chapter provides an overview of the state of the art in photocatalysis and photocatalytic reactor design procedures and configurations as pertinent to the treatment of gaseous effluents in air. Various sections in this chapter emphasize the significant value of optimal designs with high usage of irradiation as shown with relevant energy efficiency factors parameters.

Chapter 3

Scope of the Research

This PhD dissertation is aimed to consider the influence of the parameters involved in the photocatalytic degradation of airborne pollutants. In doing so, a group of model pollutants was selected and their degradation in the bench-scale photocatalytic reactor Photo-CREC-Air was studied. The contribution of this thesis lies on the area of photocatalytic reactor design and its implications to reactor performance. The key of this work is the determination of energy efficiencies performed thanks to the concurrent evaluation of macroscopic energy balance in a Photo-CREC reactor.

In this respect, the main achievements of this PhD research can be summarized as follows: a) synthesis of appropriate photocatalysts that showing adequate adhesion over the support (good coating), b) performance evaluation of the reactor by carrying out the degradation of the model pollutants and c) determination of efficiency for the entire photocatalytic process. These three major parts of the research had as principal target to reach an in-depth understanding of the relation among photocatalyst characteristics, fluid dynamics and irradiation in the photocatalytic reactor.

3.1 General Objectives of the Research

This work was planned with significant experimental and theoretical general objectives. Consistent with this, the general objectives for the experimental section of the PhD dissertation includes:

- To attain an efficient reactor design in terms of irradiation and energy usage as well as photocatalyst preparation and loading.
- To study the influence of different chemical species present and chemical species changes during the photocatalytic process either as intermediates or as byproducts.
- To demonstrate high reactor performance via degradation of model pollutants.

As well a number of theoretical general objectives for the PhD research were set as follows:

- To study the flow and radiation fields for the reactor used during the photocatalytic degradation of model pollutants in air.
- To develop kinetic model able to describe the observed photocatalytic process as well as being suitable to scale-up this type of photocatalytic reactors.

3.2 Specific Objectives of the Research

This work was also envisioned to accomplish significant specific objectives.

3.2.1 Photocatalyst Preparation and Kinetic Studies

Experimentation carried out to determine the conversion and efficiency reached during model airborne pollutant degradation in the Photo-CREC-Air Reactor. As a result the experimental program included the following:

- a) Design and implementation of the Photo-CREC-Air Reactor with unique features using recent research in previous Photo-CREC-Air reactor designs.
- b) Synthesis and characterization of the photocatalyst and determination of the optimum process to coat the support according to a proposed method.
- c) Photocatalytic degradation of airborne pollutants using model compounds (acetone, acetaldehyde, isopropanol) dissolved in room air to simulate industrial or residential conditions.
- d) Identification and quantification of reaction products, intermediates and byproducts using gas chromatography (GC).
- e) Determination of reaction mechanisms and kinetic models that best fit the experimental results. A rigorous estimation of kinetic parameters in the proposed kinetics models with the use of the MATLAB© software.

3.2.2 Irradiation and Flow Field Studies

The reactor configuration (design) has been established considering fluid-photocatalyst contact and UV irradiation field. This approach allowed studying the relation between major reactor design parameters and the efficiency achieved during the reaction. Thus, the PhD dissertation includes the following:

- a) Determination of the amount of radiation absorbed by the photocatalyst-support medium by performing experimental macroscopic balances. Specific equipment and specially designed devices should be used to undertake these tasks.
- b) Assessment of the effect of the reactor configuration in the photocatalytic degradation process based on the UV radiation field inside the reactor.
- c) Experimental evaluation of the flow field in the Photo-CREC-Air reactor and its implications to the performance of the reactor.
- d) Analysis of the flow field for the reactor while working on airborne pollutant photocatalytic degradation.

3.2.3 Energy Efficiency Evaluation

Energy efficiency established considering the following issues:

- a) Determination of the light utilization by calculating the quantum yields (QY) as a measurement of the efficiency reached by the Photo-CREC-Air reactor.
- b) Evaluation of the Photochemical Thermodynamic Efficiency Factor ($PTEF$) to show the ability of the reactor to achieve high conversions of pollutant on a thermodynamic basis.

Chapter 4

Experimental Setup

4.1 Introduction

The Photo-CREC-Air Reactor of the present project was designed at the Chemical Reactor Engineering Centre (CREC) at Western University. This unit was manufactured and assembled with the help of the University Machine Services.

The objective of this unit design was to implement a photocatalytic reactor offering great flexibility for the determination of the various kinetics, mixing and irradiation required in a high efficiency photocatalytic unit.

The chosen design incorporates: i) minimum pressure drop, ii) uniform photocatalyst coating with firm particle attachment to a stainless steel mesh, iii) good irradiation transmission and distribution in the reaction section, iv) high external mass transfer between the fluid and the photocatalyst. The selected design also incorporates a cylindrical reaction section with an aerodynamic bullet nose, promoting a uniform flow distribution over the photocatalyst.

The Photo-CREC-Air Reactor in its present configuration was operated in the batch mode. The photocatalyst was supported by a cylindrical stainless steel mesh. In every experiment, a given amount of model pollutant was injected in a set volume of air. Since the dew points of the model pollutants were higher than their concentrations in the air stream, vaporization occurred almost instantaneously.

4.2 Photo-CREC-Air Reactor

The designed Photo-CREC Unit is a reactor with the capability of carrying out photocatalytic experiments in both air and water media. The plumbing system can be easily changed either when the blower is working with air or when the pump recirculates water. It has to be stressed that the scaled Photo-CREC Unit (55.1 liters) implemented in this project, is the result of several improvements and previous experience of CREC researchers on previous photocatalytic reactors. The implemented Photo-CREC Unit also takes advantage of the experience of the CREC researcher group in spectrophotometric radiation measurements and supported TiO_2 photocatalysts.

Figure 9 shows a picture of the Photo-CREC-Air Reactor showing its main and auxiliary components as follows: a) near UV lamps placed in lamp holders, b) TiO₂ supported on the stainless steel mesh, c) air blower for air recirculation, d) reaction section.

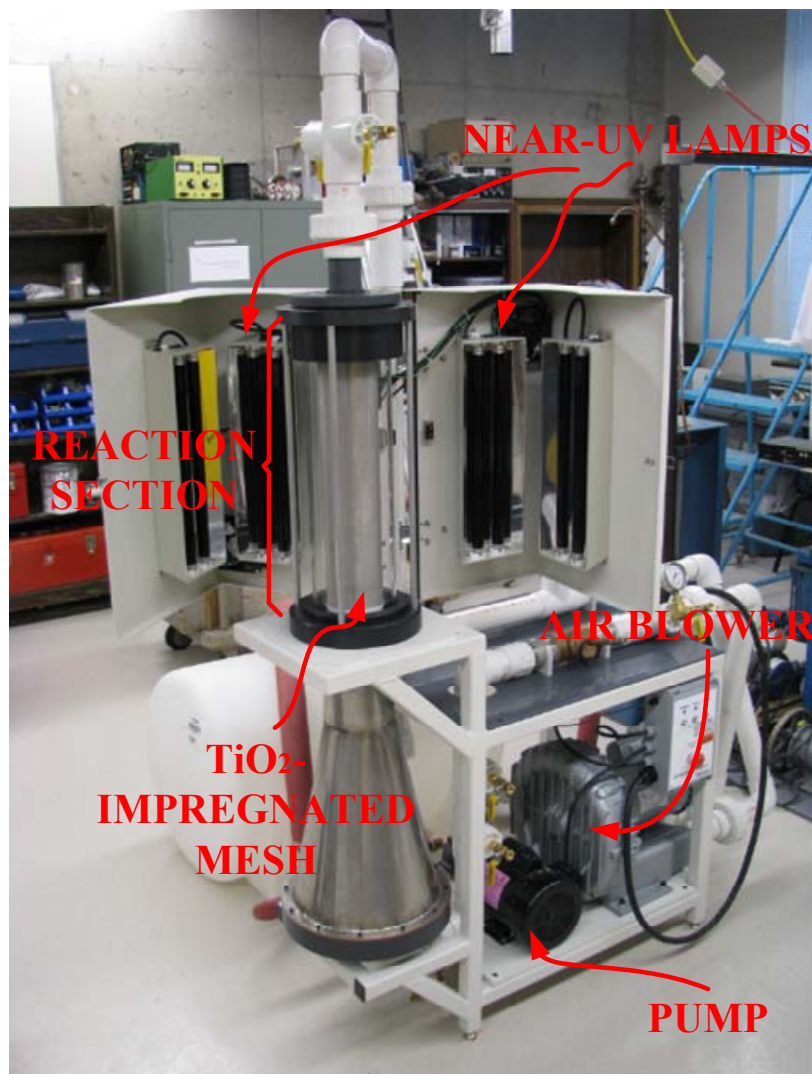


Figure 9: Picture of Photo-CREC-Air Reactor showing its main components. The protecting enclosure holding the 8 near UV lamps is open for a better description of Photo-CREC-Air components

The Photo-CREC-Air Reactor was designed on the basis of maximizing interaction between fluid-catalyst-radiation, as recommended by our research group (Ibrahim, 2001; Ibrahim and de Lasa, 2002; Ibrahim and de Lasa, 2003; Romero-Vargas Castrillón et al., 2006; Romero-Vargas Castrillón, 2007). This process has also taken

into account the results of flow pattern studies performed on this type of design using CFD simulation (Romero-Vargas Castrillón et al., 2006).

CFD simulation results were embodied in a design involving a cylindrical reaction section with an aerodynamic bullet nose that presents a uniform flow distribution over a photocatalyst. A more detailed drawing of the reactor showing the dimensions of the various sections is given in Figure 10. This Photo-CREC-Air Unit has a total volume of 55.1 liters. It is made of non-reactive plastic materials and a stainless steel Venturi section. This reactor incorporates a set of 8 near-UV lamps (UVP Inc., Upland CA). Each of these lamps supplies 15 watts nominal power at a principal irradiation wavelength of 365 nm. The lamps are symmetrically mounted around the reaction section (Figure 9). They irradiate a TiO₂-coated stainless steel cylindrical mesh which has a surface area of 192 cm². The radiation enters the reaction section through a UV-transparent quartz cylinder surrounding the metallic mesh.

There are several ports on the top of the reaction section used to determine the radiation field distribution. This is achieved by introducing an optical fiber sensor connected to a spectroradiometer. The fluid velocity in this section of the reactor was also measured using a thermal anemometer.

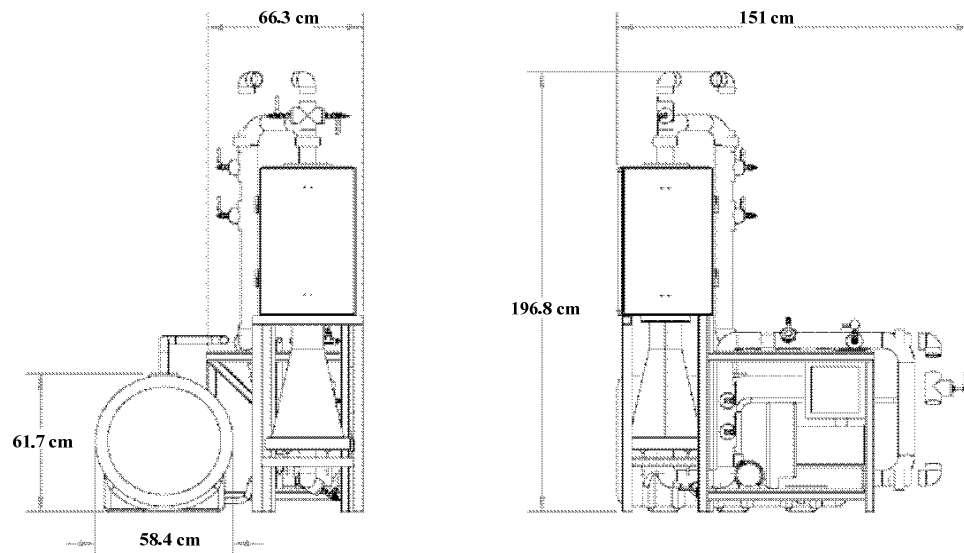


Figure 10: Detailed drawing of the Photo-CREC-Air Reactor dimensions.

Figure 11a describes the reaction section of the unit, a Venturi section containing a cylindrical stainless steel mesh which is impregnated with a TiO_2 photocatalyst. The base of this cylinder (bullet nose) supports the mesh. The air flow through the Venturi throat and around the base is described in Figure 11b. This secures cross-flow through the mesh and uniform contact between the fluid and the TiO_2 -coated mesh. Once these conditions of steady and stabilized cross-flow in the Venturi section are achieved, the lamps in the Photo-CREC-Air unit are turned on.

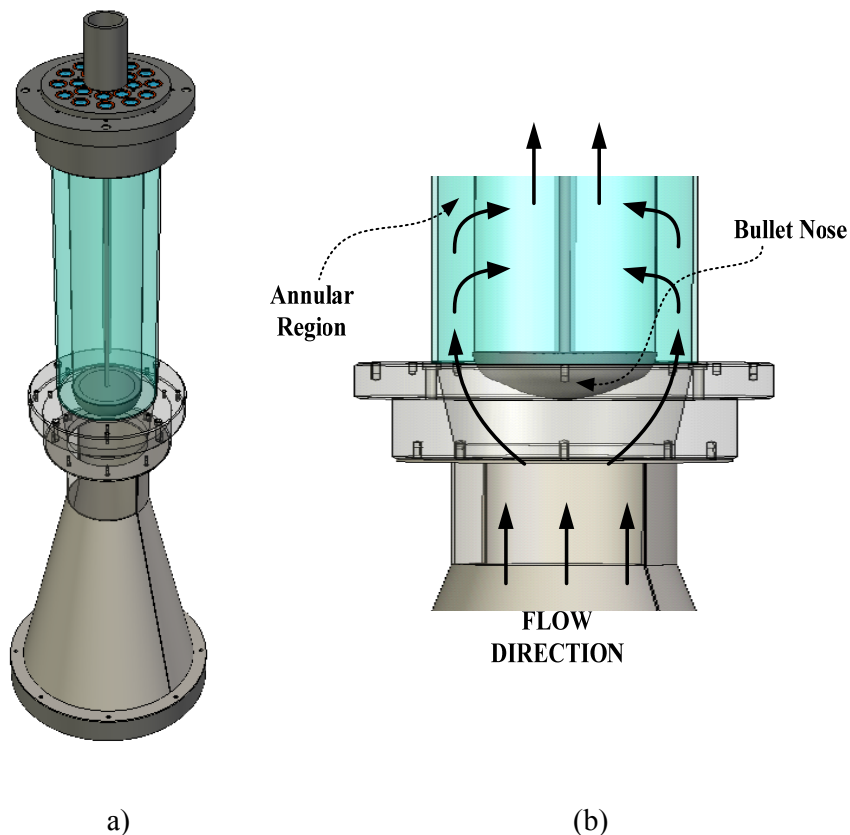


Figure 11: (a) Diagram of the Photo-CREC-Air Reactor, isometric view. (b) Description of the Venturi divergent section

As described, the Photo-CREC-Air Reactor offers advantages from the standpoint of energy usage and also presents special features for photocatalysis. These advantages can be listed as follows:

- Significant irradiation area per unit reactor volume
- High utilization of the available UV radiation
- Effective means for measuring irradiation and velocity field distribution

- Uniform velocity distribution that ensures contact between fluid and photocatalyst
- High loadings of well supported and attached photocatalyst to a metallic mesh (support)

4.3 UV Sources

Due to electricity charges and bulb replacement, the light source will tend to be the most costly component of any photocatalytic reactor. It is essential to utilize the photons effectively and to ensure that most photons emitted contact the catalyst and initiate photooxidization.. All reactor surfaces must receive adequate irradiation from the light source, making certain that no flow paths through the reactor exist where the catalyst is not illuminated.

The Photo-CREC-Air Reactor uses 8 black-light-bulb near-UV lamps (UVP Inc., Upland CA, USA) with 15 Watts nominal power each, and 4 watts actual power output. The main irradiation wavelength supplied by the lamps is 365 nm (300-420 nm range). These lamps offer a stable emission that guarantees accuracy and reproducibility. Their life is between 5000-8000 hours depending on the use. The lamps are held by aluminum housings with internal reflective walls; ensuring in this way, that most of the irradiation is directed towards the reaction section. There are a total of 4 housings, each one holding 2 lamps. All of these housings and the lamps are fixed to a specially designed enclosure that does not allow the near-UV radiation to exit the reactor. The lamps and their housings are located around the sealed quartz cylinder surrounding the TiO₂-impregnated mesh, as showed in Figure 12.

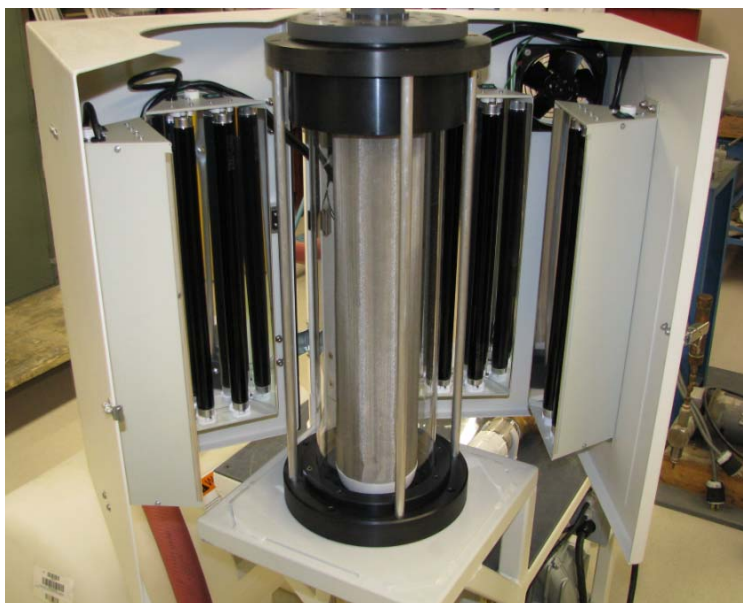


Figure 12: Detail of the reaction section in the Photo-CREC-Air Reactor showing the near-UV lamps distributed circumferentially around the reaction section.

4.4 Photocatalyst Support

The material of the mesh used as a photocatalyst support influences the activity, homogeneity and adhesion of the TiO_2 catalyst to its surface. Considering all these facts, the synthesis and the immobilization of photocatalytic materials have been the subject of research by both scientists and engineers during recent years (Yu et al., 2003; Chen and Dionysiou, 2008).

In this respect, the accessibility of the photocatalytic surface to the photons and reactants must be optimized since the external mass transfer plays a significant role, particularly at low fluid flow rates. Different materials such as fibers, plastics and glass have been used as supports (Ibrahim, 2001; Herbig and Lobmann, 2004; Portela et al., 2007).

The mechanical and chemical properties shown by certain materials such as metallic meshes, particularly stainless steel, allow considering their use as catalyst supports. These types of meshes present an extensive superficial area compared to that shown by flat surfaces and can be covered easily by one or several layers of catalyst. Moreover, the selected materials for the mesh have to be resistant to corrosion and not prone to adsorbing intermediate species that could cause catalyst deactivation.

Moreover, properties of stainless steel meshes enable prolonged contact between catalyst and pollutant and facilitate the access of the photons to the catalytic surface. All this allows good mass transfer promoting pollutant conversion.

The mesh cylinders used in the Photo-CREC-Air Reactor are made of stainless steel (type 304 woven wire mesh) with 40 openings per linear inch. These openings were measured from the center of any wire. The wire diameter is 0.010 of an inch and the openings in the mesh are 0.015 inch square showing 36% of open mesh area, (Ferrier Wire Goods Company, Toronto ON).

The mesh cylinders were manufactured at Western University Machine Services. Some dimension details of the stainless steel mesh used as a support for the photocatalyst are shown in Figure 13.

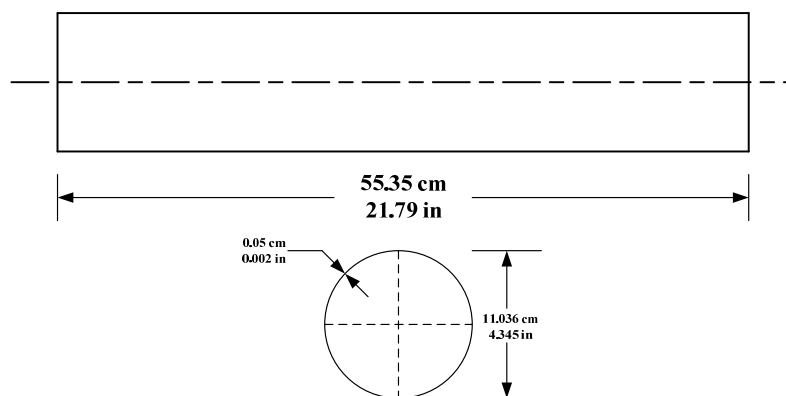


Figure 13: Cylindrical mesh used as catalyst support.

Two photos of the stainless steel mesh cylinder covered by the commercial photocatalyst Degussa P25 are shown in Figures 14 and 15. Figure 15 also shows the uniform photocatalyst distribution covering the metallic mesh.



Figure 14: Stainless steel mesh cylinder coated with Degussa P25.

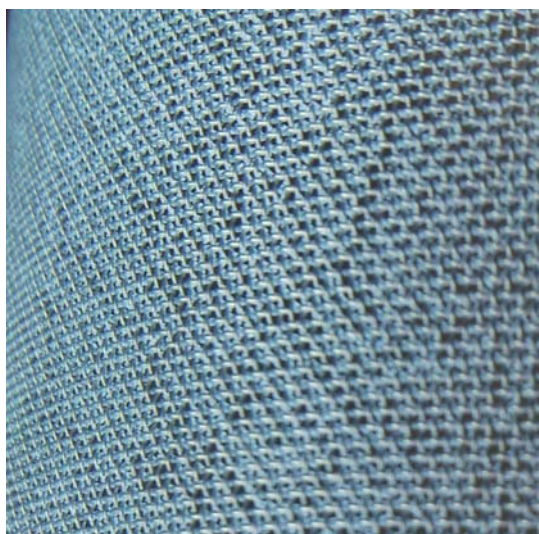


Figure 15: Picture showing the Degussa P25 photocatalyst covering the metallic mesh.

4.5 Photocatalyst Impregnation

The method of impregnation and the type of resulting TiO₂-mesh bonding is a critical step in the development of a suitable immobilized photocatalyst.

Given the nature of the special stainless steel mesh employed as catalyst support, an impregnation method had to be developed. It involved painting the mesh surface to be irradiated using a TiO₂-water slurry solution and having a carefully selected TiO₂ loading. The mesh was then left drying for 24 hours to ensure water removal. The commercial catalyst Degussa P25, which was used in this study, forms agglomerates while mixed with water. These agglomerates have a wide particle size distribution of a bimodal nature (Ibrahim and de Lasa, 2003; Suttiponparnit et al., 2011). Changes in the TiO₂ slurry concentration in the 6-10 wt% range allow preparing TiO₂-coated stainless steel meshes with different TiO₂ loadings.

It was observed that increasing TiO₂ loading produced a thicker catalyst layer. This increase of TiO₂ yielded higher rates of UV photon absorption and therefore higher photoconversion rates. However, 8 wt% TiO₂ water slurries yielded an optimal photocatalyst thickness. Surpassing this critical thickness did not enhance the photon absorption and the photoconversion rates. This critical layer thickness was estimated in our study to be in the 5.4 μm range. This is in agreement with the information reported by other authors with respect to the UV-radiation absorption using TiO₂ based photocatalysts (Hernández-Alonso et al., 2011; Peral and Ollis, 1992). In order to use the optimal amount of catalyst and trying to avoid agglomerate formation, the mesh was painted with a solution containing 8-8.8 wt% of Degussa P25 as previously suggested (Ibrahim and de Lasa, 2002).

4.6 Irradiation Field Analysis

Irradiation measurements and calculations are of key importance in the evaluation of a photocatalytic reactor such as Photo-CREC-Air Reactor. This involves: a) the different irradiation components emitted by the lamps, b) the irradiation reaching the photocatalyst surface and c) the irradiation absorbed by the photocatalyst. This was accomplished using a spectrometer Stellarnet EPP2000, which is able to measure the irradiance power at various wavelengths (200 nm-1100 nm).

In this respect, the design of the Photo-CREC-Air Reactor includes a top perforated plate. These series of spaced perforations allow introducing a specially designed probe connected to the spectrometer. Figure 16 shows the top plate of the reaction section with its perforations. Using this top plate, it is possible to determine the irradiation at different positions relative to the supported catalyst in the stainless steel mesh section. To accomplish this, a fiber optic probe housed in a periscopic device (aluminum pipe) and held in position using a clamping ring was used. A sensor on the fiber optic tip measured irradiance at various strategic locations. Using a 90 degree angled rotating receiver with internally polished walls, the incident irradiance at various reactor positions was measured. The narrow aperture of this device allowed the irradiation to be measured locally along the near-UV lamps. The details of the attachment holding the sensor are shown in Figure 17.

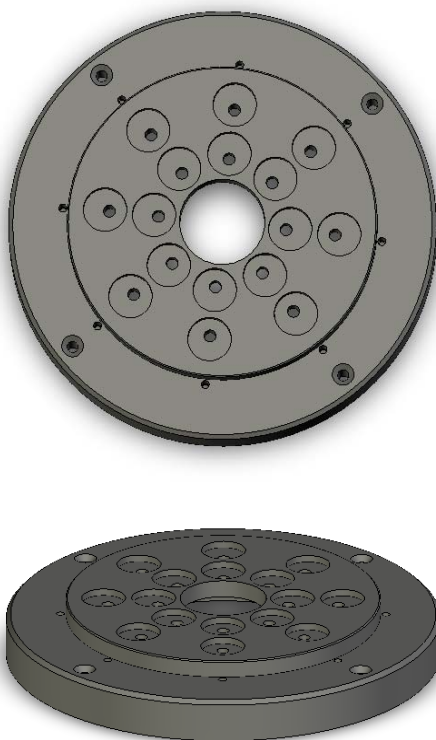


Figure 16: Top and Side View of the Perforated Reaction Section Top Plate.

Using this periscopic device as described in Figure 18, the following results were obtained: a) rate of photons emitted by the lamps, including both the irradiation

directly emitted by the lamps and that coming from the reflectors (P_e); b) rate of photons reaching the photocatalyst surface once transmitted through the UV-transparent quartz cylinder (P_{el}), c) rate of photons evolving without being absorbed by the photocatalyst (P_t).

The irradiation absorbed was calculated performing the following macroscopic irradiation balance (de Lasa et al., 2005):

$$P_a = P_{el} - P_t \quad (6)$$

It has to be emphasized that the gas phase was assumed to be radiation transparent in these calculations and the rate of backward contribution was considered negligible. It is known that air, model pollutants and water vapor do not absorb radiation in the wavelength range of interest (Alfano and Cassano, 2008; Negishi et al., 2007).

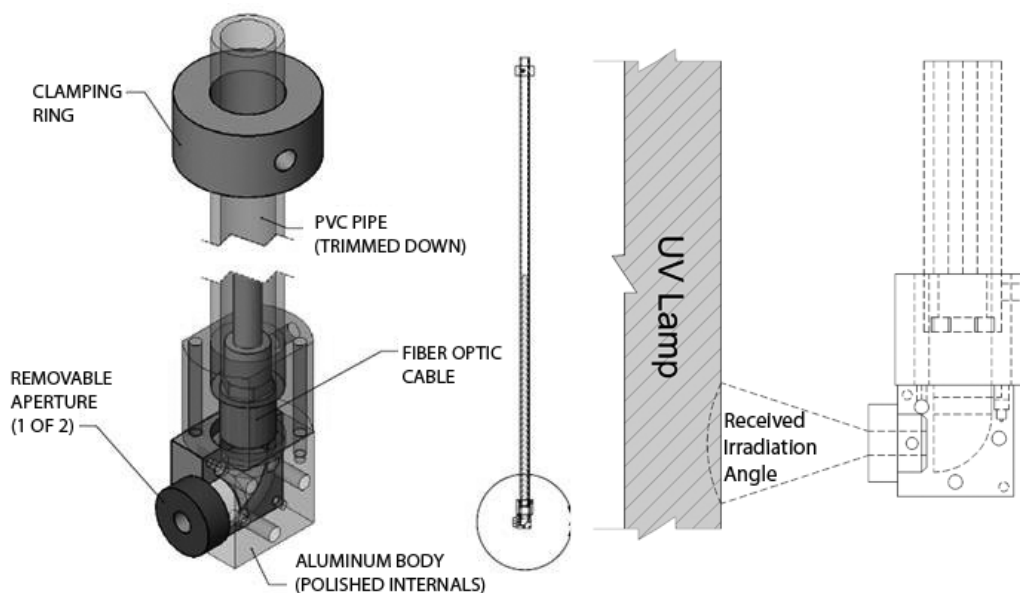


Figure 17: Schematics of the specially designed Periscopic Irradiation Receiver showing the angle of acceptance

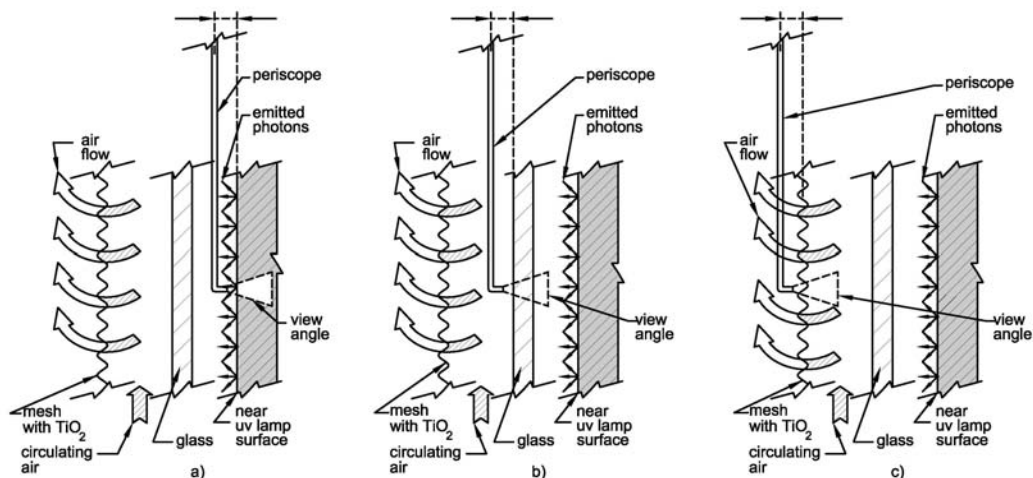


Figure 18: Schematic Diagrams of the Periscope Irradiation Receiver showing the irradiation acceptance angle placed at three positions: a) Periscope placed between the glass tube and the near UV lamps measuring “ P_e ”, (b) periscope placed between the impregnated mesh and the glass tube measuring “ P_{el} ”, (c) Periscope placed at the back of the mesh measuring “ P_i ”.

4.7 Flow Field analysis

An important aspect of any heterogeneous reactor development, including photocatalytic reactors, is the fluid-photocatalyst contact. This fluid-photocatalyst contact plays a major role in any catalytic process.

Due to a well designed plumbing system, uniform flow distribution and enhanced contact between the fluid and the TiO₂ photocatalyst are achieved in the Photo-CREC-Air Reactor. As described in Figure 19, air exiting the blower enters the Venturi convergent section and flows through the Venturi throat, where its velocity increases. The impervious bullet nose located in the base of the stainless steel mesh directs the air to create a cross-flow, improving, in this way, the fluid-photocatalyst contact.

The characterization of flow patterns in the Photo-CREC-Air Unit was performed by measuring gas velocities in the near mesh region (reaction section). The top perforated top plate as described in Figure 16, allowed the positioning of an anemometer to measure fluid velocity at different locations. For this purpose, a 36 inch long probe support connected to an IFA 300 anemometer system (TSI

Incorporated) equipped with a 45 degrees Cross-Wire probe sensor Model 1242-20 was used.

Figure 20 shows some details of the probe and sensor used for the velocity measurements. The probe with the mounted anemometer was located at three axial and two radial positions with the following gas velocities obtained: i) $1.2 \text{ m/s} \pm 5\%$ at the near front mesh region, ii) $1.7 \text{ m/s} \pm 5\%$ at the near back mesh region. Thus, it was found that there was a nearly uniform velocity distribution in the reaction sections of the Photo-CREC-Air Unit both at the front and back faces of the TiO_2 impregnated mesh.

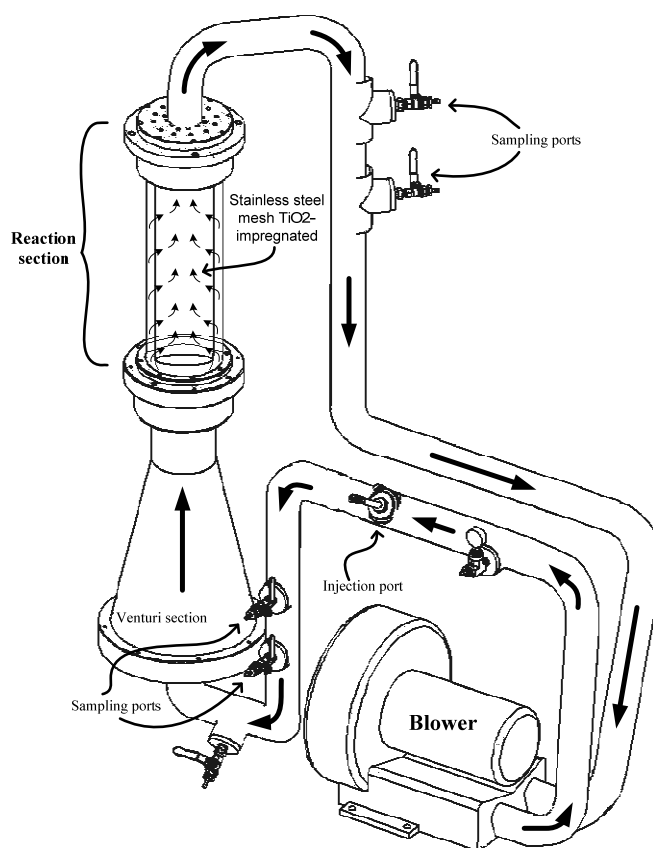


Figure 19: Schematic Diagram and Description of air circulation in Photo-CREC-Air Reactor.

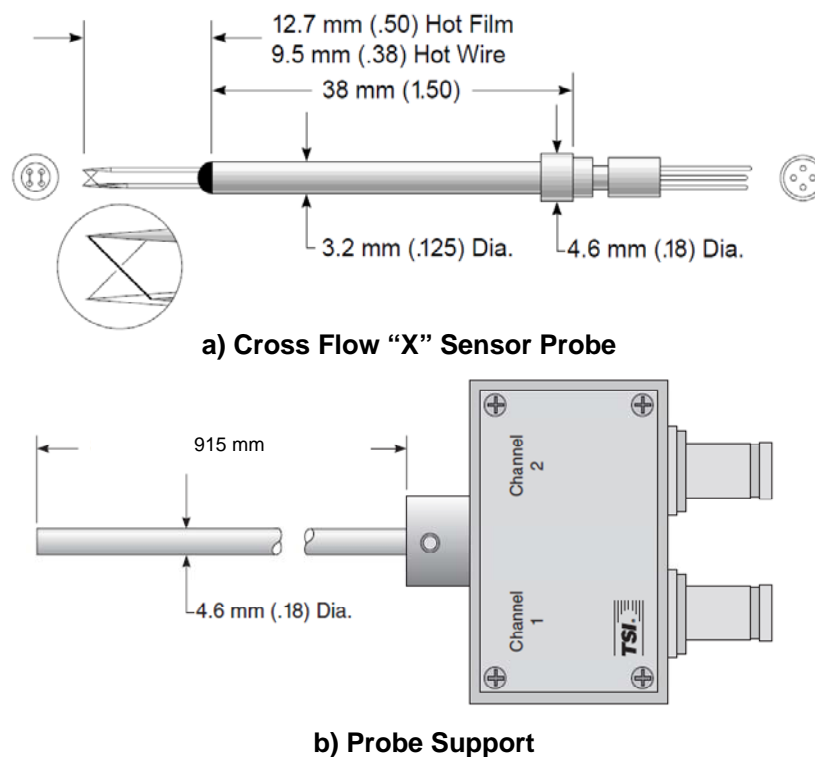


Figure 20: Cross Flow sensor probe and support (TSI Inc.) used to measure the velocity inside the reaction section.

4.8 Conclusions

This chapter highlights the main components and characteristics of the Photo-CREC-Air reactor as follows:

- a) A scaled up Photo-CREC-Air reactor unit,
- b) A large irradiated area per unit volume,
- c) An effective fluid-catalyst contact enhancing pollutant mass transfer,
- d) In-situ measurements capabilities for both irradiation distribution and gas velocity profiles in the near mesh area.

Chapter 5

Experimental Methods

5.1 Sample Analysis

Analysis of reaction samples can be accomplished using different methods including chromatography and spectroscopy. In this study, gas chromatography was implemented as the main analytical technique for product analysis.

Model pollutants and products of the photocatalytic reactions including carbon dioxide were identified and their concentration were measured using a Shimadzu gas chromatograph model 2014, equipped with a thermal conductivity detector (TCD) and a flame ionization detector (FID) connected in series. Retention times as well as their corresponding areas of the different chemical species were quantified.

A GC oven temperature program was used during the experiments to detect and quantify the different chemical species present during the experiments. This GC oven temperature program was developed to achieve good separation of the model pollutants acetone, acetaldehyde, and isopropanol. This was also performed for all the chemical species observed during the photocatalytic degradation experiments either as intermediates or products. The GC oven temperature program employed during the studies was as follows: a) an initial period of 0.5 minutes at 75°C, b) a follow-up period where the oven temperature was raised from 75°C to 185°C at the rate of 55°C/min, c) a final period where temperature was kept at 185°C for 10 minutes (Figure 21).

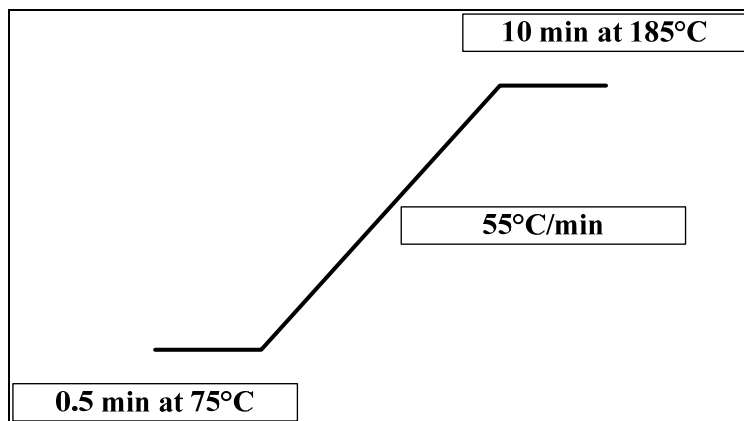


Figure 21: GC temperature program used for the experiments.

5.2 Experimental Procedure

Main classes of organic pollutants can be found in offices, buildings and factories. (Peral and Ollis, 1992). Oxygenates including ketones, acetaldehydes and alcohols are good representatives of these classes of chemical species. Thus, selected model pollutants used during the present study were acetone, acetaldehyde and isopropanol (both supplied by Caledon Laboratories Ltd., 99% purity). These species at low concentrations provide a good simulation of indoor air conditions found in industries where these materials are used as solvents.

Different amounts of model pollutant were injected into the 55.1 liter reactor to obtain the desired gas phase concentrations: 24.5, 37 and 49 $\mu\text{mol/L}$ for acetone; 160, 240 and 320 $\mu\text{mol/L}$ for acetaldehyde and 33, 50, 68, 87 and 107 $\mu\text{mol/L}$ for isopropanol.

Model compounds were specifically selected to study the functional group reactivity, such as is the case of hydroxyl and carbonyl groups. Furthermore photocatalytic conversion of acetone and acetaldehyde allows assessing the reactivity of carbonyl groups while being placed in different carbons in the hydrocarbon molecule.

The Photo-CREC-Air Reactor was operated in conjunction with a Gas Chromatograph Shimadzu 2014 equipped with a TCD and a FID connected in series using a Porapak Q packed column. Thus, the analytical system allowed the identification and quantification of all the chemical species present.

The experimental procedure adopted to carry out the various runs throughout this research was as follows:

- (a) The system was flushed with room air. The amount of humidity did not change significantly during the run of each experiment.
- (b) The pressure regulators were closed and the blower was turned on
- (c) A set amount of model pollutant entered the reactor via the injection port using a Hamilton Gastight-1001. A 10 minute period was allowed for the model pollutant to evaporate and achieve system stabilization. The injections of acetaldehyde required reducing the sample temperature below its vaporization temperature.

- (e) The lamps were turned on after the "dark reaction period" and once model pollutant adsorption equilibrium was reached,
- (f) The photocatalytic reaction was allowed to proceed. The concentration of the chemical species in the gas phase was tracked using gas samples taken at different irradiation times.
- (g) The gas samples were taken periodically and analyzed in the gas chromatography system. A highly developed system was used to take the samples and inject them into the GC automatically, so that precision and reproducibility could be achieved.
- (h) Experiments were completed at different times as planned. Once the gas phase concentration of the pollutants was undetectable, the photoconversion reaction was considered finished.
- (i) At the end of each run, lamps were turned off and the reactor was flushed with air. A complete run lasted between 45 and 180 minutes depending on the initial pollutant concentration and pollutant type.
- (j) Following these steps, the reactor was ready for a new run. The mesh was replaced after several experiments to determine any decay in photocatalytic activity. However, no measurable photocatalytic activity changes were detected.

The system was regularly checked for leaks to ensure proper operation. The only leak detected was in the blower section, during its operation. This leak was part of the normal operation of the blower and represented a small portion of the total amount of pollutant participating in the reactions. However, its effect was considered throughout the modeling and calculations were performed to take this into account as described in the upcoming sections.

5.3 Blank Experiments

Degradation of chemical species due to direct photolysis might contribute during photocatalysis. Furthermore, various materials included in the different Photo-CREC-Air reactor components may also influence model pollutant conversion.

Therefore blank experiments were performed using acetone, acetaldehyde and isopropanol at close concentrations and reaction times than the ones used in the photocatalytic runs reported in section 7. Blank runs allowed to prove the following: a) Under dark conditions (no UV radiation), with impregnated mesh placed inside the reactor, model pollutant conversions was negligible, b) With the lamps turned “on” and no impregnated mesh inside the unit model pollutant conversions were below detectable limits. Hence, it was concluded that the photocatalytic reactions proceeded in the presence of both TiO₂ and UV radiation only.

5.4 Mass Balances

The mass balance closure is a very important condition to be satisfied for reaction experiments. A good mass balance gives confidence that the experimental results obtained are consistent with the stoichiometry and provides a good basis for kinetic modeling. These balances must account for all the chemical species present during the photocatalytic process, including model pollutants, intermediates and products.

Species balance equations in the Photo-CREC-Air Unit were established considering both photocatalytic conversion and pollutant leaks. Equation (7) accounts for good gas mixing, uniform catalyst dispersion on the mesh and uniform mesh irradiation. These applicable reactor model assumptions will be justified in later sections of this PhD dissertation.

The pollutant leak term was included in equation (7), to improve kinetic parameter estimation and provide a more rigorous model. The value of the k_{leak} parameter was 7.2 m³/min for both acetone and acetaldehyde photocatalytic degradation experiments and 8.1 m³/min for isopropanol. Therefore, its contribution was typically confined to less than 1% of the total chemical species mass.

As a result, the following equation was adopted,

$$V(1 + K') \frac{dC_i}{dt} = r_{i,T} A_{irr} - k_{leak} C_i \quad (7)$$

where:

V = total hold up of the gas, m³

C_i = model pollutant concentration, μmol/m³

$r_{i,T}$ = rate of photoconversion of the model pollutant under study, $\mu\text{mol}/(\text{m}^2 \cdot \text{min})$

A_{irr} = irradiated area of catalyst, m^2

k_{leak} = parameter accounting pollutant leak, m^3/min

K' = dimensionless adsorption constant

Carbon balances of the model pollutants acetone, acetaldehyde and isopropanol were calculated by subtracting the carbon available both in the injected amount of model pollutant and the carbon dioxide at the beginning of the experiment from carbon dioxide at the end of the experiment. Carbon balances closed within $\pm 10\%$. The amount of carbon from adsorbed intermediates that could remain on the mesh at the end of every experiment was considered insignificant. Moreover, the carbon from possible carbonyl species present in the air used during the experiments, was considered insignificant while compared to the carbon available in the injected model pollutant.

Chapter 6

Results and Discussion I: Kinetic Modeling

6.1 Introduction

Heterogeneous photocatalysis involves several elementary steps. However, under certain conditions some of these steps may not need to be considered to describe the photocatalytic reaction mechanism. The appearance of one or more intermediate species could lead to complex reaction mechanisms.

The photocatalytic reaction might proceed through a complex mechanism involving the formation of one or more intermediate species that can be adsorbed onto the photocatalyst surface or be detected in the gas phase and compete for active sites with the other species.

For isothermal photocatalytic reactions, the conversion rate depends on both the radiation adsorbed and the pollutant concentration, which can be approached with a Langmuir-Hinshelwood model. Therefore, the development of any model that could describe the behavior of a photocatalytic process must account for all these issues.

This kinetics includes the reaction and adsorption effects of all the chemical species detected in the analyses as well as their interactions. These kinetic models are used to evaluate the energy efficiencies of the various photocatalytic processes as is shown in the upcoming sections.

6.2 Photocatalysis Kinetics Modeling

In spite of its complexity, the photocatalytic degradation of volatile organic compounds (VOCs), can be well described using a first order unimolecular decomposition reaction of the VOC adsorbed species on the catalyst surface:

$$r = -\frac{dC}{dt} = kC_s \quad (8)$$

where k is the global kinetic coefficient of the oxidation reaction, and C_s is the sorbed-phase concentration of the VOC.

Regarding the C_s , it can be estimated by using the Langmuir adsorption isotherm model such as:

$$C_s = f(C) = \frac{C_s^0 KC}{1 + KC} \quad (9)$$

with C_s^0 and K being the Langmuir parameters.

Substituting this equation in (8) gives the following:

$$r = -\frac{dC}{dt} = \frac{k' KC}{1 + KC} \quad (10)$$

Thus, the kinetics of photocatalytic reactions can be modeled using a Langmuir-Hinshelwood rate expression set at these initial conditions.

In equation (10), k' ($\mu\text{mol}/\text{m}^3 \text{ s}$) involves both the intrinsic kinetic coefficient of the reaction k and the sorbed-phase concentration corresponding to the monolayer coverage on the catalyst surface, C_s^0 . Equation (10) can be rewritten as:

$$\frac{1}{r} = \frac{1}{kK} \frac{1}{C} + \frac{1}{k} \quad (11)$$

As a result, the values of $1/kK$ and $1/k$ can be obtained experimentally. However, due to the presence of other chemical species in air and even intermediate species formed during the photocatalytic reaction, a modified Langmuir-Hinshelwood equation can be used. These species compete for catalyst sites at the surface influencing the VOC sorbed-phase concentration. This can be expressed in the following equation as:

$$C_s = f(C_i) = \frac{C_s^0 KC}{1 + \sum_{i=1}^n K_i C_i} = 1, 2, \dots, n \quad (12)$$

with the terms K_i and C_i representing the Langmuir-Hinshelwood parameters and the gas phase concentrations of species i , respectively; where n is the total number of present species.

Equation (12) can be introduced in Equation (8) giving the following:

$$r = \frac{kKC}{1 + \sum_{i=1}^n K_i C_i} \quad (13)$$

where K is the equilibrium adsorption constant and the terms $\sum K_i C_i$ represent the combined effect of all adsorbed intermediate species.

This proposed model has been successfully implemented by different authors (Ibrahim, 2001; Ibrahim and de Lasa, 2003; Garcia-Hernandez et al; 2010, 2012) to describe the kinetics of photoconversion of diverse organic compounds with TiO_2 as photocatalyst. This model has been proven adequate to describe the observed changes of the chemical species concentrations in the gas phase (Ibrahim and de Lasa, 2004).

In order to adopt this model, a number of conditions must apply:

- a) The gas phase was UV transparent with absorption. The scattering and reflection of the light were all negligible.
- b) The mixing in the Photo-CREC-Air-Reactor was intense, given the high air recirculation. Gas phase concentrations of all species could be considered constant at any given time.
- c) The windows in the reaction section were free of deposited particles. The adsorption of reactants on the reactor wall materials was negligible.
- d) The mesh supporting the TiO_2 was constantly irradiated by the near UV lamps with an intensity of light that did not change significantly during the experiments.
- e) The contribution of the thermal reactions to the photoconversion process was insignificant.

Based on the above conditions, the following equation was proposed:

$$V \frac{dC}{dt} = rA_{irr} \quad (14)$$

where V represents the total hold up of the gas in the reactor (m^3), where C is the pollutant concentration ($\mu\text{mol}/\text{m}^3$), where r is the rate of photocatalytic reaction ($\mu\text{mol}/\text{min cm}^2$) and where A_{irr} is the irradiated mesh area (cm^2).

6.3 Acetone Photocatalytic Degradation Modeling

The acetone photocatalytic degradation kinetics can be modeled by using the following reaction stoichiometry:



This model hypothesizes that: a) the key intermediate species in the photocatalytic acetone conversion are the OH^\bullet groups, a likely scenario if the treated air contains ambient humidity, b) acetone and CO_2 are the only carbon containing chemical species coexisting in the reaction media.

On this basis, the following stoichiometric relationship can be considered and expressed as:

$$\frac{r_{ACETONE}}{\nu_{ACETONE}} = \frac{r_{OH^\bullet}}{\nu_{OH^\bullet}} \quad \Rightarrow \quad r_{OH^\bullet} = \frac{\nu_{OH^\bullet}}{\nu_{ACETONE}} r_{ACETONE} \quad (16)$$

where:

$\nu_{ACETONE}$ = stoichiometric coefficient for acetone

ν_{OH^\bullet} = stoichiometric coefficient for OH^\bullet

Thus,

$$r_{OH^\bullet} = \frac{-16}{-1} r_{ACETONE} = 16r_{ACETONE} \quad (17)$$

It is known that the amount of acetone in the fluid phase is the result of adsorption and photoconversion processes. Thus, the mole balance for acetone is as follows:

$$N_{ACETONE,T} = N_{ACETONE,g} + N_{ACETONE,s} \quad (18)$$

where $N_{ACETONE,T}$ is the total number of moles of acetone, $N_{ACETONE,g}$ is the number of moles of acetone in the gas phase and $N_{ACETONE,s}$ is the number of moles adsorbed on the solid photocatalyst.

By dividing all terms in equation (18) by V , the total system volume, the following equation can be expressed:

$$C_{ACETONE,T} = C_{ACETONE,g} + \frac{N_{ACETONE,s}}{V} \quad (19)$$

where $C_{ACETONE,T}$ is the total concentration of acetone ($\mu\text{mol}/\text{m}^3$), $C_{ACETONE,g}$ is the number of moles of acetone in the gas phase ($\mu\text{mol}/\text{m}^3$) and V is the total system volume (m^3).

Moreover, if during the photocatalytic process, the equilibrium is reached at all times, the amount of acetone is given by:

$$N_{ACETONE,s} = q_{ACETONE}W = \zeta_{ACETONE}Wq_{ACETONE,max} \quad (20)$$

$$\text{with } \zeta_{ACETONE} = \frac{q_{ACETONE}}{q_{ACETONE,max}} \quad (21)$$

and $q_{ACETONE}$ being the specific amount of acetone adsorbed on the photocatalyst ($\mu\text{mol}/\text{g}$), $q_{ACETONE,max}$ being the maximum acetone adsorbed on the photocatalyst ($\mu\text{mol}/\text{g}$) and W being the total weight of the adsorbent substrate (g).

The value of $\zeta_{ACETONE}$ can be related to the acetone concentration in the gas phase. This is done through a pseudo equilibrium constant evaluated at one point of the adsorption equilibrium isotherm:

$$\zeta_{ACETONE} = K^A_{ACETONE} C_{ACETONE} \quad (22)$$

Thus, the total concentration of acetone can be defined as:

$$C_{ACETONE,T} = C_{ACETONE,g} (1 + K'_{ACETONE}) \quad (23)$$

where the dimensionless adsorption constant is given by:

$$K'_{ACETONE} = \frac{K^A_{ACETONE} W q_{ACETONE,max}}{V} \quad (24)$$

As a result, the total reaction rate for acetone photoconversion can be obtained by taking the derivative of equation (23), as in equation (25):

$$r_{ACETONE,T} = r_{ACETONE,g} (1 + K'_{ACETONE}) \quad (25)$$

where $r_{ACETONE,T}$ is the total reaction rate ($\mu\text{mol}/(\text{m}^2 \cdot \text{min})$) and $r_{ACETONE,g}$ is the reaction rate involving the observed chemical species concentration changes in the gas phase ($\mu\text{mol}/(\text{m}^2 \cdot \text{min})$).

Taking into account the operation conditions under which the reaction takes place where: a) the rate of acetone consumption follows a Langmuir-Hinshelwood model, as described in equation (13), b) Acetone and CO_2 are the only detectable carbon containing species, c) CO_2 adsorbs weakly on the photocatalyst surface; the following applies:

$$r_{ACETONE,g} = \frac{dC_{ACETONE,g}}{dt} \frac{V}{A_{irr}} = - \frac{k_{ACETONE} K^A_{ACETONE} C_{ACETONE,g}}{1 + K^A_{ACETONE} C_{ACETONE,g}} \frac{V}{A_{irr}} \quad (26)$$

This expression can also be -written as,

$$r_{ACETONE,g} = - \frac{C_{ACETONE,g}}{\theta_{A1} + \theta_{A2} C_{ACETONE,g}} \frac{V}{A_{irr}} \quad (27)$$

where:

$r_{ACETONE,g}$ = rate of acetone photocatalytic degradation as assessed by changes in the gas phase concentrations, $\mu\text{mol}/(\text{m}^2 \cdot \text{min})$

$C_{ACETONE,g}$ = acetone concentration in the gas phase, $\mu\text{mol}/\text{m}^3$

A_{irr} = irradiated mesh area holding the catalyst, m^2

$K^A_{ACETONE}$ = acetone adsorption constant, $\text{m}^3/\mu\text{mol}$

$k_{ACETONE}$ = reaction rate constant, $\mu\text{mol}/(\text{m}^3 \cdot \text{min})$

$\theta_{A1} = 1/(k_{ACETONE} K^A_{ACETONE})$, min

$\theta_{A2} = 1/k_{ACETONE}$, $\text{m}^3 \cdot \text{min} / \mu\text{mol}$

In this case, the kinetic model involving the θ_{A1} and θ_{A2} parameters can be used to fit the experimental data. In this case, the objective function to be minimized is defined as:

$$\sum_{i=1}^{1-n} \left(\frac{C_{ACETONE,EXPERIMENTAL,i} - C_{ACETONE,MODEL,i}}{C_{ACETONE,EXPERIMENTAL,i}} \right)^2 \quad (28)$$

where n represents the number of experimental data points.

6.4 Acetaldehyde Photocatalytic Degradation Modeling

Acetaldehyde photocatalytic degradation can be described using the overall stoichiometry in a similar way as it was done for acetone:



It is assumed in equation (29) that a) the key intermediate species in the photocatalytic acetaldehyde conversion are the OH^\bullet groups, a likely scenario if the treated air contains ambient humidity, b) acetaldehyde and CO_2 are the only coexisting carbon containing species.

As a result, the rate of photoconversion of acetaldehyde and the OH^\bullet group consumption rate can be related as follows:

$$\frac{r_{ACETALDEHYDE}}{v_{ACETALDEHYDE}} = \frac{r_{OH^\bullet}}{v_{OH^\bullet}} \quad \text{and} \quad r_{OH^\bullet} = \frac{v_{OH^\bullet}}{v_{ACETALDEHYDE}} r_{ACETALDEHYDE} \quad (30)$$

where:

$v_{ACETALDEHYDE}$ = stoichiometric coefficient for acetaldehyde

v_{OH^\bullet} = stoichiometric coefficient for OH^\bullet

Thus, according to stoichiometry:

$$r_{OH^\bullet} = \frac{-10}{-1} r_{ACETALDEHYDE} = 10r_{ACETALDEHYDE} \quad (31)$$

Since the adsorption and photoconversion processes determine the amount of acetaldehyde in the fluid phase, the mole balance for acetaldehyde is as follows:

$$N_{ACETALDEHYDE,T} = N_{ACETALDEHYDE,g} + N_{ACETALDEHYDE,s} \quad (32)$$

where $N_{ACETALDEHYDE,T}$ is the total number of moles of acetaldehyde, $N_{ACETALDEHYDE,g}$ is the number of moles of acetaldehyde in the gas phase and $N_{ACETALDEHYDE,s}$ is the number of moles of acetaldehyde adsorbed on the photocatalyst.

One can divide all the terms of equation (32) by the total system volume V as shown below:

$$C_{ACETALDEHYDE,T} = C_{ACETALDEHYDE,g} + \frac{N_{ACETALDEHYDE,s}}{V} \quad (33)$$

where $C_{ACETALDEHYDE,T}$ is the total acetaldehyde concentration ($\mu\text{mol}/\text{m}^3$), $C_{ACETALDEHYDE,g}$ is the number of moles of acetaldehyde in the gas phase ($\mu\text{mol}/\text{m}^3$) and V is the total system volume (m^3).

If equilibrium is reached at all times during the photocatalytic process, the amount of acetaldehyde is given by:

$$N_{ACETALDEHYDE,s} = q_{ACETALDEHYDE} W = \zeta_{ACETALDEHYDE} W q_{ACETALDEHYDE,max} \quad (34)$$

$$\text{with } \zeta_{ACETALDEHYDE} = \frac{q_{ACETALDEHYDE}}{q_{ACETALDEHYDE,max}} \quad (35)$$

and $q_{ACETALDEHYDE}$ being the specific amount of acetaldehyde adsorption on the photocatalyst ($\mu\text{mol}/\text{g}$), $q_{ACETALDEHYDE,max}$ being the maximum amount of acetaldehyde adsorption on the photocatalyst ($\mu\text{mol}/\text{g}$) and W being the total weight of the adsorbent substrate (g).

As in the case of acetone, the value of the parameter $\zeta_{ACETALDEHYDE}$ is related to the concentration of acetaldehyde in the gas phase. This takes place through a pseudo equilibrium constant evaluated at one point of the adsorption equilibrium isotherm as follows:

$$\zeta_{ACETALDEHYDE} = K^A_{ACETALDEHYDE} C_{ACETALDEHYDE} \quad (36)$$

Thus, the total concentration of acetaldehyde is given by:

$$C_{ACETALDEHYDE,T} = C_{ACETALDEHYDE,g} (1 + K'_{ACETALDEHYDE}) \quad (37)$$

where the dimensionless adsorption constant is defined as:

$$K'_{ACETALDEHYDE} = \frac{K^A_{ACETALDEHYDE} W q_{ACETALDEHYDE,max}}{V} \quad (38)$$

Moreover, considering the time derivative of equation (38), it is possible to obtain the total reaction rate for acetaldehyde photodegradation as follows:

$$r_{ACETALDEHYDE,T} = r_{ACETALDEHYDE,g} (1 + K'_{ACETALDEHYDE}) \quad (39)$$

where $r_{ACETALDEHYDE,T}$ is the total reaction rate ($\mu\text{mol}/(\text{m}^2 \cdot \text{min})$), $r_{ACETALDEHYDE,g}$ is the reaction rate defined with concentration changes in the gas phase ($\mu\text{mol}/(\text{m}^2 \cdot \text{min})$) and $K'_{ACETALDEHYDE}$ is a dimensionless adsorption parameter.

Given the operation conditions under which the photocatalytic reaction takes place where: a) the rate of acetaldehyde consumption follows a Langmuir-Hinshelwood model, as described in equation (13), b) acetaldehyde and CO_2 are the only detectable carbon containing species, c) the CO_2 adsorbs weakly on the photocatalyst surface, the following applies:

$$r_{ACETALDEHYDE,g} = \frac{dC_{ACETALDEHYDE,g}}{dt} \frac{V}{A_{irr}} = - \frac{k_{ACETALDEHYDE} K^A_{ACETALDEHYDE} C_{ACETALDEHYDE,g}}{1 + K^A_{ACETALDEHYDE} C_{ACETALDEHYDE,g}} \frac{V}{A_{irr}} \quad (40)$$

This rate expression can be rewritten as:

$$r_{ACETALDEHYDE,g} = - \frac{C_{ACETALDEHYDE,g}}{\theta_{AA1} + \theta_{AA2} C_{ACETALDEHYDE,g}} \frac{V}{A_{irr}} \quad (41)$$

where:

$r_{ACETALDEHYDE,g}$ = rate of acetaldehyde photocatalytic degradation as assessed by changes in the gas phase concentrations, $\mu\text{mol}/(\text{m}^2 \cdot \text{min})$

$C_{ACETALDEHYDE,g}$ = acetaldehyde concentration in the gas phase, $\mu\text{mol}/\text{m}^3$

A_{irr} = illuminated mesh area, m^2

$K^A_{ACETALDEHYDE}$ = acetaldehyde adsorption constant, $\text{m}^3/\mu\text{mol}$

$k_{ACETALDEHYDE}$ = reaction rate constant, $\mu\text{mol}/(\text{m}^3 \cdot \text{min})$

$\theta_{AA1} = 1/(k_{ACETALDEHYDE} K^A_{ACETALDEHYDE})$, min

$\theta_{AA2} = 1/k_{ACETALDEHYDE}$, $\text{m}^3 \cdot \text{min} / \mu\text{mol}$

Values for the parameters θ_{AA1} and θ_{AA2} can be obtained using nonlinear regression, with minimization of the following objective function:

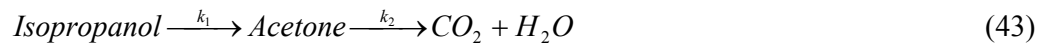
$$\sum_{i=1}^{i=n} \left(\frac{C_{ACETALDEHYDE,EXPERIMENTAL,i} - C_{ACETALDEHYDE,MODEL,i}}{C_{ACETALDEHYDE,EXPERIMENTAL,i}} \right)^2 \quad (42)$$

6.5 Isopropanol Photocatalytic Degradation Modeling

In contrast with the photocatalytic conversion of acetone and acetaldehyde, it was observed that the photocatalytic conversion of isopropanol involves three observable carbon containing species: isopropanol, acetone and CO₂. No other carbon containing by-products were detected in the photocatalytic degradation under the studied conditions.

In order to describe these chemical changes, an in-series step mechanism is postulated. The first step involves a transformation of isopropanol into acetone. This is followed by an acetone oxidation conversion step into carbon dioxide and water. Thus, based on this and on the weak CO₂ adsorption, it can be speculated that both isopropanol and acetone molecules compete for the same TiO₂ sites.

As a result, the following reaction equations can be put forth to establish the kinetic modeling of the isopropanol photocatalytic degradation using the initial rate of photoconversion:



Following this, a stoichiometric relationship can be postulated as:

$$\frac{r_{\text{ISOPROPANOL}}}{V_{\text{ISOPROPANOL}}} = \frac{r_{\text{OH}^\bullet}}{V_{\text{OH}^\bullet}} \quad \text{and} \quad r_{\text{OH}^\bullet} = \frac{V_{\text{OH}^\bullet}}{V_{\text{ISOPROPANOL}}} r_{\text{ISOPROPANOL}} \quad (45)$$

where:

$V_{\text{ISOPROPANOL}}$ = stoichiometric coefficient for isopropanol

V_{OH^\bullet} = stoichiometric coefficient for OH[•]

Thus:

$$r_{\text{OH}^\bullet} = \frac{-16}{-1} r_{\text{ISOPROPANOL}} = 16r_{\text{ISOPROPANOL}} \quad (46)$$

It is known that the amount of isopropanol in the fluid phase is the result of adsorption and photoconversion processes. The mole balance for isopropanol is as follows:

$$N_{ISOPROPANOL,T} = N_{ISOPROPANOL,g} + N_{ISOPROPANOL,s} \quad (47)$$

where $N_{ISOPROPANOL,T}$ is the total number of moles of isopropanol, $N_{ISOPROPANOL,g}$ is the number of moles of isopropanol in the gas phase and $N_{ISOPROPANOL,s}$ is the number of moles of isopropanol adsorbed on the photocatalyst.

Equation (47) can be modified to include the concentration in each of the phases:

$$N_{ISOPROPANOL,T} = C_{ISOPROPANOL,g}V + q_{ISOPROPANOL}W \quad (48)$$

where $C_{ISOPROPANOL,g}$ is the number of moles of isopropanol in the gas phase ($\mu\text{mol}/\text{m}^3$), V is the total system volume (m^3), $q_{ISOPROPANOL}$ is the isopropanol adsorption capacity ($\mu\text{mol}/\text{g}_{\text{cat}}$) and W is the total weight of the adsorbent substrate (g).

This equation can be rewritten to include the fraction adsorption coverage of isopropanol on the photocatalyst surface:

$$N_{ISOPROPANOL,T} = C_{ISOPROPANOL,g}V + \zeta_{ISOPROPANOL}q_{ISOPROPANOL,max}W \quad (49)$$

$$\text{with } \zeta_{ISOPROPANOL} = \frac{q_{ISOPROPANOL}}{q_{ISOPROPANOL,max}} \quad (50)$$

and $q_{ISOPROPANOL,max}$ being the maximum amount of isopropanol adsorbed on the photocatalyst ($\mu\text{mol}/\text{g}$). According to the adsorption equilibrium between phases, the value of $\zeta_{ISOPROPANOL}$ can be related to the isopropanol concentration in the gas phase. This is done through the use of a pseudo equilibrium constant evaluated at one point of the adsorption equilibrium isotherm:

$$\zeta_{ISOPROPANOL} = K^A_{ISOPROPANOL}C_{ISOPROPANOL,g} \quad (51)$$

Therefore, equation (51) can be rewritten as follows:

$$N_{ISOPROPANOL,T} = C_{ISOPROPANOL,g}V + K^A_{ISOPROPANOL}C_{ISOPROPANOL,g}q_{ISOPROPANOL,max}W \quad (52)$$

or

$$N_{ISOPROPANOL,T} = \left(V + K^A_{ISOPROPANOL} q_{ISOPROPANOL,max} W \right) C_{ISOPROPANOL,g} \quad (53)$$

Thus, the total concentration of isopropanol can be defined as:

$$C_{ISOPROPANOL,T} = \left(1 + \frac{K^A_{ISOPROPANOL} q_{ISOPROPANOL,max} W}{V} \right) C_{ISOPROPANOL,g} \quad (54)$$

By differentiating equation (54), it becomes:

$$\frac{dC_{ISOPROPANOL,T}}{dt} = \left(1 + K'_{ISOPROPANOL} \right) \frac{dC_{ISOPROPANOL,g}}{dt} \quad (55)$$

Using a similar procedure for acetone, it results:

$$\frac{dC_{ACETONE,T}}{dt} = \left(1 + K'_{ACETONE} \right) \frac{dC_{ACETONE,g}}{dt} \quad (56)$$

where the dimensionless isopropanol and acetone adsorption constants are given by:

$$K'_{ISOPROPANOL} = \frac{K^A_{ISOPROPANOL} q_{ISOPROPANOL,max} W}{V} \quad (57)$$

$$K'_{ACETONE} = \frac{K^A_{ACETONE} q_{ACETONE,max} W}{V} \quad (58)$$

It is possible to express the isopropanol reaction rate equation by considering the total change in the moles of isopropanol as follows:

$$\frac{dN_{ISOPROPANOL,T}}{dt} = A_{irr} r_{ISOPROPANOL,T} \quad (59)$$

or

$$\frac{dC_{ISOPROPANOL,T}}{dt} = \frac{A_{irr}}{V} r_{ISOPROPANOL,T} \quad (60)$$

Introducing equation (56) in equation (60) gives the following:

$$(1 + K'_{ISOPROPANOL}) \frac{dC_{ISOPROPANOL,g}}{dt} = \frac{A_{irr}}{V} r_{ISOPROPANOL,T} \quad (61)$$

$$r_{ISOPROPANOL,T} = \frac{dC_{ISOPROPANOL,g}}{dt} \frac{A_{irr}}{V} (1 + K'_{ISOPROPANOL}) = r_{ISOPROPANOL,g} (1 + K'_{ISOPROPANOL}) \quad (62)$$

Following this approach, the total rate of photocatalytic conversion of isopropanol can be defined. This is done by taking as a basis, the rate of photocatalytic conversion in the gas phase and introducing a $(1 + K'_{ISOPROPANOL})$ correction factor.

$$r_{ISOPROPANOL,T} = r_{ISOPROPANOL,g} (1 + K'_{ISOPROPANOL}) \quad (63)$$

Similarly, the total change of acetone in the reacting system can be expressed in terms of the change of acetone in the gas phase. It is important to notice that given that acetone is involved in two different reaction steps, the total rate of acetone photoconversion has to include both acetone production and consumption. This is expressed in the following equation:

$$r_{ACETONE,T} = \frac{dC_{ACETONE,g}}{dt} \frac{A_{irr}}{V} (1 + K'_{ACETONE}) = r_p - r_c \quad (64)$$

where

r_p = rate of acetone production ($\mu\text{mol}/\text{cm}^2 \cdot \text{min}$)

r_c = rate of acetone consumption ($\mu\text{mol}/\text{cm}^2 \cdot \text{min}$)

or ,

$$\frac{V}{A_{irr}} (1 + K'_{ACETONE}) \frac{dC_{ACETONE,g}}{dt} = r_{ISOPROPANOL,g} (1 + K'_{ISOPROPANOL}) - r_{ACETONE,g} (1 + K'_{ACETONE}) \quad (65)$$

and

$$\frac{dC_{ACETONE,g}}{dt} = \frac{A_{irr}}{V} \left(r_{ISOPROPANOL,g} \frac{(1 + K'_{ISOPROPANOL})}{(1 + K'_{ACETONE})} - r_{ACETONE,g} \right) \quad (66)$$

Thus, changes of acetone concentration in the gas phase are given by the following equation:

$$\frac{dC_{ACETONE,g}}{dt} = \frac{A_{irr}}{V} (r_{ISOPROPANOL,g} \cdot \phi - r_{ACETONE,g}) \quad (67)$$

with

$$\phi = \frac{(1 + K'_{ISOPROPANOL})}{(1 + K'_{ACETONE})} \quad (68)$$

As stated above, the only carbon containing species detected in the gas phase during isopropanol photocatalytic conversion were, besides the isopropanol itself, acetone and carbon dioxide. Given that the adsorption of carbon dioxide was negligible, a rate of isopropanol photoconversion using a Langmuir-Hinshelwood model involved both isopropanol and acetone species competing for the same catalyst sites. Thus, the following can be postulated:

$$r_{ISOPROPANOL,g} = \frac{dC_{ISOPROPANOL,g}}{dt} \frac{V}{A_{irr}} = - \frac{(k_1 + k_3) K^A_{ISOPROPANOL} C_{ISOPROPANOL,g}}{1 + K^A_{ISOPROPANOL} C_{ISOPROPANOL,g} + K^A_{ACETONE} C_{ACETONE,g}} \frac{V}{A_{irr}} \quad (69)$$

where:

$r_{ISOPROPANOL,g}$ = rate of isopropanol photodegradation as assessed by changes in the gas phase concentrations, $\mu\text{mol}/(\text{m}^2 \cdot \text{min})$

$C_{ISOPROPANOL,g}$ = isopropanol concentration in the gas phase, $\mu\text{mol}/\text{m}^3$

$C_{ACETONE,g}$ = acetone concentration in the gas phase, $\mu\text{mol}/\text{m}^3$

A_{irr} = irradiated mesh area holding the catalyst, m^2

$K^A_{ISOPROPANOL}$ = isopropanol adsorption constant, $\text{m}^3/\mu\text{mol}$

$K^A_{ACETONE}$ = acetone adsorption constant, $\text{m}^3/\mu\text{mol}$

k_1 = reaction rate constant of the isopropanol to acetone reaction, $\mu\text{mol}/(\text{m}^3 \cdot \text{min})$

k_3 = reaction rate constant of the isopropanol to CO_2 reaction, $\mu\text{mol}/(\text{m}^3 \cdot \text{min})$

The rate of acetone photoconversion can be represented in a similar manner with the following expression:

$$r_{ACETONE,g} = \frac{dC_{ACETONE,g}}{dt} \frac{V}{A_{irr}} = \frac{k_1 K^A_{ISOPROPANOL} C_{ISOPROPANOL,g} \phi - k_2 K^A_{ACETONE} C_{ACETONE,g}}{1 + K^A_{ISOPROPANOL} C_{ISOPROPANOL,g} + K^A_{ACETONE} C_{ACETONE,g}} \frac{V}{A_{irr}} \quad (70)$$

where k_2 is the intrinsic rate constant for acetone conversion in the isopropanol photoconversion as described in equation (43), expressed in $\mu\text{mol}/(\text{m}^3 \cdot \text{min})$.

Furthermore, the kinetic modeling of the photocatalytic isopropanol conversion in the Photo-CREC-Air reactor involves the simultaneous evaluation of the following set of equations:

$$\frac{dC_{ISOPROPANOL,g}}{dt} = \frac{A_{irr}}{V} r_{ISOPROPANOL,g} \quad (71)$$

$$\frac{dC_{ACETONE,g}}{dt} = \frac{A_{irr}}{V} (r_{ISOPROPANOL1,g} \cdot \phi - r_{ACETONE,g}) \quad (72)$$

$$\frac{dC_{CO_2}}{dt} = \frac{A_{irr}}{V} 3(r_{ACETONE,g} + r_{ISOPROPANOL2,g}) \quad (73)$$

The following set of equations can be expressed in terms of the kinetic and adsorption constants as:

$$r_{ISOPROPANOL,g} = - \frac{(k_1 + k_3) K^A_{ISOPROPANOL} C_{ISOPROPANOL,g}}{1 + K^A_{ISOPROPANOL} C_{ISOPROPANOL,g} + K^A_{ACETONE,g} C_{ACETONE,g}} \quad (74)$$

$$r_{ACETONE,g} = \frac{k_1 K^A_{ISOPROPANOL} C_{ISOPROPANOL,g} \phi - k_2 K^A_{ACETONE,g} C_{ACETONE,g}}{1 + K^A_{ISOPROPANOL} C_{ISOPROPANOL,g} + K^A_{ACETONE,g} C_{ACETONE,g}} \quad (75)$$

$$r_{CO_2,g} = \frac{3(k_2 K^A_{ACETONE,g} C_{ACETONE,g} + k_3 K^A_{ISOPROPANOL} C_{ISOPROPANOL,g})}{1 + K^A_{ISOPROPANOL} C_{ISOPROPANOL,g} + K^A_{ACETONE,g} C_{ACETONE,g}} \quad (76)$$

Once the kinetic model for the isopropanol photocatalytic degradation is established, a numerical regression is required to obtain the values of the different parameters involved.

In order to accomplish this, the sum of the experimental and theoretical concentration differences is to be minimized. In the case of isopropanol photocatalytic degradation, the following minimization of objective function is proposed:

$$\sum_{i=1}^{i=n} \frac{(C_{ACETONE,EXPERIMENTAL,i} - C_{ACETONE,MODEL,i})^2 + (C_{ISOPROPANOL,EXPERIMENTAL,i} - C_{ISOPROPANOL,MODEL,i})^2}{(C_{ISOPROPANOL,EXPERIMENTAL,i} - C_{ACETONE,EXPERIMENTAL,i})^2} \quad (77)$$

where the subindex i allows one to fit the model to the data of the different experiments.

6.6 Conclusions

- a) This chapter describes the kinetic models suitable for the photocatalytic degradation of model pollutants in air.
- b) A Langmuir-Hinshelwood rate equation is considered for acetone and acetaldehyde photocatalytic degradation with Degussa P25. This equation involves a one-site adsorption based mechanism.
- c) A similar Langmuir-Hinshelwood rate equation is adopted for the photocatalytic degradation of isopropanol with Degussa P25. The proposed mechanism involves a one-site adsorption mechanism. Measurable chemical species compete for adsorption on the same site.
- d) Parameters related to each one of the kinetic models are proposed to be calculated using nonlinear regression.
- e) Evaluated kinetic parameters are considered very valuable for establishing quantum efficiencies and Photochemical Thermodynamic Efficiency Factors.

Chapter 7

Results and Discussion II: Energy Efficiencies in Previous Versions of the Photo-CREC-Air Reactor

7.1 Introduction

This chapter considers the calculation of the quantum yields and the Photochemical Thermodynamic Efficiency Factors (*PTEF*) for the various experiments performed during the present PhD Dissertation.

This chapter describes the application of these factors to experimental results obtained in a previous version of the Photo-CREC-Air Reactor with a volume of 14.7 liters. This procedure has been helpful to establish comparative values and start delimiting the capabilities of photocatalysis as an air treatment technology.

To accomplish this, results reported by Ibrahim (2001) and Ibrahim and de Lasa (2004) for the photocatalytic degradation of acetone and acetaldehyde with the commercial photocatalysts Hombikat UV-100 and Degussa P25 were used. The kinetic model proposed by these authors was based on a Langmuir-Hinshelwood rate equation.

Results reported in this chapter, are part of a paper already published by Garcia-Hernandez et al. in 2010. This paper represents a first attempt to implement the Photochemical Thermodynamic Efficiency Factor (*PTEF*) as an energy efficiency parameter for air treatment applications in the technical literature.

7.2 Quantum Efficiency in Previous Photo-CREC-Air Reactor Versions

The definition of quantum yield was modified in the present study. It accounts for the rate of OH^\bullet radicals converted at any particular time during the photoconversion over the rate of photons reaching the photocatalyst as described in equation (78),

$$QY_{app} = \frac{\text{number of } OH^\bullet \text{ consumed}}{\text{number of photons reaching the photocatalyst with } \lambda \leq 388nm} \quad (78)$$

This definition considers the key role played by OH^\bullet radicals as the driving force of the photocatalytic reaction as proposed by Pichat (2010).

It has to be noted that in the previous Photo-CREC-Air Unit (Ibrahim, 2001), the irradiation measurement reaching the surface of the photocatalyst was the only available irradiation data. This fact is reflected in the denominator of equation (78). However, and later in the upcoming chapters of this PhD dissertation, an improved definition of the quantum yields will be considered based on absorbed photons as a more adequate approach for energy efficiency calculations.

Quantum yield calculations using equation (80) for the photocatalytic degradation of acetone with the data as reported by Ibrahim and de Lasa (2004) are shown in Figures 22 and 23. Figure 22 shows the results using the Hombikat UV-100 photocatalyst while Figure 23 shows the results using the Degussa P25 photocatalyst.

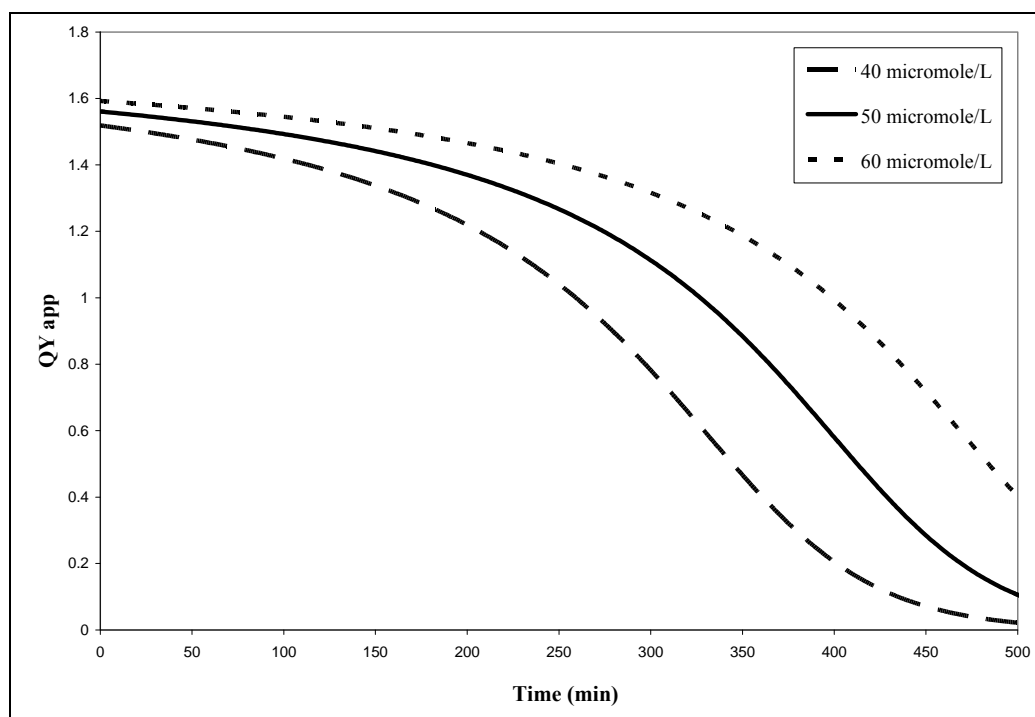


Figure 22: QY_{app} for acetone using experimental data reported by Ibrahim and de Lasa (2004) with the catalyst Hombikat UV-100. Three initial concentrations in $\mu\text{mol/L}$: 40, 50 and 60.

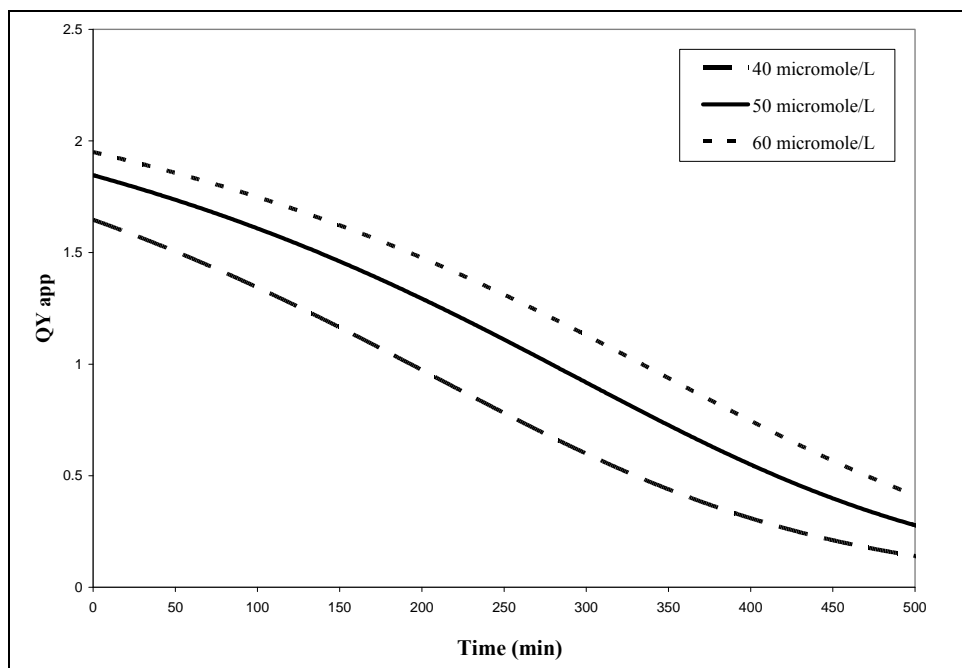


Figure 23: QY_{app} for acetone using experimental data reported by Ibrahim and de Lasa (2004) with the catalyst Degussa P25. Three initial concentrations in $\mu\text{mol/L}$: 40, 50 and 60.

Figure 24 depicts the quantum yields for the photocatalytic degradation of acetaldehyde over Hombikat UV-100, whereas Figure 25 shows the same parameter with Degussa P25.

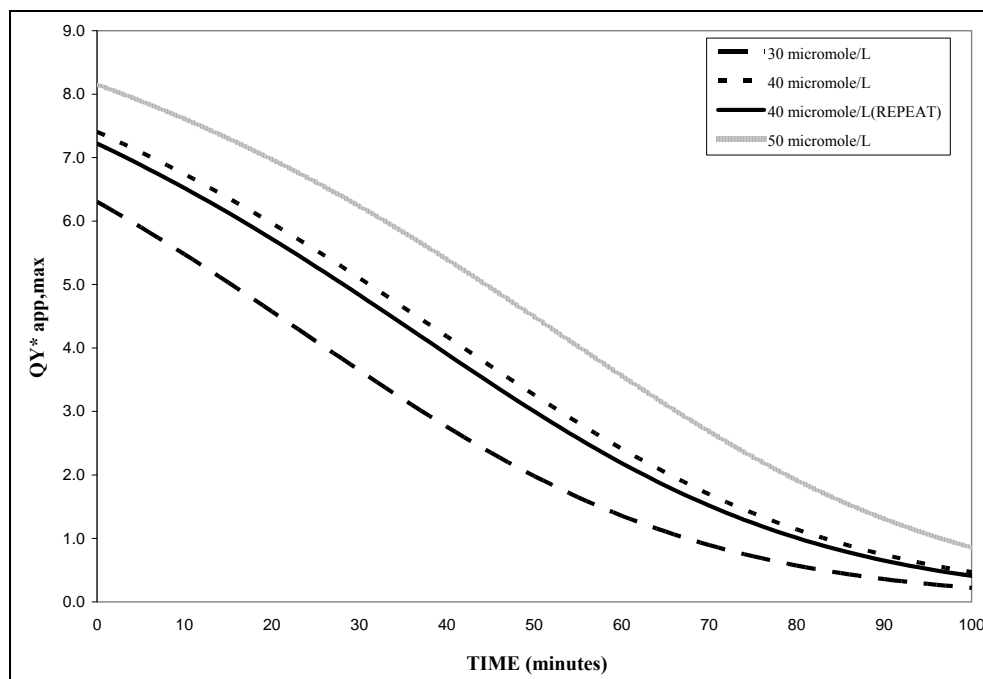


Figure 24: QY_{app} for acetaldehyde using experimental data reported by Ibrahim and de Lasa (2004) with the catalyst Hombikat UV-100. Three initial concentrations in $\mu\text{mol/L}$: 30, 40 and 50.

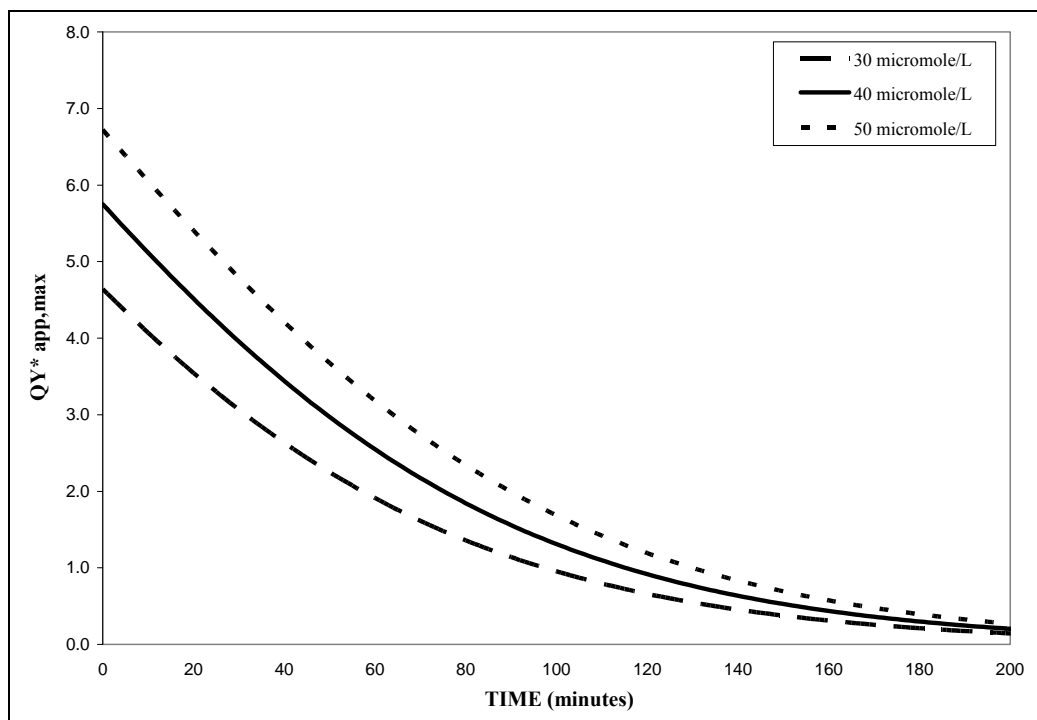


Figure 25: QY_{app} for acetaldehyde using experimental data reported by Ibrahim and de Lasa (2004) with the catalyst Degussa P25. Three initial concentrations in $\mu\text{mol/L}$: 30, 40 and 50.

It is noticeable that quantum yields for both acetone and acetaldehyde photocatalytic degradation are, during most of the irradiation period, in excess of the theoretical maximum of 133% (Appendix A).

More specifically, in the case of the photocatalytic degradation of acetone, at initial irradiation conditions, the quantum yields fall in the 1.5-1.6 range (equivalent to 150-160%) when Hombikat UV-100 is used and in the 1.65-1.95 range (equivalent to 165-195%) when Degussa P25 is used,

Furthermore, during initial irradiation, the quantum yields obtained for the photocatalytic degradation of acetaldehyde based on the consumed OH^\bullet groups, once again surpass the value of 1. These quantum yields are in the 6.3-8.15 range (equivalent to 630-815%) for Hombikat UV-100 and in the 4.6-6.7 (equivalent to 460-670%) for Degussa P25.

7.3 Photochemical-Thermodynamic Efficiency Factor (*PTEF*) in Previous Photo-CREC-Air Reactor Versions.

The Photochemical Thermodynamic Efficiency Factor (*PTEF*) was defined as the product of *QY* and η_{OH^\bullet} . *QY* accounts for the fraction of photons absorbed by the photocatalyst leading to the formation of OH^\bullet radicals (quantum yield) as follows:

$$PTEF_{app} = QY_{app} \eta_{OH^\bullet} \quad (79)$$

where η_{OH^\bullet} is the fraction of photon energy used in forming an OH^\bullet radical. This is given by

$$\eta_{OH^\bullet} = \frac{\Delta H_{OH^\bullet}}{E_{av}} \quad (80)$$

with ΔH_{OH^\bullet} being the enthalpy of formation of an OH^\bullet group ($J\ mol^{-1}$) and E_{av} being the average energy of a photon (Appendix B).

The *PTEFs* obtained during the photocatalytic degradation of acetone at three different initial concentrations using Hombikat UV-100 and Degussa P25 were calculated using equation (79). They are reported in Figures 26 and 27 for the acetone photocatalytic degradation and in Figures 28 and 29 for the photocatalytic degradation of acetaldehyde. The values of the *PTEFs* were calculated again on the assumption that the OH^\bullet groups consumed are the only ones driving the photocatalytic degradation.

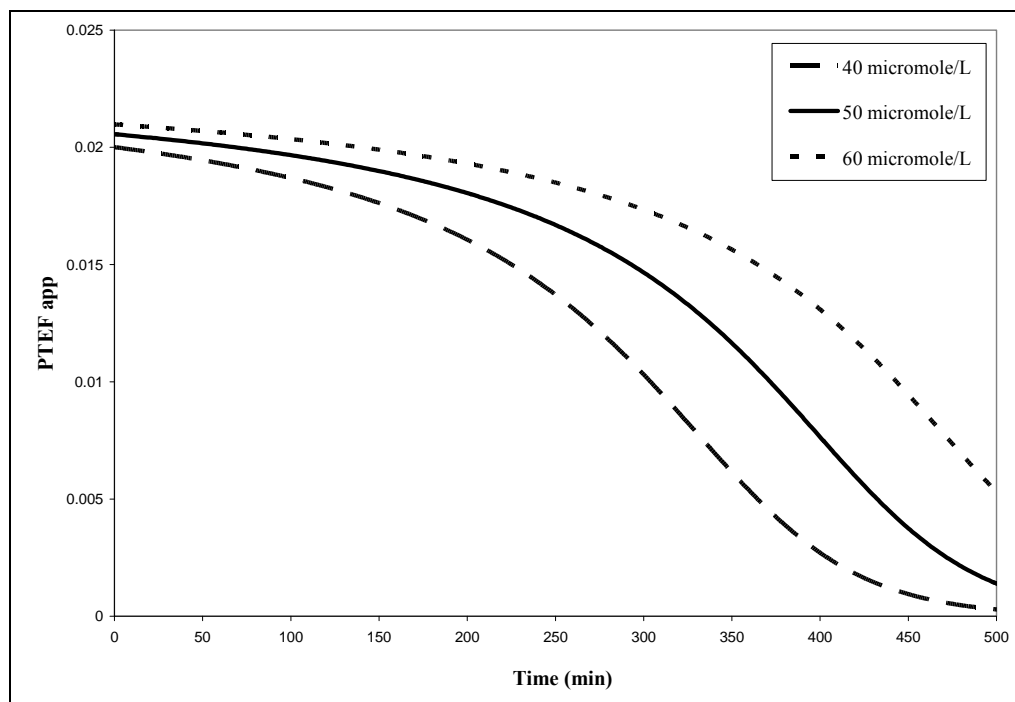


Figure 26: $PTEF_{app}$ for acetone using experimental data reported by Ibrahim and de Lasa (2004) with the catalyst Hombikat UV-100. Three initial concentrations in $\mu\text{mol/L}$: 40, 50 and 60.

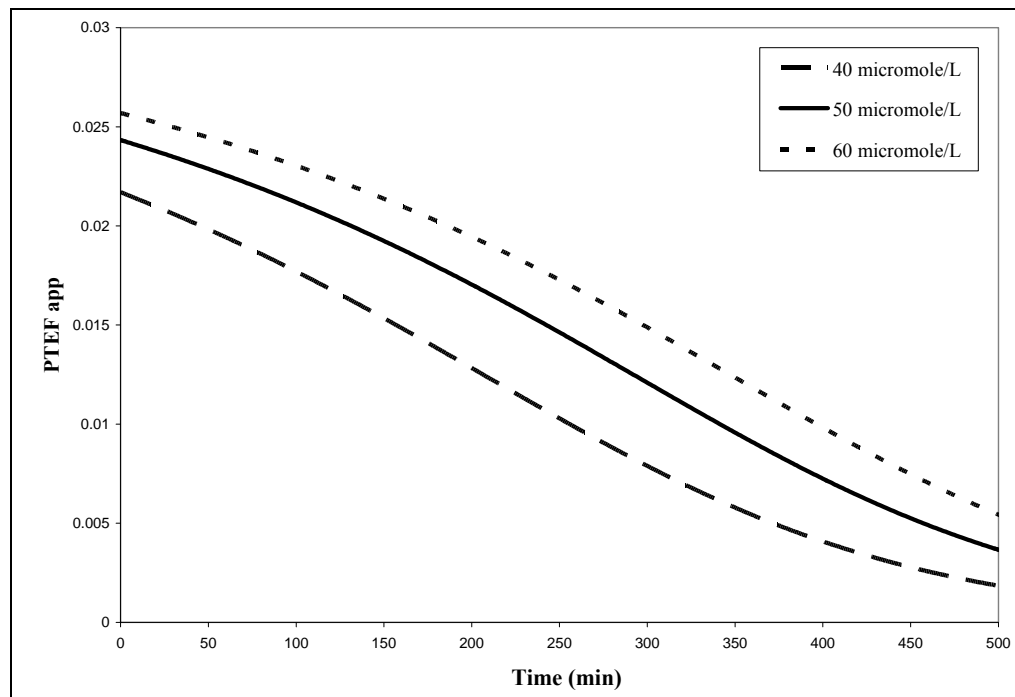


Figure 27: $PTEF_{app}$ for acetone using experimental data reported by Ibrahim and de Lasa (2004) with the catalyst Degussa P25. Three initial concentrations in $\mu\text{mol/L}$: 40, 50 and 60.

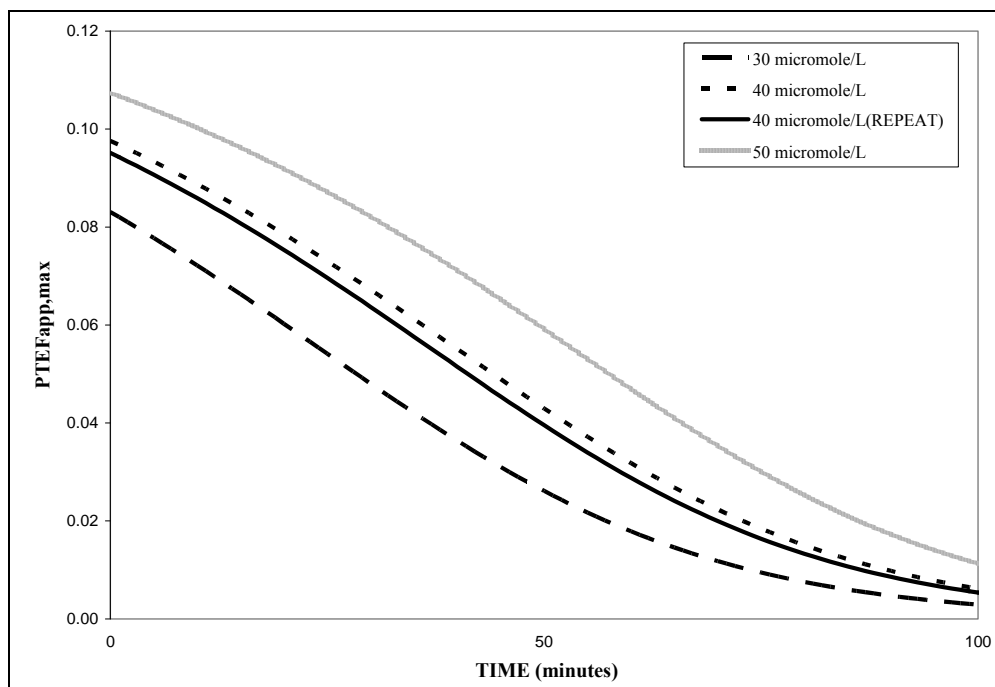


Figure 28: $PTEF_{app}$ for acetaldehyde using experimental data reported by Ibrahim and de Lasa (2004) with the catalyst Hombikat UV-100. Three initial concentrations in $\mu\text{mol/L}$: 30, 40 and 50.

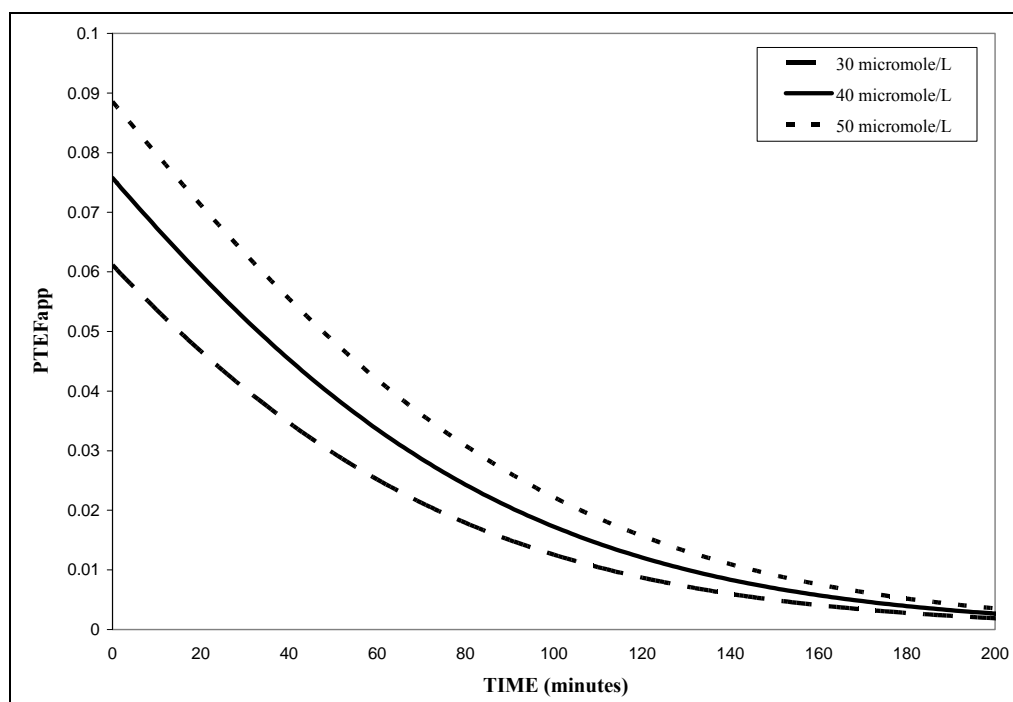


Figure 29: $PTEF_{app}$ for acetaldehyde using experimental data reported by Ibrahim and de Lasa (2004) with the catalyst Degussa P25. Three initial concentrations in $\mu\text{mol/L}$: 30, 40 and 50.

It is stated that during the photocatalytic degradation of acetone, the *PTEFs* remained in the 0.02-0.021 (2.0-2.1%) range when using Hombikat UV-100 and in the 0.0215-0.025 (2.15-2.5%) range when using Degussa P25. On the other hand, for the photocatalytic degradation of acetaldehyde, the *PTEFs* efficiencies remained, in the 0.08-0.10 (8-10%) range and in the 0.06-0.087 range (6-8.7%) for Hombikat UV-100 and Degussa P25 respectively.

Thus, the resulting energy efficiencies gave, in many instances, quantum -yields higher than 1 with the *PTEF* remaining below 1 as required by thermodynamics:

$$QY_{app} \geq 1 \text{ and } PTEF < 1$$

One should note that the high values of *QY* calculated in this chapter are consistent with *QYs* reported in the technical literature. *QYs* reported previously are based on both photoconverted pollutant molecules and formed carbon dioxide molecules as reported by Raupp et al., (1993), Cassano et al., (1995); Nimlos et al., (1996); Ibrahim and de Lasa,(2003).

7.4 Conclusions

- a) Energy Efficiency parameters are obtained using acetone and acetaldehyde photocatalytic degradation data obtained in a previous Photo-CREC-Air Reactor of 14.7 L of capacity developed by Ibrahim (2001).
- b) *QYs* in excess to 1 or equivalent to 100% were calculated. *QYs* varied in an ample range with pollutant concentrations favoring a higher *OH*[•] utilization during the initial steps of photocatalytic degradation.
- c) *PTEFs* were consistently below 1 for all runs and conditions. Thus, the following consistently applied: $PTEF_{app,ACETONE} \leq 1$ with $QY_{app,ACETONE} \geq 1$ and $PTEF_{app,ACETALDEHYDE} \leq 1$ with $QY_{app,ACETALDEHYDE} \geq 1$.

Chapter 8

Results and Discussion III: Energy Efficiency in the 55.1 L Version of the Photo-CREC-Air Reactor

8.1 Introduction

One of the most significant obstacles in the application of photocatalytic processes is their perceived low energy efficiency. Therefore, it is important to establish how the irradiation is being used and how this energy efficiency varies with different operating conditions. It is also necessary to pay special attention to the reactor design allowing for optimal use of irradiation.

A useful parameter in the determination of energy efficiencies in photocatalytic processes is the quantum yield (QY), a reactor-dependent parameter discussed in Chapter 7. This parameter can also help in the discrimination of possible reaction pathways.

Chapter 2 reports how different definitions of the quantum yield have been proposed for various photocatalytic reactors, leading to different approaches in assessing their energy performance. The Photocatalytic Thermodynamic Efficiency Factor ($PTEF$) is a parameter based on thermodynamic considerations. This parameter was first proposed by Serrano and de Lasa (1997) for water purification to overcome the uncertainty of the lack of bounds for quantum efficiency.

The calculation of the $PTEF$ with experimental data obtained by Ibrahim (2001) in a 14.7 L Photo-CREC-Air Reactor, as well as the evaluation of related apparent quantum yields was performed as a part of this PhD dissertation. This has been the first reported use of the $PTEF$ parameter to assess the effectiveness of a photocatalytic reactor for air purification (Garcia-Hernandez, 2010). However, these energy efficiency factors were obtained using the number of photons reaching the surface of the photocatalyst. Results of these evaluations are well described in Chapter 7.

This chapter describes the evaluation of the values of quantum yields and $PTEF$ achieved while performing air purification in a scaled up 55.1 liter version of the Photo-CREC-Air Reactor. This unit was developed in the context of the present PhD

Dissertation. With this objective, the photocatalytic degradation of acetone, acetaldehyde and isopropanol were carried out. Results obtained are compared to those reported in Chapter 7 for the 14.7 liter capacity Photo-CREC-Air Unit. It has to be highlighted that the initial concentrations of model pollutants used in the new scaled up reactor are between 5 to 10 times smaller than those implemented in the 14.7 L capacity unit. The information presented in this chapter represent part of an article already accepted for publication by Garcia-Hernandez et al. in 2012.

8.2 Energy Efficiency Factors

The *quantum yield* (QY) is a parameter used to evaluate the photon efficiency. This parameter considers the ratio of pollutant molecules degraded over the number of absorbed photons with energy superseding the photocatalyst band gap.

This definition can be modified and established in a more phenomenologically meaningful manner using the ratio of the rate of consumed OH^\bullet radicals over the rate of photons absorbed by the photocatalyst with $\lambda < 388\text{nm}$ (Garcia-Hernandez et. al., 2010; 2012; Serrano et al., 2009; 2010). This QY definition accounts for the critical role assigned to OH^\bullet radicals in the purification of ambient air using photocatalysis. Thus, for near UV lamps, the following definition can be adopted:

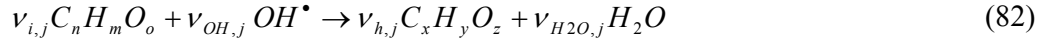
$$QY = \frac{\text{number of } OH^\bullet \text{ consumed}}{\text{number of photons absorbed by the photocatalyst with } \lambda \leq 388\text{nm}} \quad (81)$$

The denominator in equation (81) is clearly different from the one used in the calculations performed with the results obtained in the previous Photo-CREC-Air reactor (Chapter 7). Quantum yields, in that case, were defined on the basis of the number of photons reaching the photocatalyst giving an apparent quantum yield. Apparent quantum yields provide an approximate efficiency assessment only.

The quantum yield as defined by equation (81) assigns to the OH^\bullet radicals the role of being the sole drivers of the photoconversion process. This is based on the stoichiometric requirements for oxidation of the observable chemical species (Garcia-Hernandez et. al., 2010; 2012; Serrano et al., 2009).

For instance, in the “ j ” reaction step, one can consider that both the OH^\bullet groups and two organic species with different degrees of oxidation are involved. The “ i ” species ($C_nH_mO_o$) represents the species at the lower oxidation state while the “ h ” species

($C_xH_yO_z$) stands for the one at the higher oxidation state. These two species have to comply with oxygen, carbon, and hydrogen elemental balances as set by stoichiometric requirements. Thus, stoichiometry sets the OH^\bullet 's needed in every “ j ” photocatalytic step, where “ i ” ($C_nH_mO_o$) species are transformed into “ h ” ($C_xH_yO_z$) species as follows,



with $v_{i,j}$ and $v_{h,j}$ representing the stoichiometric coefficients for $C_nH_mO_o$ and $C_xH_yO_z$ respectively in the “ j ” step with:

$$v_{i,j}n - v_{h,j}x = 0 \quad (\text{Elemental carbon balance}) \quad (83a)$$

$$v_{i,j}m + v_{OH^\bullet,j} - v_{h,j}y - 2v_{H_2O,j} = 0 \quad (\text{Elemental hydrogen balance}) \quad (83b)$$

$$v_{i,j}o + v_{OH^\bullet,j} - v_{h,j}z - v_{H_2O,j} = 0 \quad (\text{Elemental oxygen balance}) \quad (83c)$$

As a result,

$$r_{OH^\bullet,T} = \sum r_{OH^\bullet,j} = \sum \frac{v_{OH^\bullet,j}}{v_{i,j}} r_{i,j} \quad (84)$$

where $r_{OH^\bullet,j}$ is the rate of consumption of OH^\bullet radicals in step “ j ” of the reaction network, where $r_{i,j}$ is the reaction rate of the compound “ i ” in step “ j ”, and where $v_{i,j}$ is the stoichiometric coefficient of compound “ i ” in step “ j ”. One should mention that sometimes stoichiometric coefficients in equation (84) may be zero. This depends on the contribution of the “ i ” species in a specific reaction step “ j ”.

The total rate of OH^\bullet consumption can be calculated using an “*indirect method*” as in equation (84). This involves the summation of the rates of every single oxidation step multiplied by the ratio of the corresponding stoichiometric coefficients as,

$$QY = \frac{-A_{irr} \sum_1^j r_{OH^\bullet,j}}{\int_{\lambda_{min}}^{\lambda_{max}=388nm} \frac{RA_{irr} \lambda d\lambda}{hc}} = \frac{A_{irr} \sum_1^j \frac{v_{OH^\bullet,j}}{v_{i,j}} r_{i,j}}{\int_{\lambda_{min}}^{\lambda_{max}=388nm} \frac{RA_{irr} \lambda d\lambda}{hc}} \quad (85)$$

with,

$r_{OH^{\bullet},j}$ = rate of OH^{\bullet} radicals consumption in step “j” (mol/cm²_{irr}·s)

$r_{i,j}$ = rate of “i” pollutant molecules degraded in the step “j” of the photoconversion process (mol/cm²_{irr}·s)

$\nu_{i,j}$ = stoichiometric coefficient involved in the photoconversion of the species “i” in step “j”

R = radiation intensity, W/(cm²·nm)

A_{irr} = the total area of irradiated photocatalyst-impregnated mesh, 192 cm²

h = Planck’s constant, 6.63×10^{-34} J·s

c = speed of light in vacuum, 3×10^{10} cm/s

λ_{min} = the lower wavelength of the spectrum in the range of interest, 300 nm

λ_{max} = the higher wavelength of the spectrum in the range of interest, 388 nm

Equation (85) involves almost the complete spectrum of the near-UV lamps used in the current Photo-CREC-Air Unit, with 93% of the photons used in the photocatalyst activation (Appendix D). This is in contrast with the lamps used in a previous Photo-CREC-Air Reactor where 92% of the photons could be used for photocatalytic transformations (Appendix C).

The Photochemical Thermodynamic Efficiency Factor (*PTEF*) for photocatalytic air treatment units is defined as the energy utilized for the OH^{\bullet} radical formation over the photocatalyst absorbed energy. This definition has to include as in the case of *QY*, the γ factor or the photon energy fraction with a wavelength smaller than the one superseding the semiconductor band gap:

$$PTEF = \frac{Q_{used}}{Q_{abs}\gamma} = \frac{-r_{OH^{\bullet},T}\Delta H_{OH^{\bullet}}A_{irr}}{Q_{abs}\gamma} \quad (86)$$

with $r_{OH^{\bullet},T}$ being in mol min⁻¹cm²_{irr}⁻¹, A_{irr} in cm²_{irr}, $\Delta H_{OH^{\bullet}}$ in J mol⁻¹, Q_{abs} in J min⁻¹ and γ without units.

In the case analyzed in this chapter, with $\gamma = 0.93$ (refer to the Appendix D), equation (86) simply becomes:

$$PTEF = \frac{Q_{used}}{\gamma Q_{abs}} = \frac{-r_{OH^\bullet, T} \Delta H_{OH^\bullet} A_{irr}}{0.93 Q_{abs}} \quad (87)$$

The *PTEF* can also be defined as the product of *QY* and η_{OH^\bullet} . *QY* accounts for the fraction of photons absorbed by the photocatalyst leading to the formation of *OH*[•] radicals as shown in the following equation:

$$PTEF = QY_{abs} \eta_{OH^\bullet} \quad (88)$$

where η_{OH^\bullet} is the fraction of photon energy used in forming an *OH*[•] radical, and is given by:

$$\eta_{OH^\bullet} = \frac{\Delta H_{OH^\bullet}}{E_{av}} \quad (89)$$

with ΔH_{OH^\bullet} being the enthalpy of formation of an *OH*[•] group (J mol⁻¹) and E_{av} being the average energy of a photon (J) (refer to Appendix B).

It is possible in this manner, to use the *PTEF* for the assessment of photocatalytic reactors for air treatment. This can be done by selecting the appropriate photocatalytic reaction network and reaction kinetics as well as the relevant thermodynamic and irradiation parameters.

8.3 Stoichiometric equations and photoreaction rates

In order to establish the photocatalytic degradation kinetics, the following pertinent assumptions were considered: a) The gas is transparent to near-UV irradiation with absorption, scattering and reflection being negligible, b) The mixing in the Photo-CREC-Air Reactor is intense, given the high air recirculation. Gas phase concentrations of all species can be considered uniform at any given time; c) The internal wall of the quartz cylinder enclosing the reaction section is free of deposited particles. The adsorption of reactants on the walls of the reaction can be neglected; d) The metallic mesh supporting the TiO₂ is constantly irradiated by the near UV lamps with an intensity of light that does not change significantly during the experiments; e) The contribution of the thermal reactions to the photo-conversion process is insignificant.

8.3.1 Acetone Photocatalytic Degradation Stoichiometry

Assuming that acetone photocatalytic degradation is the result of the OH^\bullet group consumption rate only, the following stoichiometry can be proposed:



This stoichiometry is considered adequate at any irradiation time during the photoconversion, given that no intermediate species were detected. As a result, the following relationships can be considered:

$$\frac{r_{ACETONE}}{v_{ACETONE}} = \frac{r_{OH^\bullet}}{v_{OH^\bullet}} \quad \text{and} \quad r_{OH^\bullet} = \frac{v_{OH^\bullet}}{v_{ACETONE}} r_{ACETONE} \quad (91)$$

where:

$v_{ACETONE}$ = stoichiometric coefficient for acetone

v_{OH^\bullet} = stoichiometric coefficient for OH^\bullet

8.3.2 Acetaldehyde Photocatalytic Degradation Stoichiometry

In a similar manner, and as it is postulated for acetone, the following stoichiometry can be adopted for acetaldehyde degradation. It is assumed that the only radical species driving the photocatalytic degradation are OH^\bullet radicals.



This stoichiometry also assumes that there are no intermediates. As a result, the rate of photoconversion of acetaldehyde and the OH^\bullet group consumption rate can be written as follows:

$$\frac{r_{ACETALDEHYDE}}{v_{ACETALDEHYDE}} = \frac{r_{OH^\bullet}}{v_{OH^\bullet}} \quad \text{and} \quad r_{OH^\bullet} = \frac{v_{OH^\bullet}}{v_{ACETALDEHYDE}} r_{ACETALDEHYDE} \quad (93)$$

where:

$v_{ACETALDEHYDE}$ = stoichiometric coefficient for acetaldehyde

ν_{OH^\bullet} = stoichiometric coefficient for OH^\bullet

8.3.3 Isopropanol Photocatalytic Degradation Stoichiometry

Under the assumption that the isopropanol photocatalytic degradation is driven only by the rate of the OH^\bullet group consumption, the following stoichiometry can be postulated:



This stoichiometry is considered adequate at any irradiation time during the photoconversion. Given that the presence of acetone as an intermediate species was detected during the reaction, the following relationships can be considered:

$$\frac{r_{ISOPROPANOL}}{\nu_{ISOPROPANOL}} = \frac{r_{OH^\bullet}}{\nu_{OH^\bullet}} \quad \text{and} \quad r_{OH^\bullet} = \frac{\nu_{OH^\bullet}}{\nu_{ISOPROPANOL}} r_{ISOPROPANOL} \quad (95)$$

where:

$\nu_{ISOPROPANOL}$ = stoichiometric coefficient for isopropanol

ν_{OH^\bullet} = stoichiometric coefficient for OH^\bullet

8.4 Photocatalytic modeling

As stated in Chapter 6, the photocatalytic reaction kinetics can be modeled with a Langmuir-Hinshelwood expression as follows:

$$r = \frac{-k^* I^\alpha KC}{1 + KC + \sum K_i C_i} \quad (96)$$

with $\alpha = 1$. K is the equilibrium adsorption constant for the model pollutant. The term $\sum K_i C_i$ represents the combined effect of all adsorbed intermediate species.

This model has proved to be adequate in describing the observed changes of the chemical species concentrations in the gas phase of the photocatalytic conversion of acetone, acetaldehyde and isopropanol (Ibrahim, 2001; Ibrahim and de Lasa, 2002)

8.4.1 Acetone Photocatalytic Degradation Modeling

The total acetone photocatalytic degradation rate can be evaluated using the rate of photoconversion in the gas phase as follows:

$$r_{ACETONE,T} = r_{ACETONE,g} (1 + K'_{ACETONE}) \quad (97)$$

where $r_{ACETONE,T}$ is the total reaction rate ($\mu\text{mol}/(\text{m}^2 \cdot \text{min})$), $r_{ACETONE,g}$ is the reaction rate calculated with concentration changes in the gas phase ($\mu\text{mol}/(\text{m}^2 \cdot \text{min})$) and $K'_{ACETONE}$ is a dimensionless adsorption parameter .

Furthermore, given that acetone was the only detectable species and given the rate of consumption for the i species followed a Langmuir-Hinshelwood model (a detailed explanation on the derivation of these equations is given in Chapter 6), the following applies:

$$r_{ACETONE,g} = \frac{dC_{ACETONE,g}}{dt} \frac{V}{A_{irr}} = - \frac{k_{ACETONE} K^A_{ACETONE} C_{ACETONE,g}}{1 + K^A_{ACETONE} C_{ACETONE,g}} \frac{V}{A_{irr}} \quad (98)$$

This expression can also be expressed as,

$$r_{ACETONE,g} = - \frac{C_{ACETONE,g}}{\theta_{A1} + \theta_{A2} C_{ACETONE,g}} \frac{V}{A_{irr}} \quad (99)$$

where:

$r_{ACETONE,g}$ = rate of acetone photocatalytic degradation as assessed by changes in the gas phase concentrations, $\mu\text{mol}/(\text{m}^2 \cdot \text{min})$

$C_{ACETONE,g}$ = acetone concentration in the gas phase, $\mu\text{mol}/\text{m}^3$

A_{irr} = irradiated mesh area holding the catalyst, m^2

$K^A_{ACETONE}$ = acetone adsorption constant, $\text{m}^3/\mu\text{mol}$

$k_{ACETONE}$ = reaction rate constant, $\mu\text{mol}/(\text{m}^3 \cdot \text{min})$

$\theta_{A1} = 1/(k_{ACETONE} K^A_{ACETONE})$, min

$\theta_{A2} = 1/k_{ACETONE}$, $\text{m}^3 \cdot \text{min} / \mu\text{mol}$

Fitting the data shown in Figure 30 into equation (99), yields the parameters θ_{A1} and θ_{A2} for acetone reported in Table 4. This table contains statistical indicators such as correlation coefficients (r^2) and the sum of squared residuals (S.S.R.). These

parameters were obtained with a Degree of Freedom (*D.O.F.*) of 61 or 63 data points. Reported data points represent average values for 3 repeat runs at the same initial pollutant concentration. Standard deviation of data points for repeats was less than $\pm 5\%$. The built-in subroutines *lsqcurvefit* and *ode45* in MATLAB[©] were used to perform the fitting using the least squares method.

Table 4: Kinetic and Data Modeling Parameters for acetone photocatalytic degradation with Degussa P25 photocatalyst

	Current Reactor	Former Reactor (Ibrahim and de Lasa, 2003)
A_{irr}/V	0.0346	0.0348
$\theta_{A1} * 0.1$, min	1.584 \pm 0.372	10.77 \pm 0.47
$\theta_{A2} * 10^3$, m ³ ·min / μ mol	0.7604 \pm 0.015	4.88 \pm 0.19
k , μ mol/(m ³ ·min)	1315.097 \pm 30.88	204.92 \pm 9.001
$K^4 * 10^5$, m ³ / μ mol	4.8 \pm 0.0095	4.56 \pm 0.1776
r^2	0.98	0.99
<i>D.O.F.</i>	61	115
<i>S.S.R.</i> *10 ⁻⁸	0.93644	1.06

Both θ_{A1} and θ_{A2} parameters, as well as k and K^4 , were obtained with statistically desirable $\pm 5\%$ narrow confidence intervals. When the fitted parameters were used to calculate the CO₂ formation, it was observed that the model consistently predicted the CO₂ formation rate as shown in Figure 31.

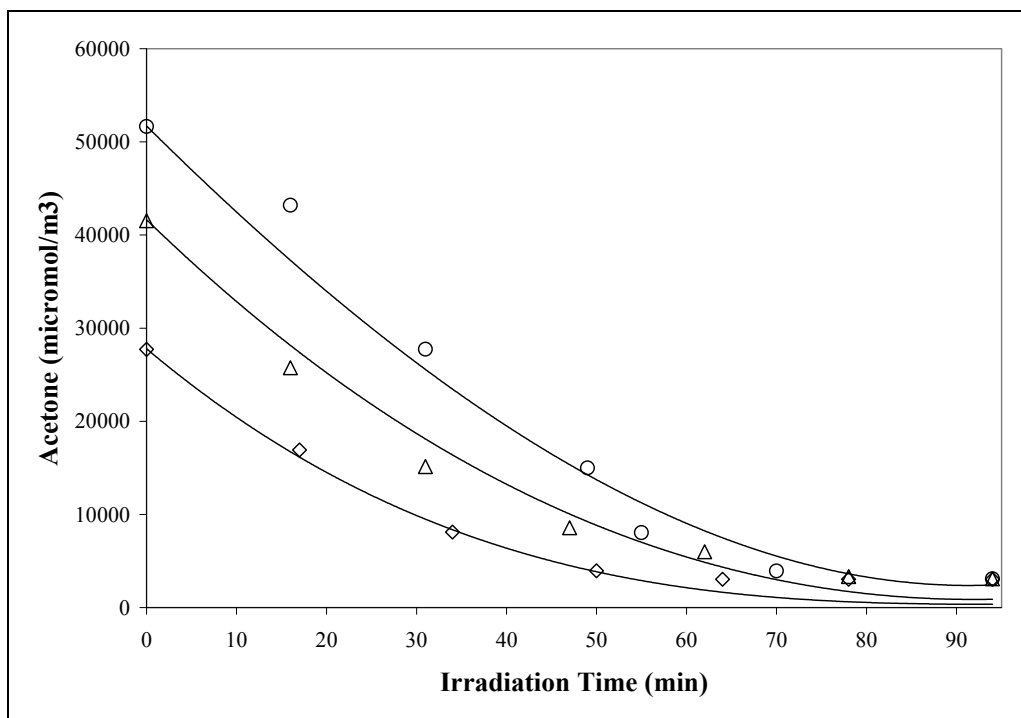


Figure 30: Changes of acetone concentrations with reaction time using the Degussa P25 as catalyst. Three initial concentrations in $\mu\text{mol/L}$ were considered: 49(○), 37(△) and 24.5(◇). (Continuous line represents model predictions using Equation 99)

The calculated values of K^A constants in this research are close to the ones reported by Ibrahim and de Lasa (2003) for a former Photo-CREC-Air Reactor. This is encouraging given that Degussa P25 was used in both studies with Photo-CREC-Air Units of different capacity.

In addition, Table 4 shows that the k parameters increase five times with respect to the ones observed in a previous Photo-CREC-Air Unit. This demonstrates that even with the design complexities involved in the scaling up of the Photo-CREC-Air Unit (55.1 liters instead of 14.7 liters), there is in this enlarged unit enhanced irradiation and high photocatalyst loadings. This leads to significantly higher intrinsic photocatalytic kinetic parameters.

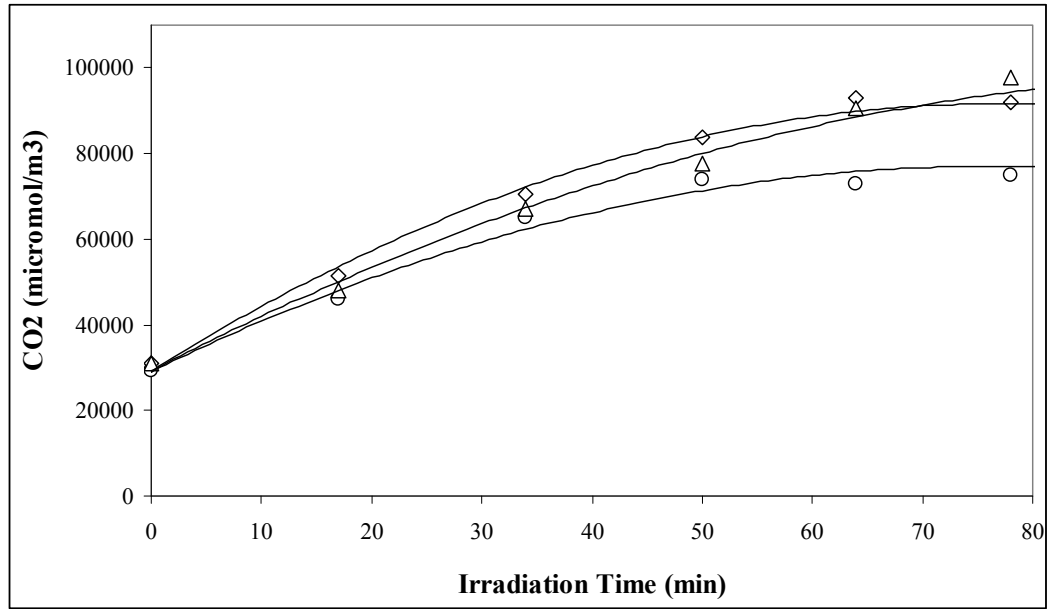


Figure 31: Changes of CO₂ concentrations with reaction time during the photocatalytic degradation of acetone using the Degussa P25 as catalyst. Three initial concentrations of acetone in μmol/L were considered: 49(◇), 37(△) and 24.5(○). (Continuous line represents model predictions)

8.4.2 Acetaldehyde Photocatalytic Degradation Modeling

Using a similar kinetic modeling procedure as in section 8.4.1, it is possible to obtain the following expression for the acetaldehyde reaction degradation rate:

$$r_{ACETALDEHYDE,T} = r_{ACETALDEHYDE,g} (1 + K'_{ACETALDEHYDE}) \quad (100)$$

where $r_{ACETALDEHYDE,T}$ is the total reaction rate ($\mu\text{mol}/(\text{m}^2 \cdot \text{min})$), $r_{ACETALDEHYDE,g}$ is the reaction rate defined by concentration changes in the gas phase ($\mu\text{mol}/(\text{m}^2 \cdot \text{min})$) and $K'_{ACETALDEHYDE}$ is a dimensionless adsorption parameter .

Considering that acetaldehyde was the only detectable species and given that the rate of consumption for “*i*” species follows a Langmuir-Hinshelwood model, as described in Chapter 6, the following applies:

$$r_{ACETALDEHYDE,g} = \frac{dC_{ACETALDEHYDE,g}}{dt} \frac{V}{A_{irr}} = - \frac{k_{ACETONE} K^A_{ACETALDEHYDE} C_{ACETALDEHYDE,g}}{1 + K^A_{ACETALDEHYDE} C_{ACETALDEHYDE,g}} \frac{V}{A_{irr}} \quad (101)$$

This rate expression can be rewritten as:

$$r_{ACETALDEHYDE,g} = -\frac{C_{ACETALDEHYDE,g}}{\theta_{AA1} + \theta_{AA2}C_{ACETALDEHYDE,g}} \frac{V}{A_{irr}} \quad (102)$$

where:

$r_{ACETALDEHYDE,g}$ = rate of acetaldehyde photocatalytic degradation as assessed by changes in the gas phase concentrations, $\mu\text{mol}/(\text{m}^2 \cdot \text{min})$

$C_{ACETALDEHYDE,g}$ = acetaldehyde concentration in the gas phase, $\mu\text{mol}/\text{m}^3$

A_{irr} = illuminated mesh area, m^2

$K^A_{ACETALDEHYDE}$ = acetaldehyde adsorption constant, $\text{m}^3/\mu\text{mol}$

$k_{ACETALDEHYDE}$ = reaction rate constant, $\mu\text{mol}/(\text{m}^3 \cdot \text{min})$

$\theta_{AA1} = 1/(k_{ACETALDEHYDE}K^A_{ACETALDEHYDE})$, min

$\theta_{AA2} = 1/k_{ACETALDEHYDE}$, $\text{m}^3 \cdot \text{min} / \mu\text{mol}$

Fitting the data of Figure 32 into equation (102), yields the parameters shown in Table 5. The values of θ_{AA1} and θ_{AA2} parameters as well as K^A are calculated. The parameters are adjusted with 99 data points and high correlation coefficients. Statistically desirable indicators are achieved: narrow confidence intervals and regression coefficients. Typical deviations on data point repeats were as in the case of the acetone experiments less than $\pm 5\%$. As in the case of acetone, MATLAB © was used to perform the fitting.

Figure 33 shows the changes in concentration of CO_2 with reaction time. When the fitted parameters were used to calculate the CO_2 formation, it was observed that the model consistently predicted the CO_2 formation rate as shown in Figure 33.

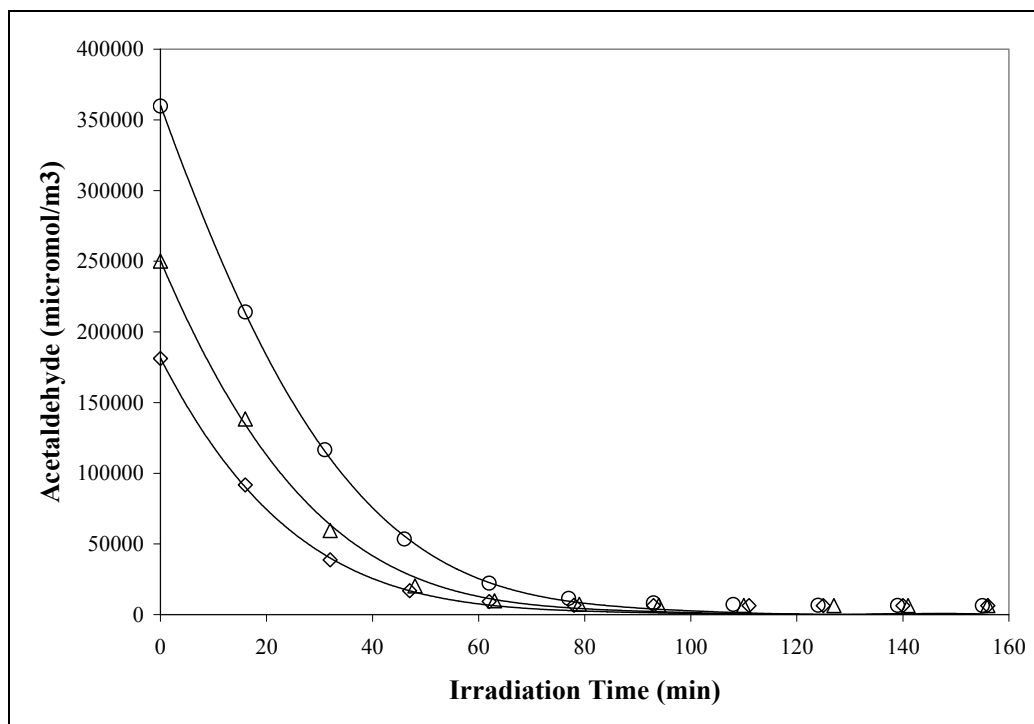


Figure 32: Changes of acetaldehyde concentrations with reaction time using Degussa P25 as catalyst. Three initial concentrations in $\mu\text{mol/L}$ were considered: 320(\diamond), 240(Δ) and 160(o). (Continuous line represents model predictions using Equation 102)

Table 5: Kinetic and Data Modeling Parameters for acetaldehyde photocatalytic degradation with Degussa P25 photocatalyst

	Current Reactor	Former Reactor (Ibrahim and de Lasa, 2003)
A_{irr}/V	0.0346	0.0348
$\theta_{AA1} * 0.1, \text{ min}$	1.6315 \pm 0.0975	5.10 \pm 0.45
$\theta_{AA2} * 10^4, \text{ m}^3 \cdot \text{min} / \mu\text{mol}$	0.5069 \pm 0.05686	3.62 \pm 1.55
$K, \mu\text{mol}/(\text{m}^3 \cdot \text{min})$	19728.15 \pm 1178.97	2762.43 \pm 243.74
$K^A * 10^6, \text{ m}^3/\mu\text{mol}$	3.107 \pm 0.348	7.098 \pm 0.304
r^2	0.99	0.97
$D.O.F.$	97	74
$S.S.R. * 10^{-8}$	6.3892	4.7

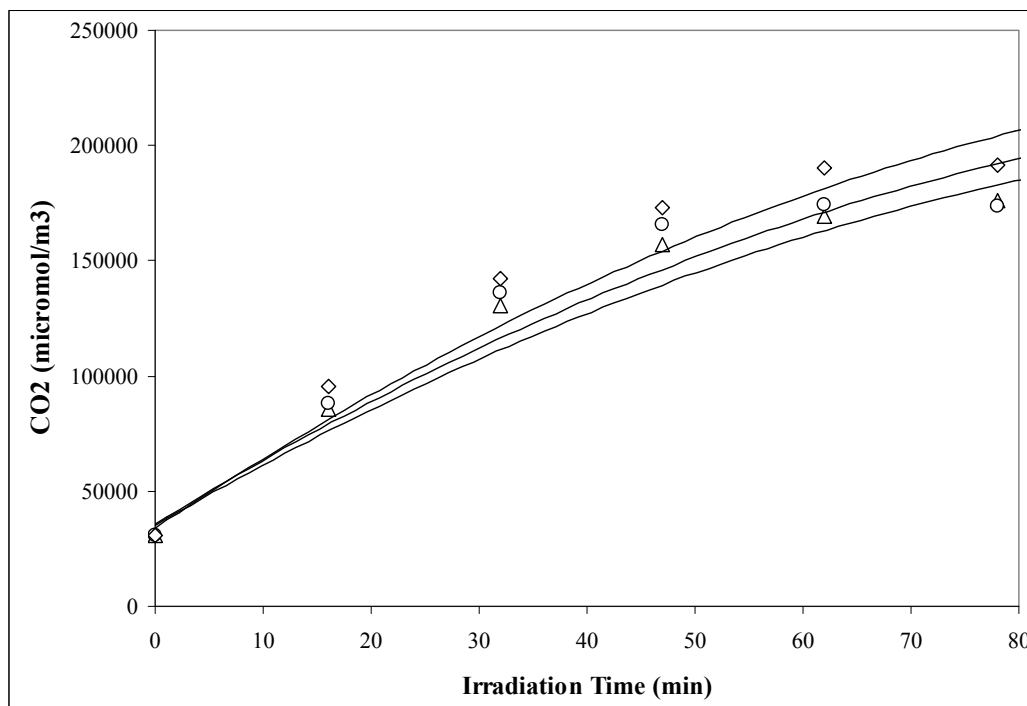
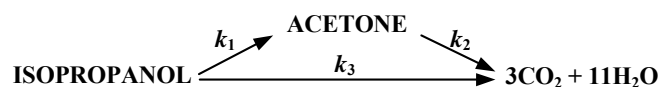


Figure 33: Changes of CO₂ during the photocatalytic degradation of acetaldehyde using Degussa P25 as catalyst. Three initial concentrations of acetaldehyde in μmol/L were considered: 320(◇), 240(Δ) and 160(○). (Continuous line represents model predictions)

It can be seen in Table 5 that the K^A adsorption constants for acetaldehyde are in the range of values reported in a previous study performed using former versions of the Photo-CREC-Air Reactor (Ibrahim and de Lasa, 2003). This is once again encouraging, as was the case for acetone, given that Degussa P25 was used in both 55.1 liter and 14.7 liter Photo-CREC-Air Units.

8.4.3 Isopropanol Photocatalytic Degradation Modeling

In the case of isopropanol photocatalytic degradation, the presence of acetone as intermediate during the process was detected. The detection of acetone allowed the study of a series-parallel kinetic model involving: a) the formation of CO₂ directly from isopropanol, b) the formation of acetone from isopropanol later converted into CO₂ as follows:



(103)

As in the cases of acetone and acetaldehyde, the total isopropanol photocatalytic degradation rate can be evaluated using the rate of photoconversion in the gas phase:

$$r_{ISOPROPANOL,T} = r_{ISOPROPANOL,g} (1 + K'_{ISOPROPANOL}) \quad (104)$$

where $r_{ISOPROPANOL,T}$ is the total reaction rate ($\mu\text{mol}/(\text{m}^2 \cdot \text{min})$), $r_{ISOPROPANOL,g}$ is the reaction rate calculated with concentration changes in the gas phase ($\mu\text{mol}/(\text{m}^2 \cdot \text{min})$) and $K'_{ISOPROPANOL}$ is a dimensionless adsorption parameter .

The total change of acetone can be expressed in terms of the change of acetone concentration in the gas phase. Given that acetone is involved in two different reaction steps, the total rate of acetone photoconversion has to include both acetone production and consumption.

$$\frac{dC_{ACETONE,g}}{dt} = \frac{A_{irr}}{V} (r_{ISOPROPANOL,g} \cdot \phi - r_{ACETONE,g}) \quad (105)$$

with

$$\phi = \frac{(1 + K'_{ISOPROPANOL})}{(1 + K'_{ACETONE})} \quad (106)$$

The only carbon containing species detected in the gas phase during isopropanol photocatalytic conversion were isopropanol, acetone and carbon dioxide. Since the rate of isopropanol photoconversion using a Langmuir-Hinshelwood model involves both isopropanol and acetone species competing for the same catalyst sites, the following equation can be written as follows:

$$r_{ISOPROPANOL,g} = \frac{dC_{ISOPROPANOL,g}}{dt} \frac{V}{A_{irr}} = - \frac{(k_1 + k_3) K^A_{ISOPROPANOL} C_{ISOPROPANOL,g}}{1 + K^A_{ISOPROPANOL} C_{ISOPROPANOL,g} + K^A_{ACETONE} C_{ACETONE,g}} \frac{V}{A_{irr}} \quad (107)$$

where:

$r_{ISOPROPANOL,g}$ = rate of isopropanol photodegradation as assessed by changes in the gas phase concentrations, $\mu\text{mol}/(\text{m}^2 \cdot \text{min})$

$C_{ISOPROPANOL,g}$ = isopropanol concentration in the gas phase, $\mu\text{mol}/\text{m}^3$

$C_{ACETONE,g}$ = acetone concentration in the gas phase, $\mu\text{mol}/\text{m}^3$

A_{irr} = irradiated mesh area holding the catalyst, m^2

k_1 = isopropanol to acetone reaction rate constant, $\mu\text{mol}/(\text{m}^3 \cdot \text{min})$

k_3 = isopropanol to CO_2 reaction rate constant, $\mu\text{mol}/(\text{m}^3 \cdot \text{min})$

$K^A_{ISOPROPANOL}$ = isopropanol adsorption constant, $\text{m}^3/\mu\text{mol}$

$K^A_{ACETONE}$ = acetone adsorption constant, $\text{m}^3/\mu\text{mol}$

The rate of acetone photoconversion can be represented in a similar manner with the following expression:

$$r_{ACETONE,g} = \frac{dC_{ACETONE,g}}{dt} \frac{V}{A_{irr}} = - \frac{k_1 K^A_{ISOPROPANOL} C_{ISOPROPANOL,g} \phi - k_2 K^A_{ACETONE} C_{ACETONE,g}}{1 + K^A_{ISOPROPANOL} C_{ISOPROPANOL,g} + K^A_{ACETONE} C_{ACETONE,g}} \frac{V}{A_{irr}} \quad (108)$$

where k_2 is the intrinsic rate constant for acetone conversion into CO_2 during the isopropanol photoconversion as described in the above mechanism, expressed in $\mu\text{mol}/(\text{m}^3 \cdot \text{min})$.

Furthermore, the kinetic modeling of the photocatalytic isopropanol conversion in the Photo-CREC-Air Reactor involves the simultaneous evaluation of the following set of equations expressed in terms of the kinetic and adsorption parameters:

$$\frac{dC_{ISOPROPANOL,g}}{dt} = - \frac{(k_1 + k_3) K^A_{ISOPROPANOL} C_{ISOPROPANOL,g}}{1 + K^A_{ISOPROPANOL} C_{ISOPROPANOL,g} + K^A_{ACETONE} C_{ACETONE,g}} \quad (109)$$

$$\frac{dC_{ACETONE,g}}{dt} = - \frac{k_1 K^A_{ISOPROPANOL} C_{ISOPROPANOL,g} \phi - k_2 K^A_{ACETONE} C_{ACETONE,g}}{1 + K^A_{ISOPROPANOL} C_{ISOPROPANOL,g} + K^A_{ACETONE} C_{ACETONE,g}} \quad (110)$$

$$\frac{dC_{CO_2,g}}{dt} = \frac{3(k_2 K^A_{ACETONE} C_{ACETONE,g} + k_3 K^A_{ISOPROPANOL} C_{ISOPROPANOL,g})}{1 + K^A_{ISOPROPANOL} C_{ISOPROPANOL,g} + K^A_{ACETONE,g} C_{ACETONE,g}} \quad (111)$$

The value of ϕ is 1.3 when using Degussa P25.

The fitting of the experimental data of Figure 34 into the equations (109) to (111) was performed using the built-in MATLAB© subroutines *lsqcurvefit* and *ode45* for the minimization of objective function and numerical solution of the ordinary differential equations, respectively. Table 6 reports the values of the kinetic constants k_1 to k_3 and

the adsorption constants $K^A_{ISOPROPANOL}$ and $K^A_{ACETONE}$ for this photocatalytic degradation. Parameters were obtained with a D.O.F. of 91 or 93 data points. The data points show the average values for 3 repeat runs developed at 5 different initial pollutant concentrations. Standard deviation of data points for repeats was less than $\pm 10\%$.

When the fitted parameters were used to calculate the formation and posterior consumption of acetone as well as the CO_2 formation, it is observed that the model consistently predicted both rates as shown in Figure 34.

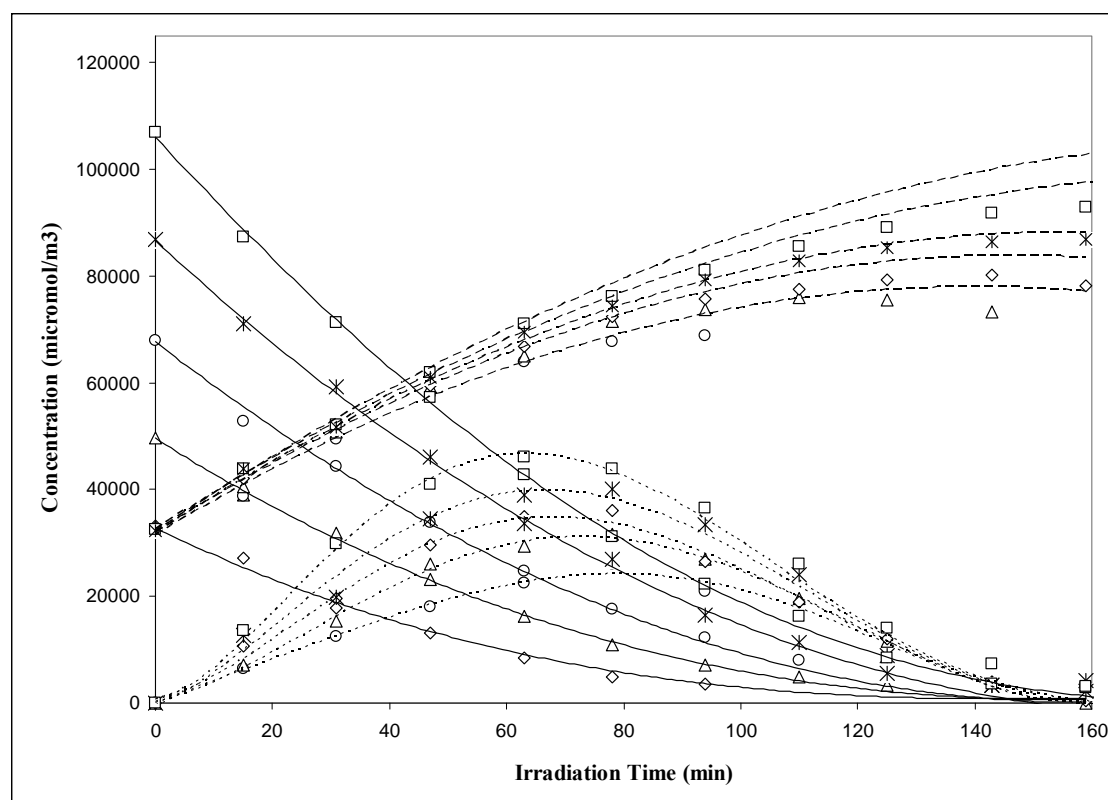


Figure 34: Changes in the concentration of all species present during the photocatalytic degradation of isopropanol using Degussa P25 as catalyst. Five initial concentrations of isopropanol in $\mu\text{mol/L}$ were considered: 33(o), 50(Δ), 68(\diamond), 87(X) and 107(\square). (Continuous and dashed lines represent model predictions using Equations 30, 31 and 32)

Table 6: Kinetic and Data Modeling Parameters for isopropanol photocatalytic degradation with Degussa P25 photocatalyst

	Photo-CREC-Air Reactor
A_{irr}/V	0.0346
$k_1 \cdot 10^{-3}$, $\mu\text{mol}/(\text{m}^3 \cdot \text{min})$	14.3756 \pm 1.5036
$k_2 \cdot 10^{-3}$, $\mu\text{mol}/(\text{m}^3 \cdot \text{min})$	98.516 \pm 3.0167
$k_3 \cdot 10^{-3}$, $\mu\text{mol}/(\text{m}^3 \cdot \text{min})$	2.4218 \pm 0.2387
$K^A_{ISOPROPANOL} \cdot 10^6$, $\text{m}^3/\mu\text{mol}$	7.976 \pm 0.5821
$K^A_{ACETONE} \cdot 10^5$, $\text{m}^3/\mu\text{mol}$	4.9342 \pm 0.5556
r^2	0.5069 \pm 0.05305
<i>D.O.F.</i>	1015.0638 \pm 31.0829
<i>S.S.R.</i> $\cdot 10^{-8}$	295.4646 \pm 4.6311

The resulting k intrinsic kinetic parameter presents the following trends:

- In the current reactor design, the k values for acetaldehyde are about several times larger than for acetone and isopropanol. This shows the higher reactivity of carbonyl groups while placed in terminal carbons, as is the case of acetaldehyde versus the reactivity of carbonyl groups in secondary carbon.
- The k s for acetaldehyde and acetone are about five times larger with respect to the k s reported previously for a former Photo-CREC-Air design (Ibrahim and de Lasa, 2003). These results confirm the successful design approach used for the scaled up 55.1 liter Photo-CREC-Air Unit with enhanced irradiation and high photocatalyst loadings.

8.5 Energy efficiency calculations

Once the photocatalytic degradation kinetics was established, quantum yields and the *PTEFs* for acetone, acetaldehyde and isopropanol were calculated using equations (85) and (88) and the parameters reported in Tables 4, 5 and 6. These quantum yields and *PTEFs* are based on a more phenomenologically sound accounting of the OH^\bullet radicals consumed as well as on the accurate absorbed irradiation.

As reported in the Figures 35, 36, 37, 38, 39 and 40, energy efficiencies decrease progressively with acetone, acetaldehyde and isopropanol concentrations, with a

common pattern being established: a higher OH^\bullet group is utilized at the higher concentrations during the initial photocatalytic degradation steps.

It can be noted that while intermediate species for the photocatalytic degradation of all model pollutants were reported (Chang et al., 2003; Sopyan, 2007; Arai et al., 2008; Besov et al., 2007; Morikawa et al., 2006; Schmidt et al., 2007), they were not detected in the cases of acetone and acetaldehyde using the Photo-CREC-Air Reactor. This result is attributed to the high photoconversion efficiency reached in the Photo-CREC-Air Unit.

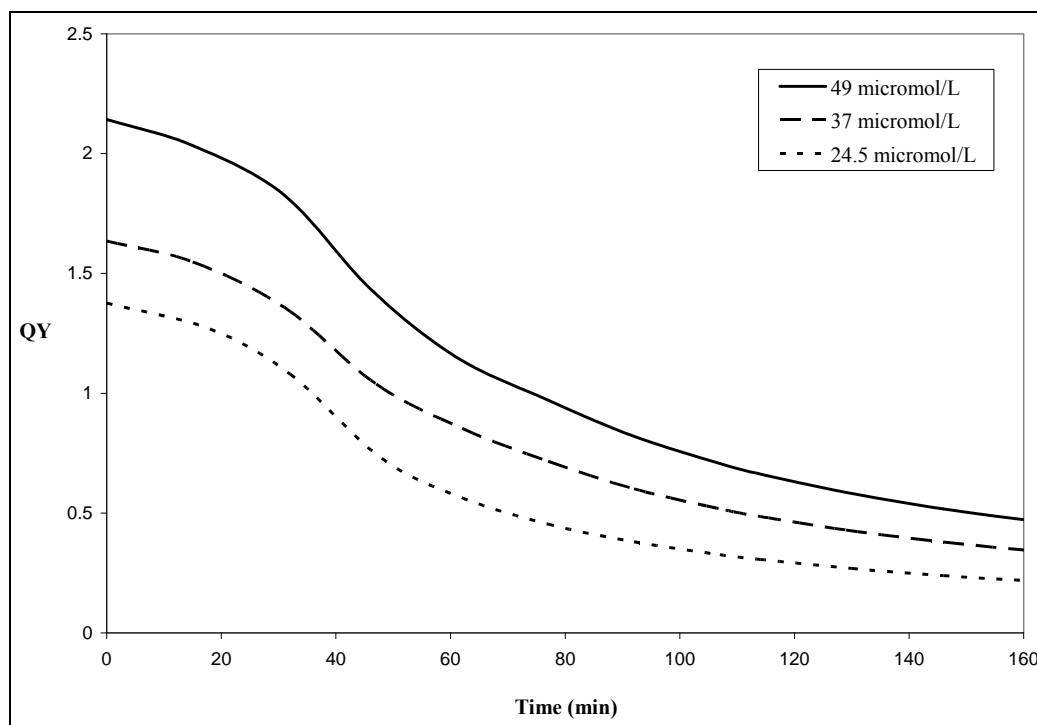


Figure 35: QY for acetone with Degussa P25 as photocatalyst. Three initial concentrations were considered in $\mu\text{mol/L}$: 49, 37 and 24.5

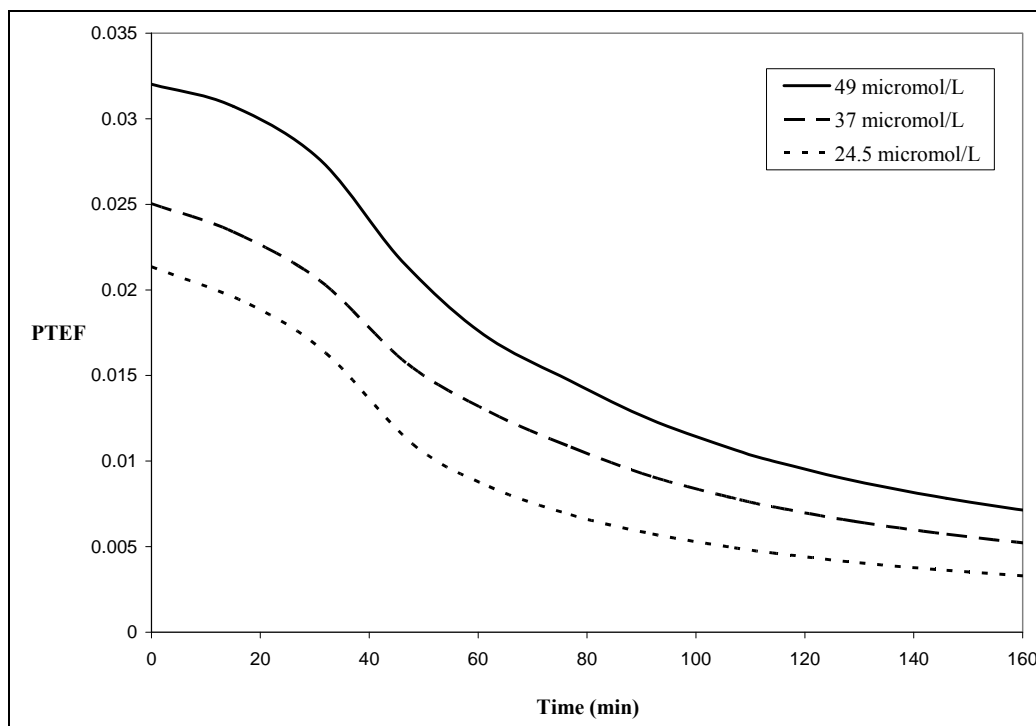


Figure 36: *PTEF* for acetone using Degussa P25 as photocatalyst. Three initial concentrations were considered in $\mu\text{mol/L}$: 49, 37 and 24.5

On the basis of the data reported in Figure 35, it can be observed that quantum yields for acetone photocatalytic degradation are, during a significant period of the irradiation, in excess to the theoretical maximum of 133% as described in Appendix A. More specifically, quantum yields fall in the 2.15-1.4 range (equivalent to 215-140%) at initial irradiation conditions. It can also be noticed that in agreement with thermodynamics, the corresponding *PTEFs* as reported in Figure 37 remain in all cases below 1 and in the 0.033-0.022 (3.3-2.2%) range.

Thus, in spite of achieving, in the Photo-CREC-Air Unit, quantum yields superseding the value of 1; *PTEFs* consistently stay below 1 such as is expressed in the following inequality:

$$QY_{ACETONE} \geq 1 \text{ with } PTEF_{ACETONE} \leq 1$$

Furthermore, the quantum yields and *PTEFs* obtained during the photocatalytic degradation of acetaldehyde at three different initial concentrations are reported in Figures 37 and 38. The quantum yields and *PTEFs* were calculated once again based on the measured values of absorbed irradiation. This was performed assuming that the

OH groups consumed during the process are the only ones driving the photocatalytic degradation.

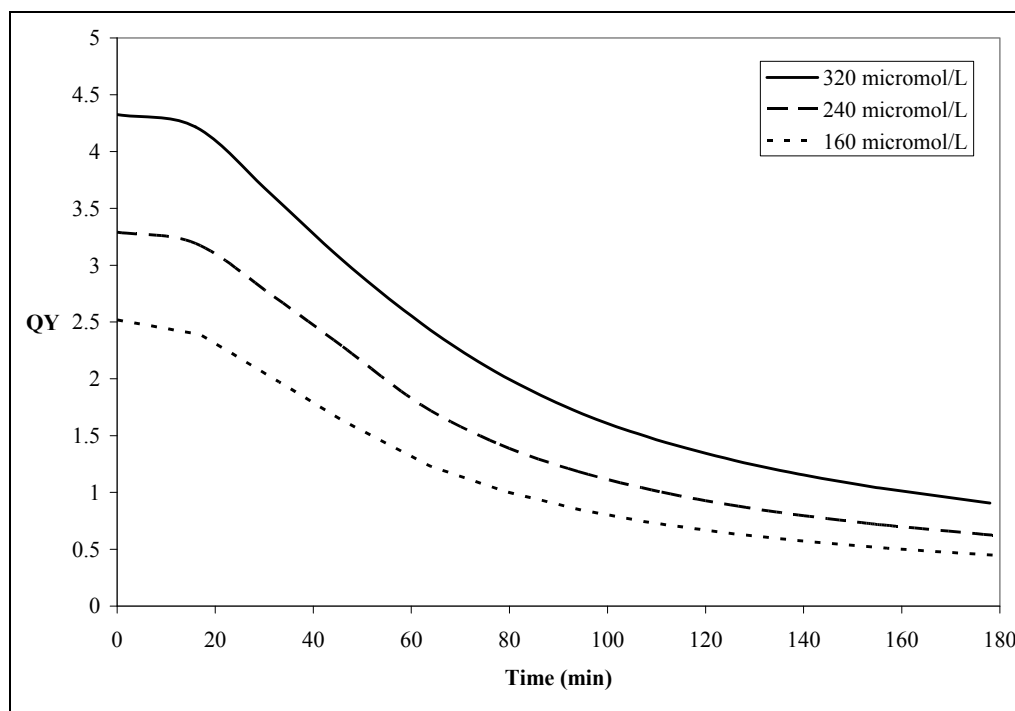


Figure 37: *QY* for acetaldehyde using Degussa P25 as photocatalyst. Three initial concentrations in $\mu\text{mol/L}$: 320, 240 and 160

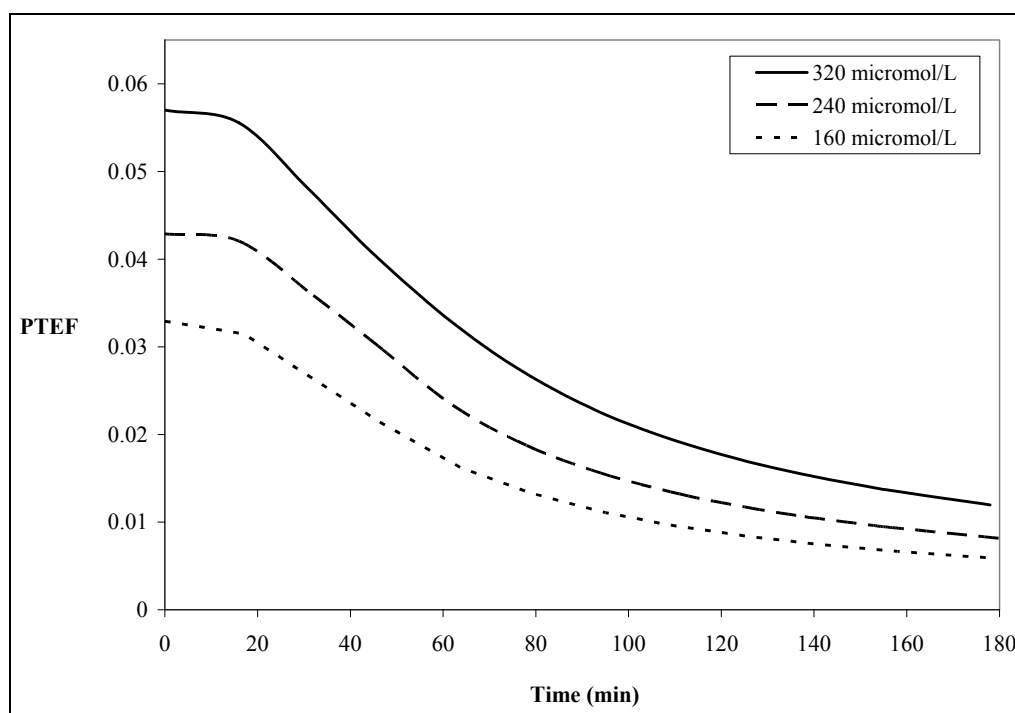


Figure 38: *PTEF* for acetaldehyde using Degussa P25 as photocatalyst. Three initial concentrations in $\mu\text{mol/L}$: 320, 240 and 160

It is possible to note again in Figure 37 that during initial irradiation, the quantum yields, obtained for acetaldehyde and based on the consumed OH^* groups, surpass the value of 1. These quantum yields are in the 4-2.5 range (equivalent to 400-250%). The $PTEF$ s efficiencies shown in Figure 38 remain however, in agreement with thermodynamics in the 0.053-0.033 (5.3-3.3%) range.

Thus, a similar condition is found for acetaldehyde photocatalytic degradation as in the case for acetone, with the following inequality applying:

$$QY_{ACETALDEHYDE} \geq 1 \text{ with } PTEF_{ACETALDEHYDE} \leq 1.$$

Table 7 reports a comparison of the quantum efficiencies of the present study with the ones found in a former reactor design for the photocatalytic degradation of acetone and acetaldehyde. The values of quantum efficiencies for both model pollutants are in a close range to those reported previously for a former Photo-CREC-Air design. This occurs in the current reactor design in spite of having initial pollutant concentrations five times lower than in the previous design of the reactor (Chapter 7).

Table 7: Comparison of Efficiency Parameters (Quantum Efficiency and $PTEF$)

	Acetone		Acetaldehyde	
	QY	$PTEF$	QY	$PTEF$
Current Reactor Design	215-140%	3.3-2.2%	400-250%	5.3-3.3%
Former Reactor Design	195-165%	2.5-2.15%	670-460%	8.7-6%

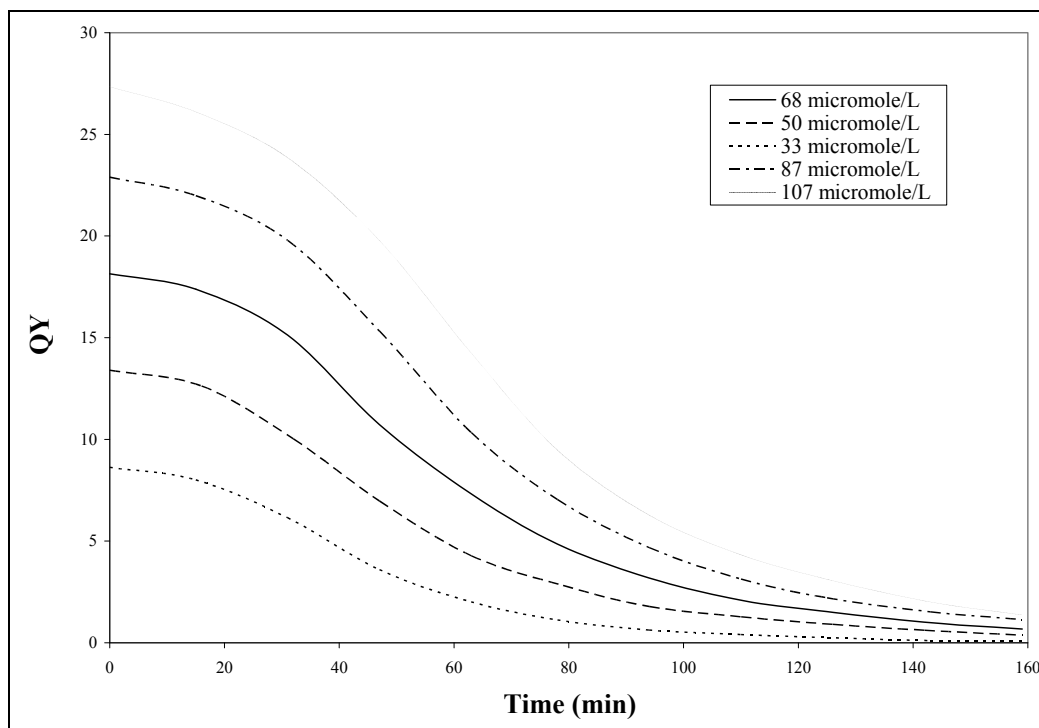


Figure 39: *QY* for isopropanol using Degussa P25 as photocatalyst. Five initial concentrations in $\mu\text{mol/L}$: 33, 50, 68, 87 and 107

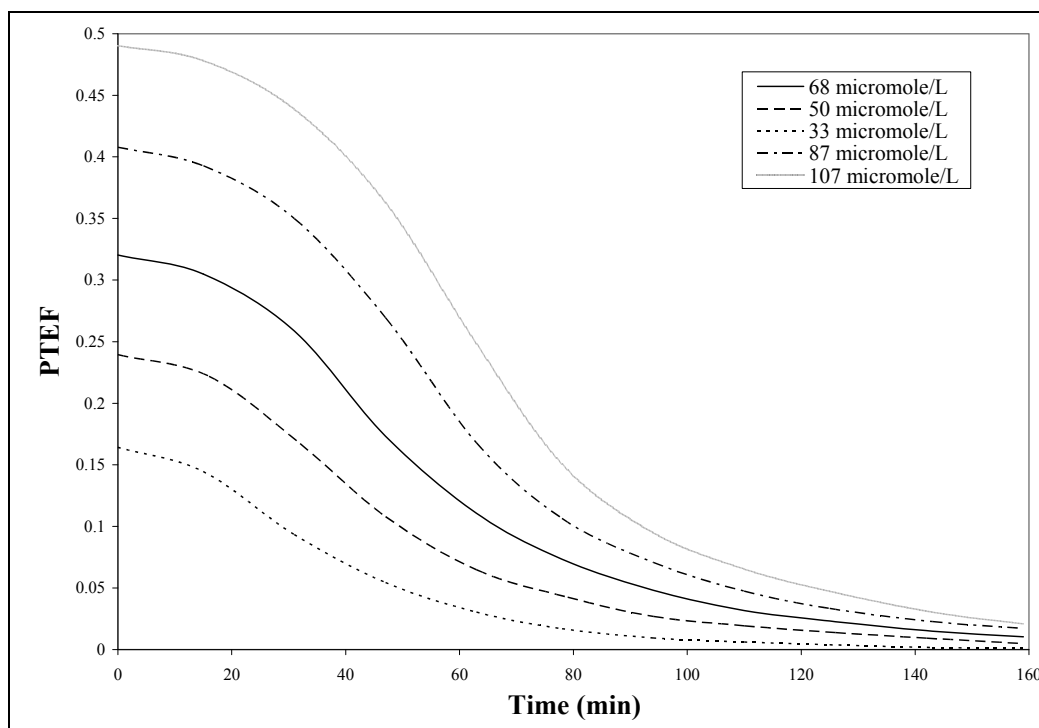


Figure 40: *PTEF* for isopropanol using Degussa P25 as photocatalyst. Five initial concentrations in $\mu\text{mol/L}$: 33, 50, 68, 87 and 107

According to the data reported in Figure 39, the quantum yields for isopropanol photocatalytic degradation are in excess to the theoretical maximum of 133% during a significant period of the irradiation time. These quantum yield values fall in the 8.5-27 range (equivalent to 850-2700%) at initial irradiation conditions. It can be noted that, as in the case of acetone and acetaldehyde photocatalytic degradation, the corresponding *PTEFs* remain in all cases in the 0.16-0.49 (16-49%) range as shown in Figure 40.

Therefore, *PTEFs* consistently stay below 1 even when the corresponding quantum yields supersede the value of 1:

$$QY_{ISOPROPANOL} \geq 1 \text{ with } PTEF_{ISOPROPANOL} \leq 1$$

Thus, in all cases studied, consisting of three model compounds and three initial concentrations, the values of *QYs* supersede in many cases the value of 1.33. In these cases, the *PTEFs* always satisfy the thermodynamic constraint of being smaller than 1.

The high values of *QYs* reported are consistent with *QYs* reported in the technical literature which were based on both photoconverted pollutant and carbon dioxide formed (Negishi et al., 2007; Cassano et al., 1995).

There are two possible contributing factors for high values of *QYs*: a) The quantum yield definitions in the present study involve absorbed photons only. These absorbed photons are the denominator in equation (85) and tend to augment the quantum yield and *PTEFs*; b) The 55.1 liter redesigned Photo-CREC-Air Unit with a catalyst carefully impregnated on a mesh and adequate irradiation leads to higher kinetic rates even at the lower pollutant concentrations.

Thus, it is possible to conclude that high photocatalyst irradiation with enhanced contact between the fluid and the photocatalyst lead to high energy efficiencies. These high *QYs*, exceeding the 1.33 theoretical level, can be justified via a free radical chain mechanism involving other radical species such as peroxy radicals. These peroxy radicals may contribute to various oxidation steps, not requiring once formed extra photons or OH^{\bullet} radicals (Choi et al., 2001; Sopyan, 2007).

8.6 Conclusions

- a) The current 55.1 liter Photo-CREC-Air Reactor shows a highly irradiated catalyst as well as high energy utilization and uniform fluid-catalyst contact.
- b) Experimental and analytical data prove the suitability of the Photo-CREC-Air Unit design as a scaled up photocatalytic reactor for air treatment.
- c) Accurate calculations of quantum yields and Photocatalytic Thermodynamic Efficiency Factors (*PTEFs*) were performed.
- d) Quantum yields for acetone, acetaldehyde and isopropanol model pollutants in a Photo-CREC-Air Unit using Degussa P25 photocatalyst supersede 1.33 (equivalent to 133%). These Quantum yields in excess of 133% are observed at the shorter contact irradiation times.
- e) *PTEFs* for acetone, acetaldehyde and isopropanol model pollutants in the Photo-CREC-Air Reactor remain in all cases below the limit of 1 (equivalent to 100%) complying in all cases with thermodynamic constraints.

Chapter 9

Conclusions and Recommendations

This thesis reports energy efficiencies in a Photo-CREC-Air Reactor Unit using quantum yields and photochemical thermodynamic efficiency factors (PTEF). This is accomplished for the photocatalytic degradation of several model pollutants.

Various energy efficiency evaluations consider the irradiation absorbed by the photocatalyst. With this goal, a Photo-CREC-Air Reactor Unit and its accessories were designed. This unit allows for irradiation macroscopic balances.

This chapter presents the most important conclusions of this PhD dissertation as well as recommendations for future work based of the results obtained.

9.1 Main Conclusions

- a) *A new and efficient design of a 55.1 liter Photo-CREC-Air Reactor was implemented.* The Photo-CREC-Air Reactor was designed and manufactured with several unique features that make it suitable for photocatalytic air purification. This was done given the high energy utilization and the uniform fluid-photocatalyst contact in the Photo-CREC-Air Reactor.
- b) *Irradiation macroscopic balances were thoroughly performed.* These macroscopic irradiation balances were done using in situ measurements of the irradiation absorbed by the photocatalyst. With this objective, a specially designed periscopic device was designed and implemented. This was done to determine the different irradiation components in a photocatalytic unit for air purification. This represents the first contribution that we are aware of, where an accurate evaluation of irradiation absorbed on the photocatalyst is reported.
- c) *The high performance of the 55.1 liter Photo-CREC-Air Reactor design was demonstrated.* This was accomplished using Degussa P25 photocatalyst and various acetone, acetaldehyde and isopropanol concentrations. These model pollutant concentrations in ambient air were 5-10 times lower than in previous studies (Ibrahim, 2001). Photoconversion was completed in 60-120 minutes only, with no intermediate species detected for acetone and acetaldehyde. In

the case of isopropanol photocatalytic degradation, acetone was the only chemical intermediate detected.

- d) *Kinetic modeling using the Langmuir-Hinshelwood model was developed.* This model accounted for the competitive pollutant adsorption of various chemical gas phase species detected in a one type site. Kinetic parameters were established using nonlinear regression. Kinetic parameters were obtained with reduced span and low cross-correlation.
- e) *Quantum yields using phenomenological relevant parameters were established.* Quantum yields accounted for the number of OH^\bullet radicals consumed during the photocatalytic process and the number of photons absorbed. Quantum yields obtained were particularly high at the shorter irradiation times: 215-140% for acetone, 400-250% for acetaldehyde and 1800-850% for isopropanol. These high quantum yields strongly confirm the high performance of the 55.1 liter capacity Photo-CREC-Air Reactor. These high quantum yields may be explained by considering the formation of OH^\bullet radicals by other mechanisms than photocatalysis. Other possible interpretation is the one of a free radical chain reaction mechanism involving radicals other than OH^\bullet .
- f) *Photochemical thermodynamic efficiency factors (PTEF) were proven to be valuable.* This PTEF application represents the first reported application of PTEF in air purification. PTEF calculations allowed establishing compliance of the photocatalytic reaction with thermodynamic constraints. This was true for all experimental conditions studied.

9.2 Recommendations for Future Work

- a) *Use of different irradiation sources.* Irradiation intensity changes in the photocatalytic Photo-CREC-Air Unit still require to be analyzed more thoroughly. This task can be accomplished by using a new set of lamps or simply by covering the UV lamps with wire mesh. One could perform a number of trials by using various wire meshes with different opening sizes. This will reduce the power reaching the supported photocatalyst. The results of such study should allow the conceptualization and design of future photocatalytic reactors.

- b) *Experimentation with different TiO₂ photocatalysts.* TiO₂-based catalysts show certain differences such as crystalline phase distribution, surface area and tendency to agglomerate. Comparison of the possible effects of various photocatalyst types on photocatalytic degradation kinetics using the same type of model compounds is recommended.
- c) *Experimentation with mixtures of model pollutants.* Indoor contaminated air streams usually may contain several different pollutant compounds. Therefore, a study of photocatalytic degradation processes of mixtures of model pollutants is advisable. This type of study may show the effects of competitive adsorption among chemical species.
- d) *In-depth analysis of photocatalytic degradation of model pollutants showing the applicability of the in series-parallel reaction mechanisms.* Conversion of some chemical species (e.g. isopropanol) may involve: i) direct transformation of model pollutant into CO₂, ii) conversion of model pollutants into intermediate species and then conversion of intermediates into CO₂. Clarification of this matter may allow the favoring of specific reactions to avoid the formation of harmful or unwanted byproducts or intermediate compounds.

References

- Aguado, S.; Polo, A.; Bernal. M. M Coronas, J.; Santamaria, J (2004) Removal of pollutants from indoor air using zeolite membranes. *Journal of Membrane Science* 240, 159-166.
- Alfano, M. O.; Cabrera, M. I.; Cassano, A. E. (1997) Photocatalytic Reactions Involving Hydroxyl Radical Attack I. Reaction Kinetics Formulation with Explicit Photon Absorption Effects. *Journal of Catalysis* 172, 370-379.
- Ao, C. H.; Lee, S. C. (2005) Indoor air purification by photocatalyst TiO₂ immobilized on an activated carbon filter installed in an air cleaner. *Chemical Engineering Science* 60, 103-109.
- Alfano, O. M.; Cassano, A. E.; (2008) Photoreactor Modeling: Applications to Advanced Oxidation Process. *International Journal of Chemical Reactor Engineering* 6, 1-18.
- Al-Ekabi, H.; Serpone, N.; Pelizzetti, E.; Minero, C.; Anne Fox, M.; Barton Draper, R. (1989) Kinetic studies in heterogeneous photocatalysis. 2. Titania-mediated degradation of 4-chlorophenol alone and in a three-component mixture of 4-chlorophenol, 2,4-dichlorophenol, and 2,4,5-trichlorophenol in air-equilibrated aqueous media. *Langmuir* 5 (1), 250-255.
- Arai, T.; Yanagida, M.; Konishi, Y.; Iwasaki, Y.; Sugihara, H.; Sayama, K. (2008) Promotion effect of CuO co-catalyst on WO₃-catalized photodegradation of organic substances. *Catalysis Communications* 9, 1254-1258.
- Benoit-Marquie, F.; Wilkenhoner, U.; Simon, V.; Braun, A.; Oliveros, E.; Maurette, M. T. (2000) VOC photodegradation at the gas-solid interface of a TiO₂ photocatalyst part I: 1-butanol and 1-butylamine; *Journal of Photochemistry and Photobiology A: Chemistry*, 132, 225-232.
- Besov, A. S.; Vorontsov, A. V. (2007) Acceleration of Acetone Destruction Process under Synergistic Action of Photocatalytic Oxidation and Barrier Discharge, *Plasma Chem. Plasma Process.* 27, 624-634.

- Bickley, R.I.; Stone, F.S. (1973) Photoadsorption and Photocatalysis at Rutile Surfaces I. Photoadsorption of Oxygen. *Journal of Catalysis*. 31, 389-397
- Bolton, J.; Safarzadeh-Amiri, A; Carter, S. (1995) The Detoxification of Waste Water Streams Using Solar and Artificial UV Light Sources; *Alternative Fuels and the Environment*; Sterrett F.(ed.); Lewis Publishers, 187-192.
- Cant, N. W.; Cole, J .R. (1992) Photocatalysis of the reaction between ammonia and nitric oxide on TiO₂ surface. *Journal of Catalysis* 134, 317-323.
- Cassano, A.; Martín, C.; Brandi, R.; Alfano, O. (1995) Photoreactor Analysis and Design: Fundamentals and Applications, *Industrial and Engineering Chemistry Research* 34, 2155-2201.
- Cerdá, J.; Marchetti, J. L.; Cassano, A. E. (1977) Radiation efficiencies in elliptical photoreactors. *Latin American Journal of Heat Mass Transfer* 1, 33-63.
- Chang, C. P.; Chen, J. N.; Lu, M. C. (2003) Heterogeneous Photocatalytic Oxidation of Acetone for Air Purification by Near UV-Irradiated Titanium Dioxide. *Jornal Environ. Sci. Health, Toxic/Hazard Subst. Environmental Engineering* 38, 1131-1143.
- Changrani, R.G.; Raupp, G. B. (1999) Monte Carlo simulation of the radiation field in a reticulated foam photocatalytic reactor. *AIChE Journal*, 45, 1085-1094.
- Changrani, R .G.; Raupp, G. B. (2000) Two-dimensional heterogeneous model for a reticulated-foam photocatalytic reactor. *AIChE Journal*, 46, 829-842.
- Chen, Y.; Dionysiou, D.; (2006) Effect of calcination temperature on the photocatalytic activity and adhesion of TiO₂ films prepared by the P-25 powder-modified sol-gel method, *Journal of Molecular Catalysis A: Chemical* 244, 73-82.
- Chen D., Ray A. K. (1999) Photocatalytic kinetics of phenol and its derivatives over UV irradiation TiO₂. *Applied Catalysis B: Environmental* 23, 143.

- Choi, W.; Ko, J. Y.; Park, H.; Chung, J. S. (2001) Investigation on TiO₂-coated optical fibers for gas-phase photocatalytic oxidation of acetone. *Applied Catalysis, B: Environmental* 31, 209-220.
- de Lasa, H.; Serrano, B.; Salaices, M.; (2005) *Photocatalytic Reaction Engineering*, First Ed., Springer: New York.
- Daisey, J. M.; Angell, W. J.; Apte, M. G. (2003) Indoor air quality, ventilation and health symptoms in schools: an analysis of existing information. *Indoor Air* 13, 53-64.
- Davydov, L.; Smirniotis, P. G.; Pratsinis, S. E. (1999) Novel Differential Reactor for the Measurement of Overall Quantum Yields. *Industrial and Engineering Chemistry Research* 38, 1376-1383.
- Dibble, J. A.; Raupp, G. B. (1992) Fluidized-bed photocatalytic oxidation of trichloroethylene in contaminated airstreams. *Environmental Science & Technology*, 26, 492-495.
- Emeline, A.V.; X. Zhang, X.; Jin, M.; Murakami, T.; Fujishima, A. (2006) Application of a "Black Body" Like Reactor for Measurements of Quantum Yields of Photochemical Reactions in Heterogeneous Systems; *The Journal of Physical Chemistry B*, 110, 7409-7413.
- Esterkin, C. R.; Negro, A. C.; Alfano, O. M.; Cassano, A. E. (2002) Radiation field inside a reactor of glass-fiber meshes coated with TiO₂. *AIChE Journal*, 48, 832-845.
- Finlayson-Pitts, B. J.; Pitts, J. N. (2000) *Chemistry of the Upper and Lower Atmosphere: Theory, Experiments, and Applications*; Academic Press: New York.
- Fox M. A.; Dulay, M. T. (1993) Heterogeneous Photocatalysis. *Chemical Reviews* 93, 341-350.
- Garcia-Hernandez, J. M., Serrano, B. and de Lasa, H. (2010) Energy Efficiencies in a Photo-CREC-Air Reactor: Conversion of Model Pollutants in Air.

- The photochemical thermodynamic efficiency factor (PTEF) in photocatalytic reactors for air treatment. *Chemical Engineering Journal* 165, 891-901.
- Garcia-Hernandez, J.M., Serrano, B. and de Lasa, H. (2012). The photochemical thermodynamic efficiency factor (PTEF) in photocatalytic reactors for air treatment. Accepted for Publication in: *Industrial & Engineering Chemistry Research*.
- Hayes, R. E.; Kolaczkowski, S. T.; Thomas, W. J. (1992) Finite-element model for a catalytic monolith reactor. *Computer Chemical Engineering* 16, 645-657.
- Henderson, M. A. (2011) A surface science perspective on TiO₂ photocatalysis. *Surface Science Reports*. 66, 185-297
- Hennezel D., Pichat O. P., Ollis D. F. (1998) Benzene and toluene gas-phase photocatalytic degradation over H₂O and HCl pretreated TiO₂: by-products and mechanisms. *Journal of Photochemistry and Photobiology A: Chemistry* 118, 197.
- Herbig, B.; Löbmann, P.; (2004) TiO₂ photocatalysts deposited on fiber substrates by liquid phase deposition. *Journal of Photochemistry and Photobiology A: Chemistry* 163, 359-365.
- Hernández-Alonso M. D.; Tejedor-Tejedor I.; (2011) Coronado, J M.; Anderson, M. A. Operando FTIR study of the photocatalytic oxidation of methylcyclohexane and toluene in air over TiO₂-ZrO₂ thin films: Influence of the aromaticity of the target molecule on deactivation. *Applied Catalysis B*. 101, 283-293.
- Hofstadler, K.; Bauer, R.; Novalic, S.; Helsfer, G. (1994) New reactor design for photocatalytic wastewater treatment with TiO₂ mobilized on fused-silica glass fibers; Photomineralization of 4-chlorophenol. *Environmental Science & Technology*, 28, 670-674.
- Hossain, M. M.; Raupp, G. B.; Hay, S. O.; Obee, T. N. (1975) Three-dimensional developing flow model for photocatalytic monolith reactor. *AIChE Journal* 45, 1309-1321.

- Hossain, M. M.; Raupp, G. B. (1998) Radiation field modeling in a photocatalytic monolith reactor. *Chemical Engineering Science* 53, 3771-3780.
- Hossain, M. M.; Raupp, G. B. (1999) Polychromatic radiation field model for a honeycomb monolith photocatalytic reactor. *Chemical Engineering Science* 54, 3027-3034.
- Ibrahim, H., (2001) Photo-catalytic reactor for the degradation of airborne pollutants: photo-conversion efficiency and kinetic modeling. Ph.D. Dissertation. The University of Western Ontario, London, Canada.
- Ibrahim, H.; de Lasa, H. (2003) Photo-catalytic degradation of air borne pollutants. Apparent quantum efficiencies in a novel photo-CREC-air reactor. *Chemical Engineering Science* 58, 943-949.
- Ibrahim, H.; de Lasa, H. (2004) Kinetic Modeling of the Photocatalytic Degradation of Air-Borne Pollutants. *AIChE Journal* 50, 1017-1027.
- Jacoby, W. A. (1993) Destruction of trichloroethylene in air via semiconductor mediated gas-solid heterogeneous photocatalysis. PhD dissertation, Department of Chemical Engineering, University of Colorado, USA.
- Kaneko, M.; Okura, I. (Eds.) (2002) *Photocatalysis: Science and Technology*, Kodansha Springer: Tokyo, Berlin, New York.
- Kim, H.; Choi, W. (2007) Effects of surface fluorination of TiO₂ on photocatalytic oxidation of gaseous acetaldehyde. *Applied Catalysis, B*, 69, 127-132.
- Kisch, H. (2010) On the Problem of comparing Rates or Apparent Quantum Yields in Heterogeneous Photocatalysis. *Angewandte Chemie International Edition* 49, 9588-9589.
- Kribus, A.; Zik, O.; Karni, J. (2000) Optical fiber and solar power generation. *Solar Energy* 68, 405-416.
- Larson, S. A.; Widegren, J. A.; Falconer, J. L. (1995) Transient studies of 2-propanol photocatalytic oxidation on titania. *Journal of Catalysis* 157, 611-625.

- Lichtin, N. N.; Avudaithai, M.; Berman, E.; Grayfer, A. (1996) TiO₂-photocatalyzed oxidation degradation of binary mixture of vaporized organic compounds. *Solar Energy* 5, 377-385.
- Lim, T. H.; Jeong, S. M.; Kim, S. D.; Gyenis, J. (2000) Photocatalytic decomposition of NO by TiO₂ particles. *Journal of Photochemistry and Photobiology A: Chemistry* 134, 209-217.
- Marinangeli, R. E.; Ollis, D. F. (1977) Photo-assisted heterogeneous catalysis with optical fibers: I. Isolated single fiber. *AIChE Journal* 23, 415-426.
- Marinangeli, R. E.; Ollis, D. F. (1980) Photo-assisted heterogeneous catalysis with optical fibers: II. Nonisothermal Single Fiber and Fiber Bundle. *AIChE Journal* 26, 1000-1008.
- Marinangeli, R. E.; Ollis, D. F. (1982) Photo-assisted heterogeneous catalysis with optical fibers. Part III: Photoelectrodes. *AIChE Journal* 28, 945-955.
- Maruyama, T.; Nishimoto, T. (1992) Light intensity profile in heterogeneous photochemical reactor. *Chemical Engineering Communications* 117, 111-116.
- Matthews, R. W.; Photocatalysis in water purification: Possibilities, problems and prospects, in *Photocatalytic purification and treatment of water and air*, Ollis, D., and Al-Ekabi, H. (eds.); Elsevier, 121-133.
- Mills, A.; Davies, R. H.; Worsley, D. (1993) Water purification by semiconductor photocatalysis. *Chemical Society Reviews* 22, 417-425.
- Mo, J. H.; Zhang, Y. P.; Yang, R. (2005) Novel insight into VOC removal performance of photocatalytic oxidation reactors. *Indoor Air* 15, 291-300.
- Mo, J. H.; Zhang, Y. P.; Yang, R.; Xu, Q. J. (2008) Influence of fins on formaldehyde removal in annular photocatalytic reactors. *Building and Environment* 43, 238-245.
- Mo, J.; Zhang Y.; Xu, Q; Lamsona, J. J.; Zhao, R. (2009) Photocatalytic purification of volatile organic compounds in indoor air: A literature review. *Atmospheric Environment* 43, 2229-2246.

- Mohseni, M.; Taghipour, F. (2004) Experimental and CFD analysis of photocatalytic gas phase vinyl chloride (VC) oxidation. *Chemical Engineering Science* 59, 1601-1609.
- Morikawa, T.; Irokawa, Y.; Ohwaki, T. (2006) Enhanced photocatalytic activity of $\text{TiO}_2\text{-xNx}$ loaded with copper ions under visible light irradiation *Applied Catalysis, A* 314, 123-127.
- Nam, W.; Kim, J.; Han, G. (2002) Photocatalytic oxidation of methyl orange in a three-phase fluidized bed reactor. *Chemosphere* 47, 1019-1024.
- Negishi, N.; Matsuzawa, S.; Takeuchi, K.; Pichat, P.; (2007) Transparent Micrometer-Thick TiO_2 Films on SiO_2 -Coated Glass Prepared by Repeated Dip-Coating/Calcination: Characteristics and Photocatalytic Activities for Removing Acetaldehyde or Toluene in Air. *Chemistry of Materials* 19, 3808-3814.
- Nimlos, M. R.; Wolfrum, E. J.; Brewer, M. L.; Fennell, J. A.; Bintner, G. (1996) Gas-Phase Heterogeneous Oxidation of Ethanol: Pathways and Kinetic Modeling *Environmental Science & Technology* 30, 3102-3110.
- Obee, T. N. (1996) Photooxidation of sub-parts-million toluene and formaldehyde levels on titania using a glass-plate reactor. *Environmental Science & Technology* 30, 3578-3584.
- Ollis, D. F. (1991) Solar-assisted photocatalysis for water purification : issues, data, questions. In *Photochemical Conversion and Storage of Solar Energy*, eds. E. Pelizzetti and M. Schiavello. Kluwer Academic Publishers, Dordrecht, The Netherlands 235.
- Parmon, V. (1997) Catalysis as a phenomenon: Aspects of terminology. *Catalysis Today* 39, 137-144.
- Paz, Y. (2009) Photocatalytic Treatment of Air: From Basic Aspects to Reactors, in: H.I. de Lasa, B. Serrano (Eds.), *Advances in Chemical Engineering* 36, 289-336.

- Peill, N. J.; Hoffmann, M. R. (1995) Development and optimization of a TiO₂-coated fiber-optic cable reactor: photocatalytic degradation of 4-chlorophenol. *Environmental Science & Technology* 29, 2974-2981.
- Peral, J.; Ollis, D. F. (1992) Heterogeneous photocatalytic oxidation of gas-phase Organics for Air Purification: Acetone, 1-Butanol, Butyraldehyde, Formaldehyde and m-Xylene Oxidation. *Journal of Catalysis* 36, 554-565.
- Peral, J.; Ollis, D. F. (1992) Heterogenous Photocatalytic Oxidation of Gas-Phase Hoffmann, M. R.; Martin, S. T.; Choi, W. (1995) Environmental Applications of Semiconductor Photocatalysis. *Chem. Rev.* 95, 69-77.
- Peral, J.; Domènech, X.; Ollis, D. F. (1997) Heterogeneous Photocatalysis for Purification, Decontamination and Deodorization of Air. *Journal of Chemical Technology & Biotechnology* 70, 117-140.
- Pichat, P. (2010) Some views about indoor air photocatalytic treatment using TiO₂: Conceptualization of humidity effects, active oxygen species, problem of C₁–C₃ carbonyl pollutants. *Applied Catalysis B* 99, 428-434.
- Portela, R.; Sánchez, B.; Coronado, J. M.; Candal, R. and Suárez, S.; (2007) Selection of TiO₂-support: UV-transparent alternatives and long-term use limitations for H₂S removal. *Catalysis Today* 129, 223-230.
- Raupp, G.; Junio, C. (1993) Photocatalytic Oxidation of Oxygenated Air Toxics. *Applied Surface Science* 72, 321-327.
- Raupp, G. B.; Nico, J. A.; Annangi, S.; Changrani, R.; Annapragada, R. (1997) Two flux radiation model for an annular packed-bed photocatalytic reactor. *AIChE Journal* 43, 792-801.
- Raupp, G. B.; Alexiadis, A.; Hossain, M. M.; Changrani, R. (2001) First-principles modeling, scaling laws and design of structured photocatalytic oxidation reactors for air purification. *Catalysis Today* 69, 41-49.

- Romero-Vargas Castrillón, S.; Ibrahim, H.; de Lasa, H.; (2006) Flowfield investigation in a photocatalytic reactor for air treatment (Photo-CREC-Air). *Chemical Engineering Science* 61, 3343-3361.
- Romero-Vargas Castrillón, S.; de Lasa, H.; (2007) Performance Evaluation of Photocatalytic Reactors for Air Purification Using Computational Fluid Dynamics (CFD). *Industrial & Engineering Chemistry Research* 46, 5867-5880.
- Salvador, P. (2007) On the Nature of Photogenerated Radical Species Active in the Oxidative Degradation of Dissolved Pollutants with TiO₂ Aqueous Suspensions: A Revision in the Light of the Electronic Structure of Adsorbed Water. *Journal of Physical Chemistry C* 111, 17038-17043
- Sauer, M. L.; Ollis, D. F. (1994) Acetone oxidation in a photocatalytic monolith reactor. *Journal of Catalysis* 149, 81-91.
- Schmidt, C. M.; Buchbinder, A. M.; Weitz, E.; Geiger, F. M. (2007) Photochemistry of the Indoor Air Pollutant Acetone on Degussa P25 TiO₂ Studied by Chemical Ionization Mass Spectrometry. *Journal of Physical Chemistry A* 111, 13023-13031.
- Sczechowski, J. G., Koval, C. A., Noble, R. D. (1995) A Taylor Vortex Reactor for Heterogeneous Photocatalysis. *Chemical Engineering Science* 50, 3163-3173.
- Serpone, N.; Emeline, A. V. (2002) Suggested terms and definitions in photocatalysis and radiocatalysis. *International Journal of Photoenergy* 4, 91-131.
- Serpone, N.; Khairutdinov, R. F. (1996) Application of nanoparticles in the photocatalytic degradation of water pollutants (review). In: Kamat, P.V., Meisel, D. (Eds.), *Studies in Surface Science and Catalysis* 103 (Semiconductor Nanoclusters: Physical, Chemical, and Catalytic Aspects). Elsevier, Netherlands, 417-444.
- Serpone, N., and Pelizzetti, E. (eds) (1989) *Photocatalysis: Fundamentals and Applications*. Wiley: New York.

- Serrano, B.; de Lasa, H. (1997) Photocatalytic degradation of water organic pollutants. Kinetic modeling and energy efficiency. *Industrial and Engineering Chemistry Research* 36, 4705-4711.
- Sopyan, I. (2007) Kinetic analysis on photocatalytic degradation of gaseous acetaldehyde, ammonia and hydrogen sulfide on nanosized porous TiO₂ films. *Science and Technology of Advanced Materials*. 8, 33-39.
- Spengler, J. D.; Chen, Q. (2000) Indoor air quality factors in designing a healthy building. *Annual Review of Energy and the Environment* 25, 567-600.
- Suttiponparnit, K; Jiang, J.; Sahu, M.; Suvachittanont, S.; Charinpanitkul, T.; Biswas, P. (2011) Role of Surface Area, Primary Particle Size, and Crystal Phase on Titanium Dioxide Nanoparticle Dispersion Properties. *Nanoscale Research Letters* 6, 27-34.
- Suzuki, K.; Satoh, S.; Yoshida, T. (1991) Photocatalytic deodorization on TiO₂ coated honeycomb ceramics; *Oenki Kagaku*, 59, 521-523.
- Tahiri, H.; Serpone, N.; Le Van Mao, R. (1996) Application of concept of relative photonic efficiencies and surface characterization of a new titania photocatalyst designed for environmental remediation. *Journal of Photochemistry and Photobiology A: Chemistry* 93, 199-203.
- Thevenet, F.; Guaitella, O.; Puzenat, E.; Guillard, C.; Rousseau, A. (2008) Influence of water vapour on plasma/photocatalytic oxidation efficiency of acetylene. *Applied Catalysis, B* 84, 813-820.
- Thiruvengkatachari, R.; Vigneswaran, S. and Moon, I. S. (2008) A review on UV/TiO₂ photocatalytic oxidation process. *Korean Journal of Chemical Engineering* 25, 64-72.
- Trillas, M.; Pujol, M.; Domenech, X. (1992) Phenol photodegradation over titanium dioxide. *Journal of Chemical Technology and Biotechnology* 55, 85-90.

- Valladares, J. E.; Bolton, J. R. (1993) in: D.E. Ollis, H. Al-Ekabi (Eds.),
Photocatalytic Purification and Treatment of Water and Air, Elsevier, New
York.
- Votruba, J.; Mikus, O.; Nguen, K.; Hlavacek, V.; Skrivanek, J. (1975) Heat and mass
transfer in monolithic honeycomb catalyst—II. *Chemical Engineering Science*
30, 201-206.
- Wang, W.; Chiang, L. W.; Ku, Y. (2003) Decomposition of benzene in air streams by
UV/TiO₂ process. *Journal of Hazardous Materials* 101, 133-146.
- Wilkins, F.; Blake, D. (1994) Use solar energy to drive chemical processes. *Chemical
Engineering and Processing* 90, 41-49.
- Yamazaki, S. (1999) Kinetic studies of oxidation of ethylene over a TiO₂
photocatalyst *Journal of Photochemistry and Photobiology A: Chemistry* 121,
55-61.
- Yamazaki-Nishida, S.; Read, H. W.; Nagano, J. K.; Jarosch, T.; Eddy, C.; Cervera-
March, S.; Anderson, M. A. (1994) Gas Phase Photocatalytic Degradation on
TiO₂ Pellets of Volatile Chlorinated Organic Compounds from a Soil Vapor
Extraction Well. *Journal of Soil Contamination* 3, 1-16.
- Yu, J. C.; Zhang, L.; Zheng, Z. and Zhao, J.; (2003) Synthesis and Characterization of
Phosphated Mesoporous Titanium Dioxide with High Photocatalytic Activity.
Chemistry of Materials 15, 2280-2286.
- Zhang, Y.; Crittenden, J. C.; Hand, D. W.; Perram, D. L. (1994) Fixed-bed
photocatalysts for solar decontamination of water. *Environmental Science and
Technology* 28, 435-442.
- Zhang, Z.; Anderson, W. A.; Moo-Young, M. (2000) Rigorous modeling of UV
absorption by TiO₂ films in a photocatalytic reactor. *AIChE Journal* 46, 1461-
1470.
- Zhao, J.; Yang, X. (2003) Photocatalytic oxidation for indoor air purification: A
literature review. *Building and Environment* 38, 645-654.

Appendix A

Mechanism of Formation of OH^\bullet Radicals in Photocatalytic Processes for Air Treatment

The formation of OH^\bullet radicals in photocatalysis applied to air treatment can be sketched with a process similar to the one proposed in water treatment. The main difference is that all the mechanistic steps involve species adsorbed on the surface of the semiconductor.

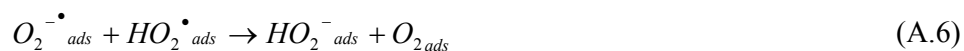
The heterogeneous photocatalytic process can be explained with the photons of light (from the sunlight or an artificial source) exciting the TiO_2 and promoting electrons from the valence band to the conduction band of the semiconductor to generate electron/hole pairs



The electron/holes pairs react with water molecules or hydroxyl ions that are adsorbed on the surface of TiO_2 to produce hydroxyl radicals as follows



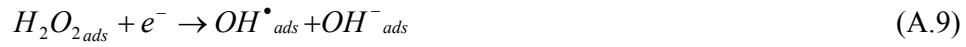
At the same time the electrons react with oxygen to form superoxide radicals. The hydrogen peroxide is formed according to equations (A.4) to (A.7).



Multiplying equations (A.2), (A.3) and (A.4) by a factor of 2 and adding all of them



Consequently there is also formation of hydroxyl radicals (OH^{\bullet}) from the hydrogen peroxide by following two extra steps



Adding these two previous equations



The combination of the equations (A.8) and (A.11) leads to the expression



Thus, the overall stoichiometry for the formation of OH^{\bullet} radicals can be described with 3 photons yielding 4 OH^{\bullet} .

Appendix B

Reaction Enthalpy for the Formation of OH^\bullet Radicals in Photocatalytic Reactors for Air Treatment

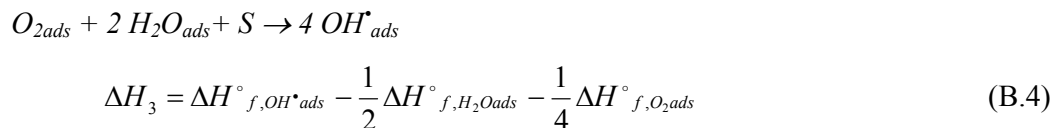
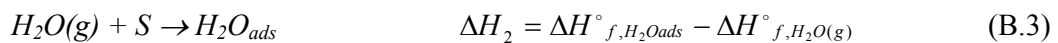
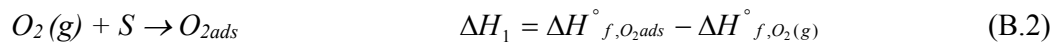
The formation enthalpy of OH^\bullet is a critical parameter for the calculation of $PTEF$ in photocatalytic reactors. According to stoichiometric requirements, OH^\bullet radicals can be formed via the following overall equation:



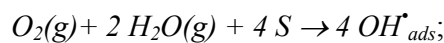
Enthalpy evaluations in equation (B.1) can consider a “likely” path for the reactant species (water vapor and oxygen) to evolve forming adsorbed OH^\bullet radicals (products). This hypothetical reaction path gives the correct numerical result; since this calculation involves enthalpies (state functions).

The proposed “likely” path for thermodynamic evaluations hypothesizes that the reaction takes place as follows: a) oxygen gas is adsorbed on the photocatalyst surface, b) water vapor is adsorbed on the photocatalyst surface, c) adsorbed OH^\bullet species are formed via reaction of adsorbed oxygen and water species. It is in this adsorbed state where OH^\bullet radicals are assumed to react with organic molecules forming intermediates first, yielding CO_2 later and reaching complete mineralization.

Thus and as reported by Garcia-Hernandez et al. (2010),



The algebraic addition of these three steps leads to the following:



$$\Delta H_{OH^\bullet} = \left[\Delta H_3 + \frac{1}{2} \Delta H_2 + \frac{1}{4} \Delta H_1 \right] = \Delta H_3 = \Delta H_{f,OH^\bullet ads}^\circ - \frac{1}{2} \Delta H_{f,H_2O(g)}^\circ - \frac{1}{4} \Delta H_{f,O_2(g)}^\circ \quad (B.5)$$

Assuming that the adsorption mechanism that possibly prevails in photocatalytic processes is one of chemisorption, a good estimation of the heat of adsorption is via the heat of condensation (Ruscic et al., 2002; Sicilia et al., 1993). As a result and using the heat of formation data reported by (Wagman et al., 1982; Kyle, 1992) the adsorption enthalpy of OH^\bullet radical species results as,

$$\Delta H_{f,OH^\bullet ads}^\circ = 38950 \text{ J/mol} - (-86490 \text{ J/mol}) = 125440 \text{ J/mol} \quad (B.6)$$

Thus, the enthalpy of formation of the OH^\bullet groups adsorbed on the photocatalyst surface having both H_2O and O_2 in the gas phase is as follows (Garcia-Hernandez et al., 2010):

$$\Delta H_{OH^\bullet} = 125440 \text{ J/mol} - \frac{1}{2}(23181 \text{ J/mol}) \quad (B.7)$$

$$\Delta H_{OH^\bullet} = 4531 \frac{\text{J}}{\text{mol of } OH^\bullet} \quad (B.8)$$

While a similar analysis was developed by Serrano et al. (2009) for a photocatalytic reactor for water purification, the enthalpy of adsorbed OH^\bullet radicals for air treatment photocatalysis is noticeably smaller than the 98300 J/mol enthalpy reported by Serrano et al. (2009). Since the enthalpy required to produce an adsorbed OH^\bullet group in an air treatment photocatalyst is 4531 J/mol of OH^\bullet , the fraction of photon energy used to form an OH^\bullet radical is

$$\eta_{OH^\bullet} = \frac{\Delta H_{OH^\bullet}}{E_{av}} = \frac{4531 \frac{\text{J}}{\text{mol of } OH^\bullet}}{343913 \frac{\text{J}}{\text{mol of photon}}} = 0.0131 \frac{\text{mol of photon}}{\text{mol of } OH^\bullet} \quad (B.9)$$

In this respect, one should also notice that the calculated η_{OH^\bullet} for photocatalysis in air is significantly smaller than the η_{OH^\bullet} parameter in water: 0.0131 in air versus 0.29 in water.

Appendix C

Calculation of the Average Photon Energy and the Fraction of Q_{irr} with a Wavelength Smaller than 388 nm (14.7 L Photo-CREC-Air Unit)

The average photon energy (E_{av}) emitted by a near UV lamp and able to activate the TiO_2 can be calculated from the irradiation spectrum. This is established using a spectroradiometer as follows:

$$E_{av} = \frac{\int_{\lambda_{min}}^{\lambda_{max}} I(\lambda)E(\lambda)d\lambda}{\int_{\lambda_{min}}^{\lambda_{max}} I(\lambda)d\lambda} \quad (C.1)$$

where:

$I(\lambda)$ = intensity of light, W/cm^2

$E(\lambda)$ = energy of a photon at a given wavelength, J

The upper integration limit λ_{max} has a wavelength with a value of 388 nm. This is the highest wavelength with enough energy to supersede the catalyst (TiO_2) band gap.

Figure C1 shows the spectral chart of the lamp used during the photoconversion of acetone and acetaldehyde. This is performed with a previous design of the Photo-CREC-Air Reactor as characterized with the Sola Scope 2000 spectroradiometer (Ibrahim, 2001). The measurements were performed every 0.5 nm for the 300-390 nm range at different locations. This confirmed uniform intensity distribution of photons reaching the glass fiber mesh holding the TiO_2 loadings.

If it is considered that $E(\lambda) = \frac{hc}{\lambda}$, where h is the Planck's constant and c is the speed of light, therefore:

$$E_{av} = \frac{hc \int_{\lambda_{min}}^{\lambda_{max}} I(\lambda) \frac{d\lambda}{\lambda}}{\int_{\lambda_{min}}^{\lambda_{max}} I(\lambda)d\lambda} \quad (C.2)$$

Thus,

$$E_{av} = \frac{hc \int_{\lambda_{\min}}^{\lambda_{\max}=388nm} I(\lambda) \frac{d\lambda}{\lambda}}{\int_{\lambda_{\min}}^{\lambda_{\max}=388nm} I(\lambda) d\lambda} = E_{av} = \frac{\left(6.63 \times 10^{-34} \frac{J \text{ sec}}{\text{photon}}\right) \left(3 \times 10^8 \frac{m}{s}\right)}{3.48 \times 10^{-7} m} = 5.71 \times 10^{-19} \frac{J}{\text{photon}}$$

$$E_{av} = \left(5.71 \times 10^{-19} \frac{J}{\text{photon}}\right) \left(6.023 \times 10^{23} \frac{\text{photon}}{\text{mol photon}}\right) = 343913 \frac{J}{\text{mol photon}}$$

(C.3)

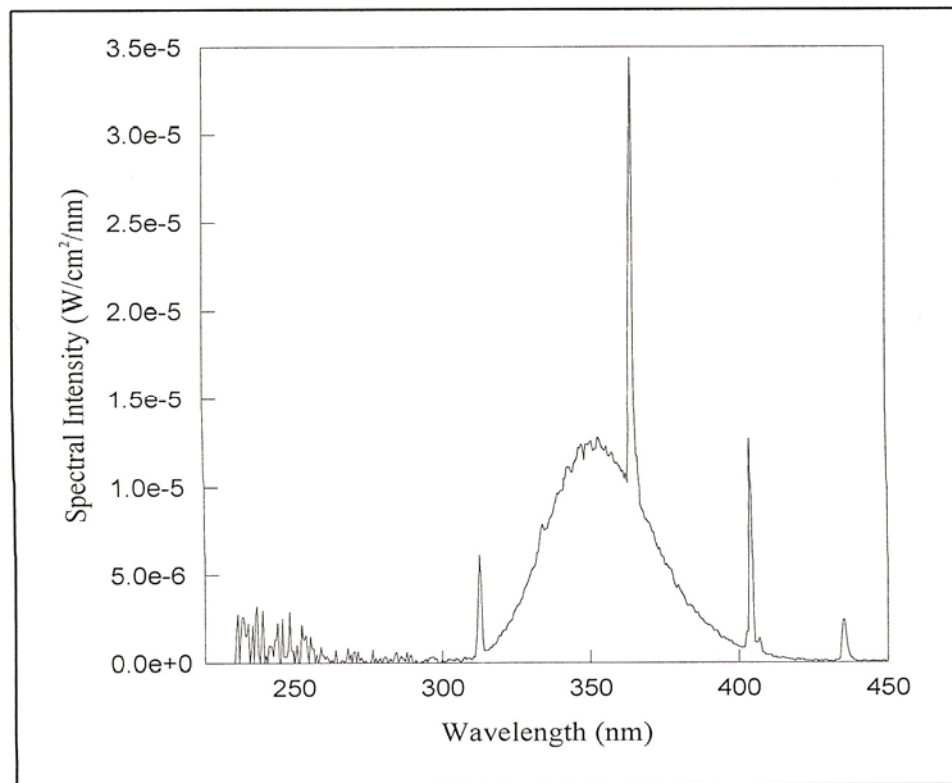


Figure C1: Spectral intensity of a new Pen-Ray lamp as measured by the Sola Scope 2000 Spectroradiometer. This reports the fraction of the total energy involved in the average photon energy calculation (Ibrahim, 2001)

Furthermore, using the same spectrum as reported in Figure C1, one can calculate the fraction of irradiated energy with a wave length smaller than 388 nm as follows:

$$\gamma = \frac{\int_{\lambda_{\max}=388nm}^{\lambda_{\min}} I(\lambda) d\lambda}{\int_{\lambda_{\min}}^{\lambda_{\max}=469nm} I(\lambda) d\lambda} \quad (\text{C.4})$$

As a result, it is possible to establish that for the case of the present study γ has a value of 0.92.

Appendix D

Calculation of the Average Photon Energy and the Fraction of Q_{ads} with a Wavelength Smaller than 388 nm (55.1 L Photo-CREC-Air Unit)

The average photon energy (E_{av}) emitted by a near UV lamp and able to activate the TiO_2 and be calculated from the irradiation spectrum which is established using a spectroradiometer

$$E_{av} = \frac{\int_{\lambda_{min}}^{\lambda_{max}} I(\lambda)E(\lambda)d\lambda}{\int_{\lambda_{min}}^{\lambda_{max}} I(\lambda)d\lambda} \quad (D.1)$$

where

$I(\lambda)$ = intensity of light, W/cm^2

$E(\lambda)$ = energy of a photon at a given wavelength, J

The upper integration limit λ_{max} is determined by the highest wavelength with enough energy to supersede the catalyst (TiO_2) band gap and has a value of 388.

Figure D1 shows the spectral chart of the 15 Watt UV lamp (UVP Inc., Upland CA) used during the photoconversion of acetone and acetaldehyde as characterized with the Stellarnet EPP2000 spectroradiometer; the measurements were performed every 0.5 nm at different locations, being the values between 300-390 nm the range in which the photons have enough energy to supersede the photocatalyst bandgap. Uniform intensity distribution of photons absorbed by the TiO_2 loadings hold by the stainless steel mesh was confirmed.

If it is defined that $E(\lambda) = \frac{hc}{\lambda}$, where h is the Planck's constant and c is the speed of light,

$$E_{av} = \frac{hc \int_{\lambda_{min}}^{\lambda_{max}} I(\lambda) \frac{d\lambda}{\lambda}}{\int_{\lambda_{min}}^{\lambda_{max}} I(\lambda) d\lambda} \quad (D.2)$$

Thus,

$$E_{av} = \frac{hc \int_{\lambda_{min}}^{\lambda_{max}=388nm} I(\lambda) \frac{d\lambda}{\lambda}}{\int_{\lambda_{min}}^{\lambda_{max}=388nm} I(\lambda) d\lambda} = E_{av} = \frac{\left(6.63 \times 10^{-34} \frac{J \text{ sec}}{\text{photon}}\right) \left(3 \times 10^8 \frac{m}{s}\right)}{3.387 \times 10^{-7} m} = 5.81245 \times 10^{-19} \frac{J}{\text{photon}}$$

$$E_{av} = \left(5.81245 \times 10^{-19} \frac{J}{\text{photon}}\right) \left(6.023 \times 10^{23} \frac{\text{photon}}{\text{mol photon}}\right) = 350084 \frac{J}{\text{mol photon}}$$

(D.3)

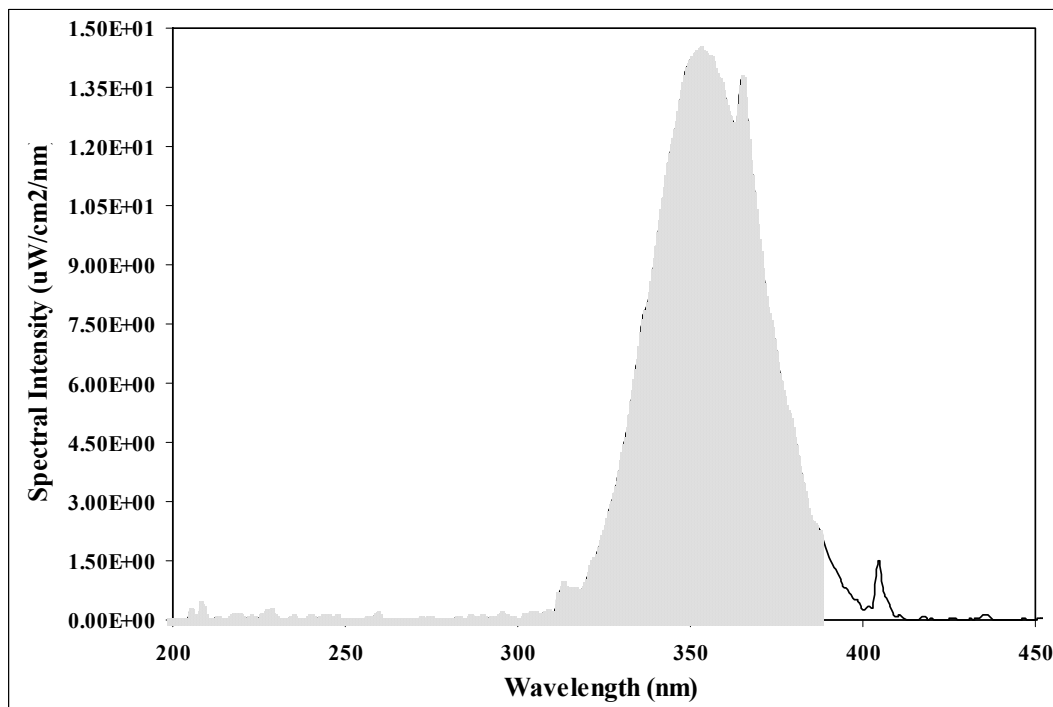


Figure D1: Spectral intensity inside the reaction section of the Photo-CREC-Air reactor reporting the fraction of the total energy involved in the average photon energy calculation

Furthermore using the same spectrum as reported in Figure D1 it is possible to calculate the fraction of irradiated energy with a wave length smaller than 388 nm as follows:

$$\gamma = \frac{\int_{\lambda_{\max}=388nm}^{\lambda_{\min}} I(\lambda) d\lambda}{\int_{\lambda_{\min}}^{\lambda_{\max}=469nm} I(\lambda) d\lambda} \quad (\text{D.4})$$

As a result, the case of the present study, it has been established a value for γ of 0.93.

APPENDIX E

Lamp Characterization

The accurate estimation of the lamp output power is a crucial factor in the evaluation of any photocatalytic performance. Without an accurate and direct physical estimate of the lamp output power, calculations of intensity field are subject to uncertainty. Therefore, determination of how efficiently is the use of irradiation in photocatalytic reactors is closely related to the lamp characterization.

The lamps used in this study (15 Watt black-light-bulb near-UV), as a part of the Photo-CREC-Air reactor, were characterized using a spectrophotometer. The spectrophotometer provides both the total emission intensity as well as the spectral chart of the lamp (Figure E1). This spectral chart played an important role in the calculation of the average photon energy used in the evaluation of efficiency parameters as described in Chapter 8.

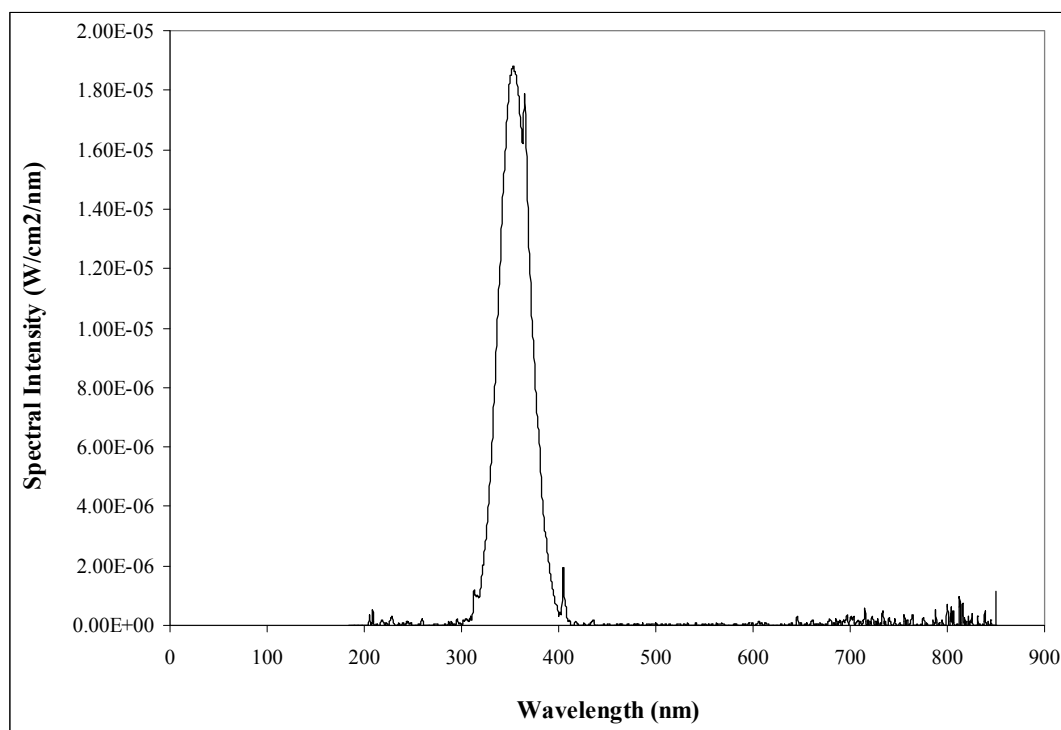


Figure E1: Spectral intensity for a new 15 W black-light-bulb near-UV lamp as measured with the spectrophotometer Stellarnet EPP2000

It is known that lamp intensity decay with utilization time. Changes in the measured intensity can be the result of the decay in the lamp spectra or the effect of changes in the sensor calibration. It has been reported by the manufacturer (UVP Inc., Upland CA) that for the type of lamps used in this study a decay of around 20 % can be expected after 500 hours of use, producing also asymmetric emission profiles (Salaices-Arredondo, 2002). However, the total time of use of the lamps during the experimental section of this research did not exceed 500 hours. Furthermore, no significant decay in the spectral intensity or variation in the emission with respect to the axial direction was measured upon completion of the experiments.

Figure E2 reports the lamp radiation flux as measured at the surface of the catalyst support, that is, once the radiation has passed through the quartz cylinder enclosing the reaction section. It can be noticed that the distance along the lamp including most of the reaction section of the reactor (between 5 and 40 cm) receives a uniform level of radiation. Therefore, the end effects of the lamp are negligible.

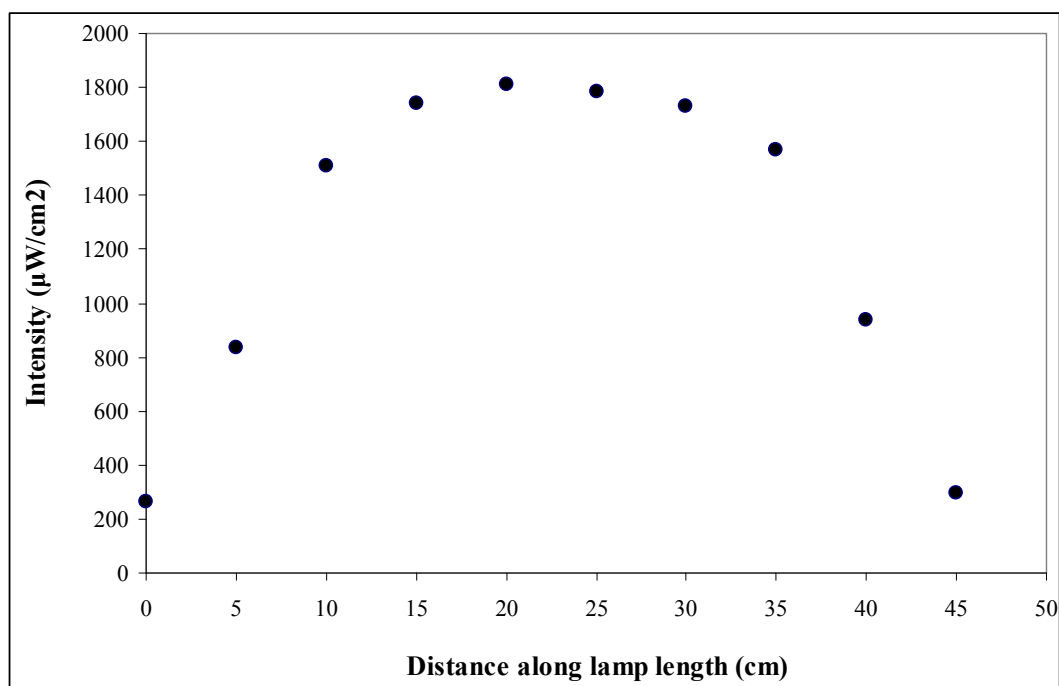


Figure E2: Typical lamp axial radiation flux as measured at the surface of the photocatalyst support

Intensity Profile at Photocatalyst Supporting Mesh

Given that the photocatalytic reactions carried out were functions of the amount of irradiation absorbed by the catalyst Degussa P25, the distribution of the available irradiation inside the reaction section of the Photo-CREC-Air unit was determined. The design of the supporting stainless steel mesh used as photocatalyst support and the location of the 8 near-UV lamps symmetrically located around the reaction section produced a uniform distribution of irradiation.

Measurements of irradiation reaching the surface of the catalyst support at different locations in the axial direction were performed (Figure E3). The irradiation profiles at these locations were very similar. The regions close to the bottom and top of the reaction section displayed less extent of irradiation. Overall these results proved a quite uniform irradiation over the photocatalyst supported surface.

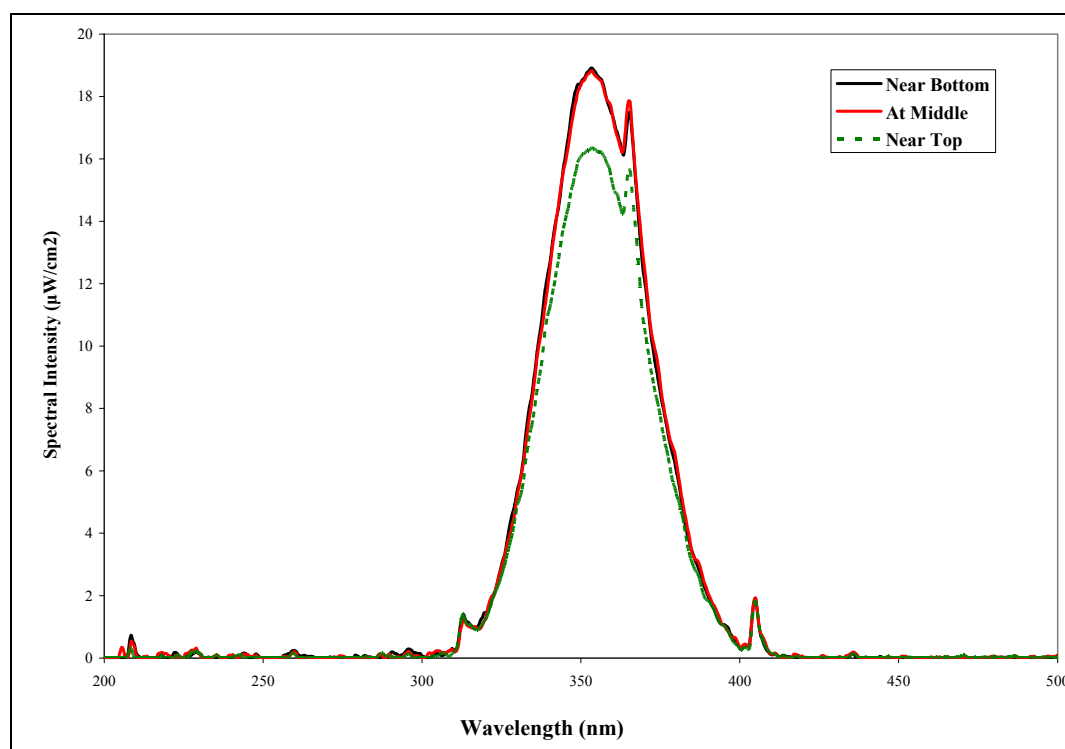


Figure E3: Spectral intensity profiles for three locations in the axial direction of the reaction section: Near the bottom, the middle and near the top

Curriculum Vitae

Name: Juan Manuel García Hernández

Post-secondary Education and Degrees: Universidad Michoacán de San Nicolás de Hidalgo
Morelia, Michoacán, México
1998-2003 Bachelor of Science in Chemical Engineering

Universidad Michoacán de San Nicolás de Hidalgo
Morelia, Michoacán, México
2003-2005 Master of Science in Chemical Engineering

The University of Western Ontario
London, Ontario, Canada
2007-2012 Doctor of Philosophy in Chemical Engineering

Honours and Awards: Faculty of Graduate Studies Scholarship
The University of Western Ontario
2007-2012

Nominated for the Teaching Assistant Award
The University of Western Ontario
2009

Full Scholarship for International PhD studies (4 years, 8 months).
Sponsored by the Federal Government of Mexico through the National Council of Science and Technology (CONACYT)
2007-2012

Related Work Experience Teaching Assistant
The University of Western Ontario
2007-2011

Research Assistant
The University of Western Ontario
2007-Present

Publications:

International peer-reviewed publications

Garcia-Hernandez, Juan M., Serrano, B. and de Lasa, H. (2012) Energy Efficiencies in a Photo-CREC-Air Reactor: Conversion of Model Pollutants in Air. Accepted for Publication in: Industrial & Engineering Chemistry Research. Impact Factor: 2.071.

Garcia-Hernandez, Juan M., Serrano, B. and de Lasa, H. (2010) The photochemical thermodynamic efficiency factor (PTEF) in photocatalytic reactors for air treatment. *Chemical Engineering Journal* 165, 891-901. Impact Factor: 3.074.

Garcia-Hernandez, Juan M., Ponce-Ortega, J.M. y Serna-Gonzalez, M. (2007) Rigorous Synthesis of Heat Exchanger Networks Using a Hybrid Method. *Mexican Journal of Chemical Engineering* 6, 89-100.

Refereed Proceedings

Juan Manuel Garcia-Hernandez, Benito Serrano-Rosales and Hugo de Lasa. "Photocatalytic Degradation of Organic Pollutants in Air. Energy Efficiency Factors in a Photo-CREC Unit" **2011 61st Canadian Chemical Engineering Conference: London, ON, Canada.**

Garcia-Hernandez, Juan M., Serrano, B. and de Lasa, H. "Efficiency Factors in Photocatalytic Reactors for Air Treatment". **2011 AIChE Annual Meeting: Minneapolis, MN, USA.**

Juan Manuel Garcia-Hernandez, Benito Serrano Rosales and Hugo de Lasa "Energy Efficiency Factors in Photocatalytic Degradation of Air Pollutants". **2011 American Catalysis Society, 22nd North American Meeting: Detroit, MI, USA.**

J. M. García Hernández, B. Serrano Rosales, H. de Lasa "Energy Efficiency in Photocatalytic Air Treatment" **2011 XXXII National Meeting and First International Congress, The Mexican Academy for Research and Teaching in Chemical Engineering (AMIDIQ): Mayan Riviera, Mexico.**

Garcia, Juan M., Ponce, J.M. and Serna, M. "A hybrid methodology for detailed heat exchanger design in the optimal synthesis of heat exchanger networks". **2006 16th European Symposium on Computer Aided Process Engineering and 9th International Symposium on Process Systems Engineering: Garmisch-Partenkirchen, Germany.**